Mid-infrared laser based trace gas sensor technologies: recent advances and applications- I I

OUTLINE

Frank K. Tittel

Dept. of Electrical & Computer Engineering, Rice University, Houston, TX 77005

http://www.ece.rice.edu/~lasersci/

Research support by NSF ERC MIRTHE, NSF-ANR NexCILAS, the Robert Welch Foundation as well as sub-awards ARPA-E from AERIS Technologies & Maxion-Thorlabs is acknowledged

GE Global Research

Houston, TX

March 9, 2016

Outline

- **Novel Laser-Based Trace Gas Sensor Technology**
  - Quartz Enhanced Photoacoustic Spectroscopy (QEPAS)
  - Mid-infrared & THz spectral ranges
  - Recent near infrared QEPAS sensor technology
  - Sensor performance improvements resulting from custom QTFs

- **Applications of QEPAS based sensor systems**
- **Five mid-infrared Trace Gas Species**
- NO, CO_2, CO, SF_6, H_2S
- **Two THz Trace Gas Species**
- H_2S and CH_3OH
- **Future Directions of QEPAS-Based Trace Gas Sensor Technologies and Conclusions**
- **I (Intra-cavity) – QEPAS**

RICE

Wide Range of Trace Gas Sensing Applications

- **Urban and Industrial Emission Measurements**
  - Industrial Plants
  - Combustion Sources and Processes (e.g. fire detection)
  - Automobile, Truck, Aircraft and Marine Emissions
- **Rural Emission Measurements**
  - Agriculture & Forestry, Livestock
- **Environmental Monitoring**
  - Atmospheric Chemistry (e.g isotopologues, climate modeling,…)
  - Volcanic Emissions
- **Chemical Analysis and Industrial Process Control**
  - Petrochemical, Semiconductor, Pharmaceutical, Metals Processing, Food & Beverage Industries, Nuclear Technology Safeguards
- **Spacecraft and Planetary Surface Monitoring**
  - Crew Health Maintenance & Life Support
- **Applications in Medical Diagnostics and the Biophotonics**
- **Technologies for Law Enforcement, Defense and Security**
- **Fundamental Science and Photochemistry**

RICE

NASA's Horizons spacecraft flew pass Pluto in July, 2015. Icy Heart of Pluto: Nitrogen, Snow and Methane Ice cover Tombaugh Region. Science, March 14, 2016

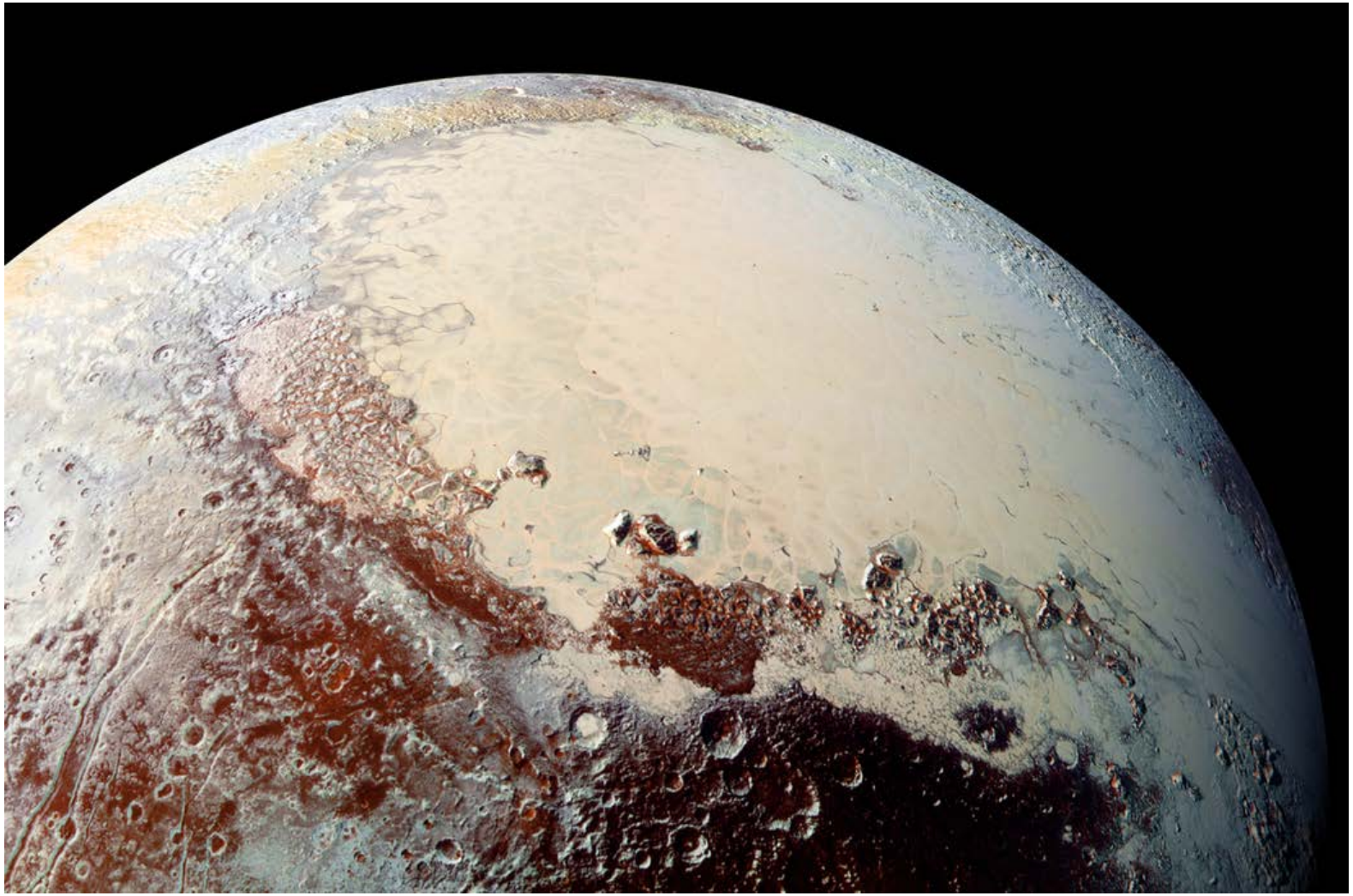

RICE

Laser-Based Trace Gas Sensing Techniques

- **Optimum Molecular Absorbing Transition**
  - Overtone or Combination Bands (NIR)
  - Fundamental Absorption Bands (Mid-IR and THz)
- **Long Optical Pathlength**
  - Multipass Absorption Gas Cell (e.g., White, Herriot, Chernin, Aeris Technologies & Circular Cylindrical Design)
  - Cavity Enhanced and Cavity Ringdown Spectroscopy
  - Open Path Monitoring (with retro-reflector or back scattering from topographic target): Standoff and Remote Detection
  - Fiberoptic & Wave-guide Evanescent Wave Spectroscopy
- **Spectroscopic Detection Schemes**
  - Frequency or Wavelength Modulation
  - Balanced Detection
  - Zero-air Subtraction
  - Photoacoustic & Quartz Enhanced Photoacoustic Spectroscopy (QEPAS)

RICE

From Conventional **PAS** to Quartz Enhanced PAS (**QEPAS**)

Q>>1000

Cell is OPTIONAL!

***V*-effective volume**

Laser beam, power P

Modulated (P or λ) at f or $f/2$

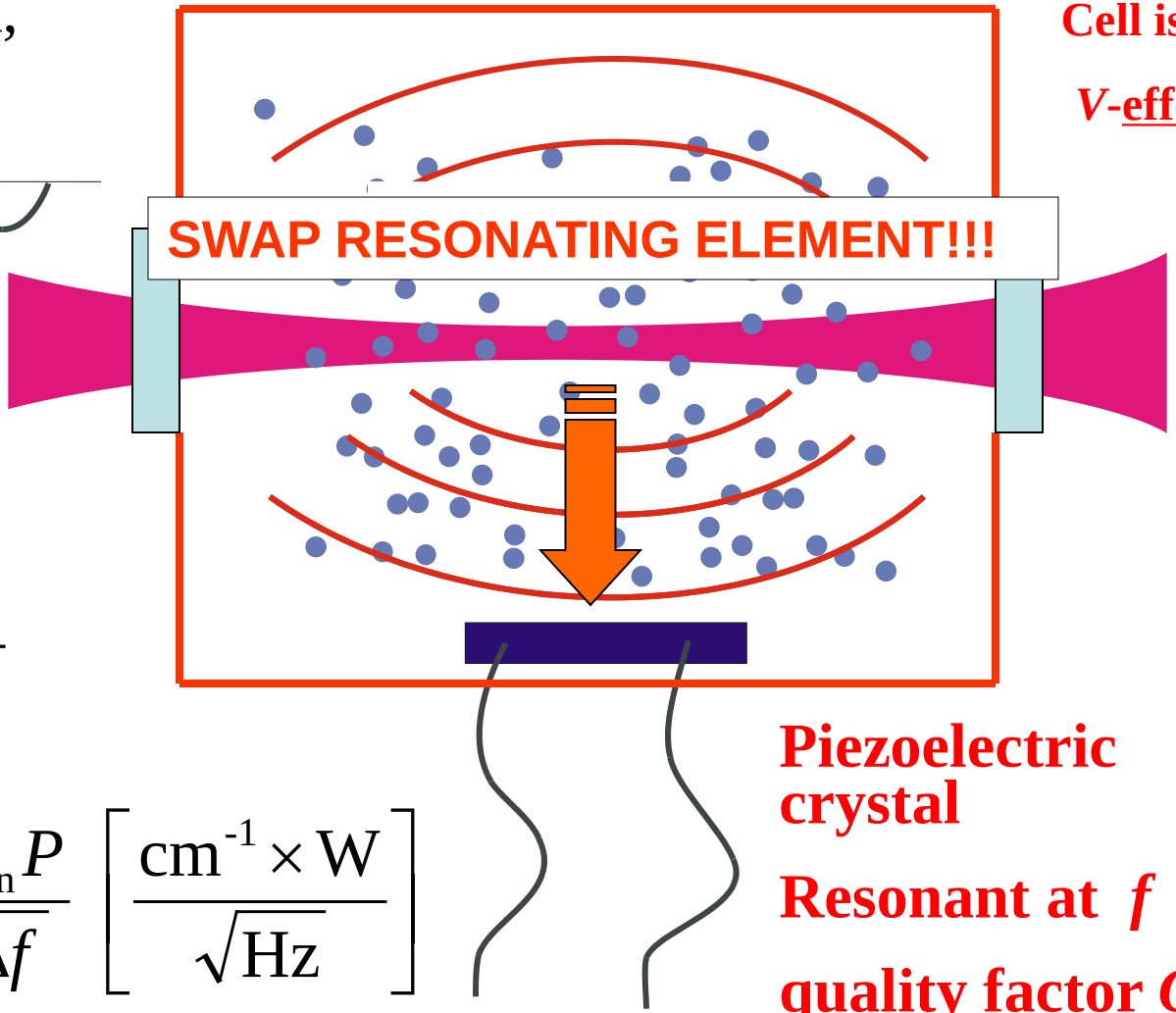

$$S \sim \frac{Q \alpha P}{f V}$$

$$NNEA = \frac{\alpha_{min} P}{\sqrt{\Delta f}} \left[\frac{\mathrm{cm}^{-1} \times \mathrm{W}}{\sqrt{\mathrm{Hz}}} \right]$$

Piezoelectric crystal

Resonant at f

quality factor Q

RICE

Conventional Photoacoustic Spectroscopy (PAS)

Cell is OPTIONAL!

***V*-effective volume**

Laser beam, power P

Modulated (P or λ) at f or $f/2$

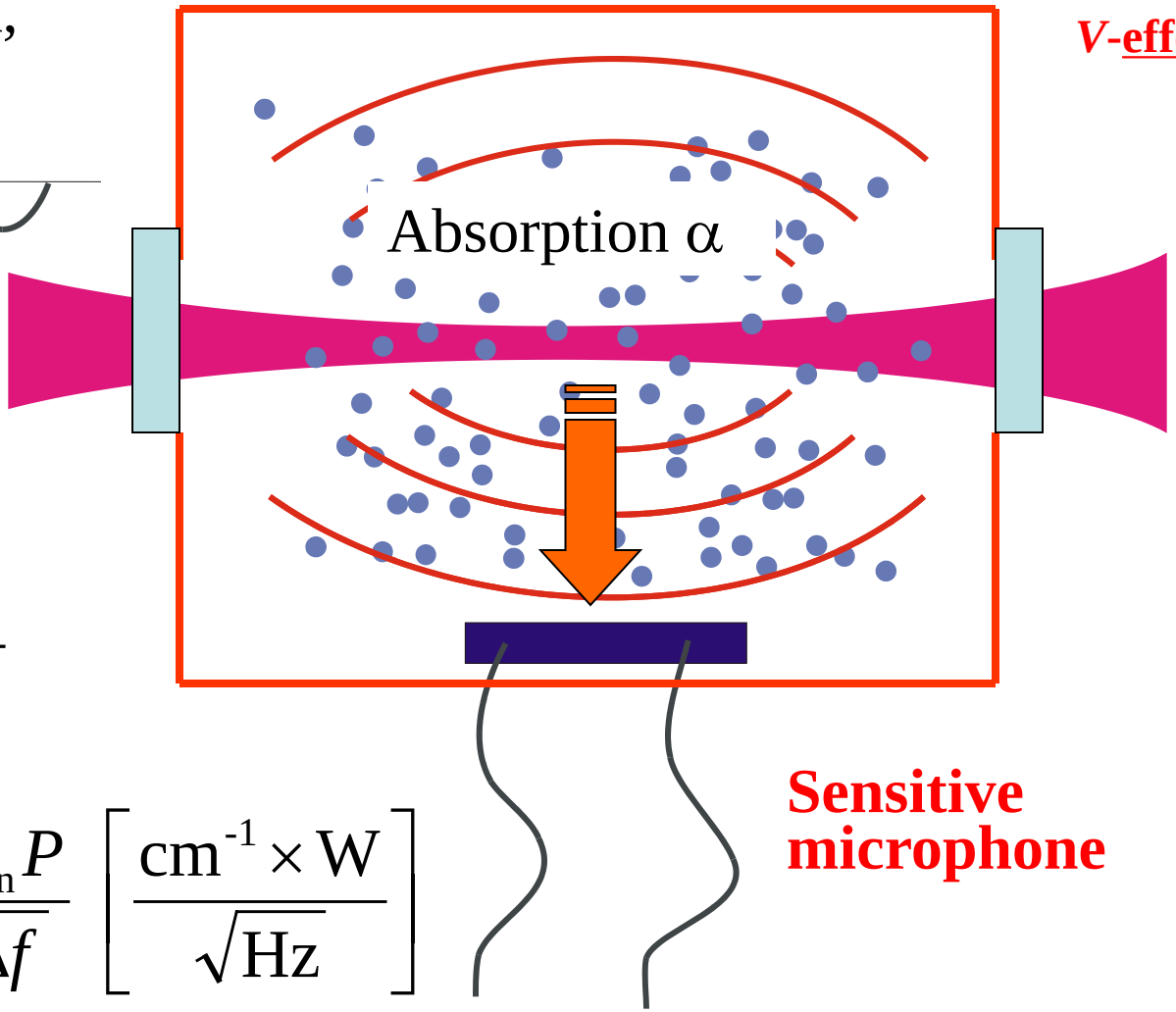

$$S \sim \frac{Q \alpha P}{f V}$$

$$NNEA = \frac{\alpha_{min} P}{\sqrt{\Delta f}} \left[\frac{cm^{-1} \times W}{\sqrt{Hz}} \right]$$

RICE

Quartz Tuning Fork as a Resonant Microphone for QEPAS

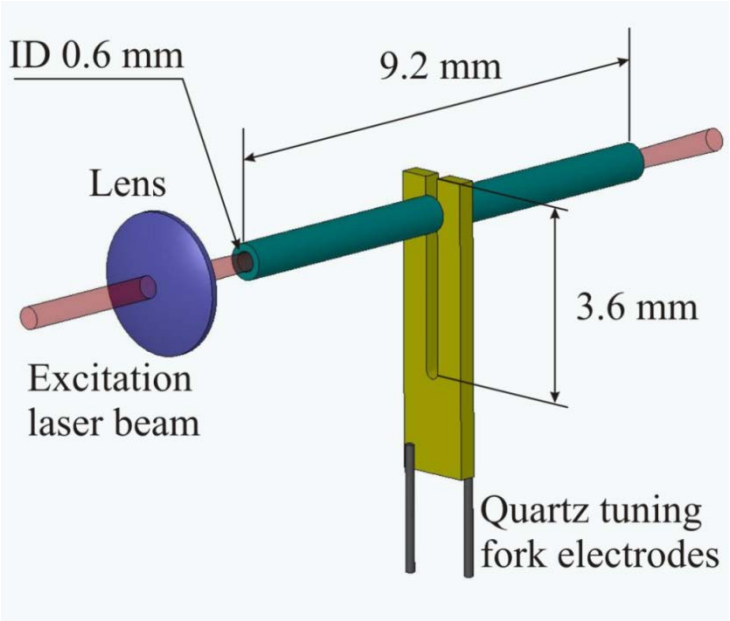

Unique Properties

- Extremely low internal losses:
  - Q ~ 10,000 at 1 atm
  - Q ~ 100,000 in vacuum
- Acoustic quadrupole geometry
  - Low sensitivity to external sound
- Large dynamic range (~10^6) – linear from thermal noise to breakdown deformation
  - 300K noise: x~10^{-11} cm
  - Breakdown: x~10^{-2} cm
- Wide temperature range: 1.6K to ~700K

Acoustic Micro-resonator (μR) Tubes

- Optimum inner diameter: 0.6 mm; μR-QTF gap is 25-50 μm
- Optimum μR tubes must be ~ 4.4 mm long (~$\lambda/4<l<\lambda/2$ for sound at 32.8 kHz)
- SNR of QTF with μR tubes: × 30 (depending on gas composition and pressure)

Motivation for Nitric Oxide Detection

- **NO in medicine and biology**
  - Important signaling molecule in physiological processes in humans and mammals (1998 Nobel Prize in Physiology/Medicine)
  - Treatment of asthma, chronic obstructive pulmonary disease (COPD) & lung rejection
- **Environmental pollutant gas monitoring**
  - Ozone depletion
  - Precursor of smog and acid rain
  - NO_X monitoring from automobile exhaust and power plant emissions
- **Atmospheric Chemistry**

RICE

HITRAN Simulated Mid-Infrared Molecular Absorption Spectra

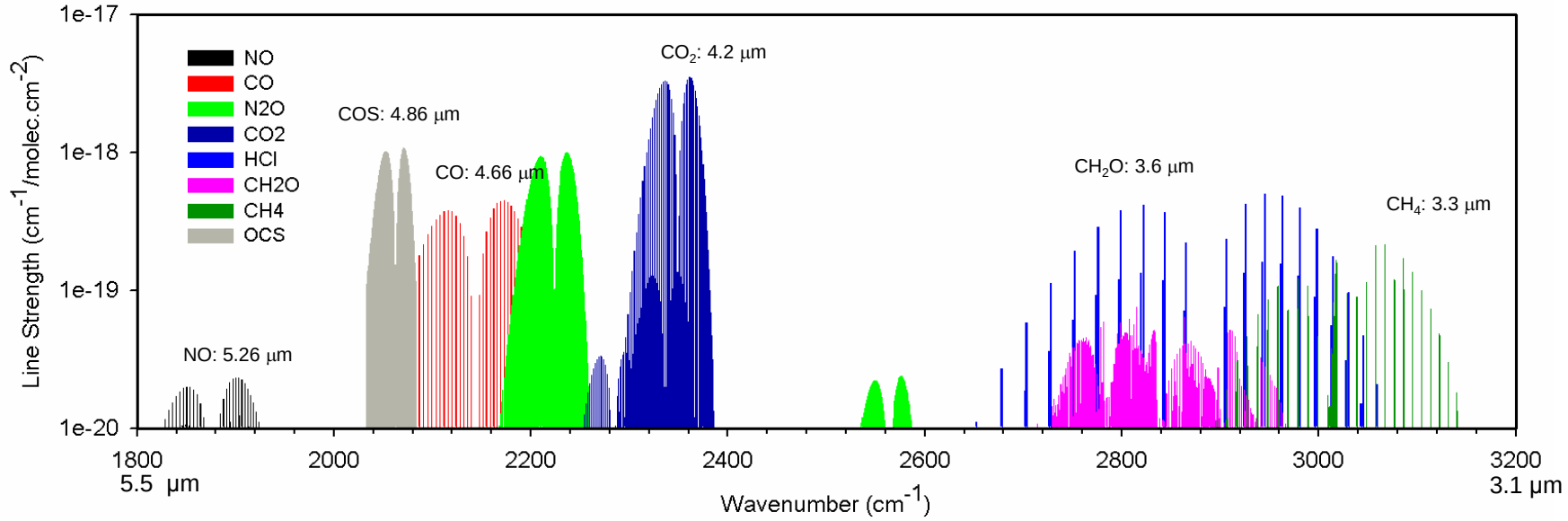

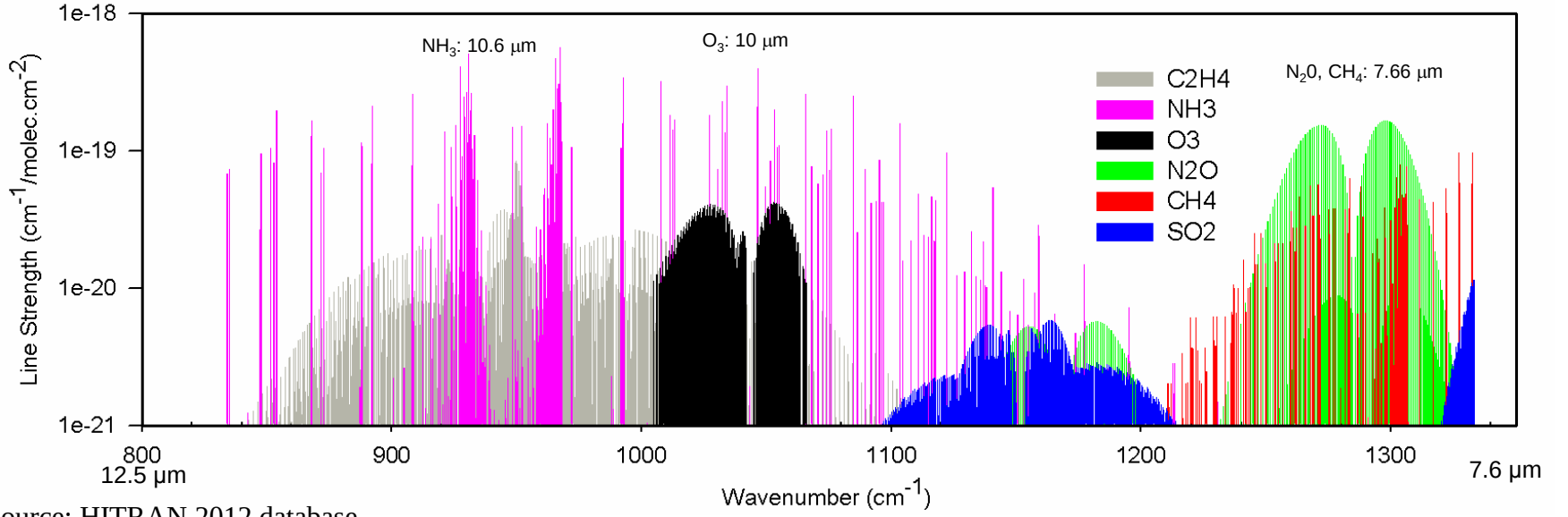

Source: HITRAN 2012 database

Emission spectra of a 1900cm^{-1} TEC DFB QCL and HITRAN simulated spectra of NO, H_2O & CO_2

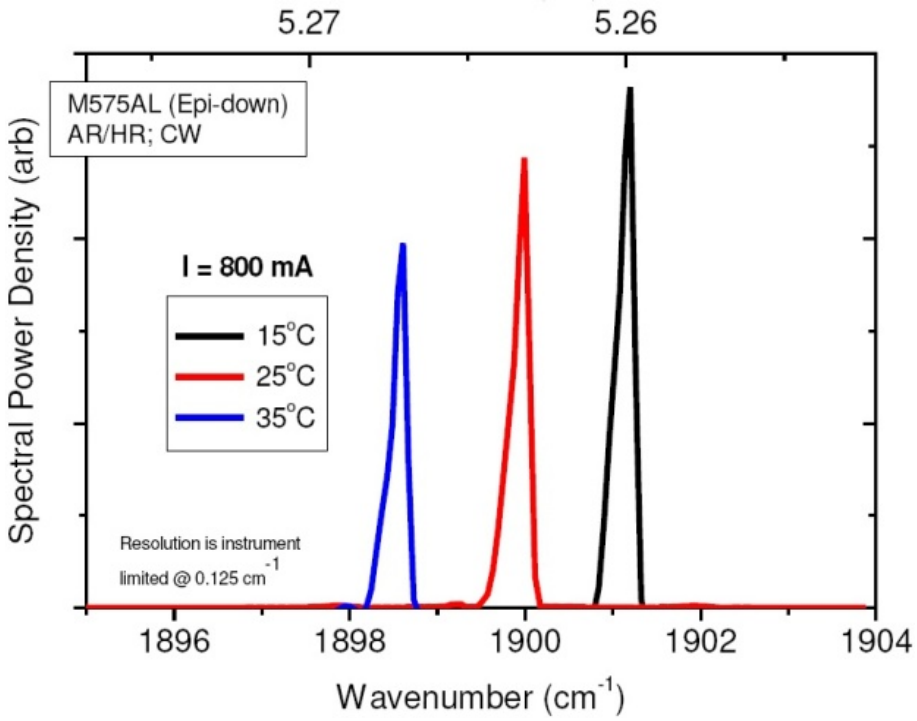

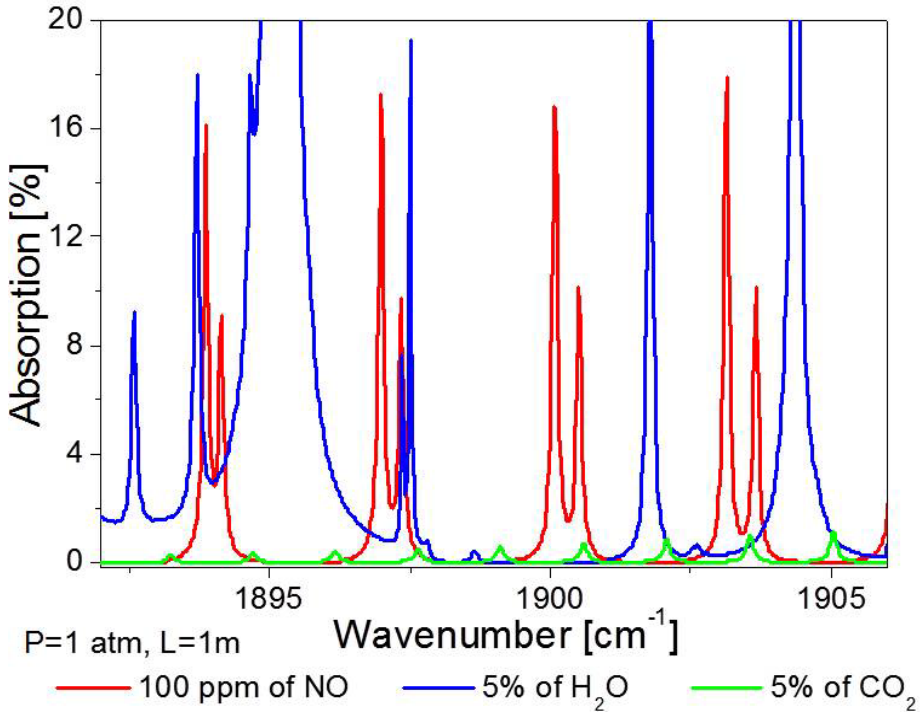

Output power: 117 mW @ 25 C
Thorlabs/Maxion

RICE

Performance of a 5.26 μm CW HHL TEC DFB-QCL

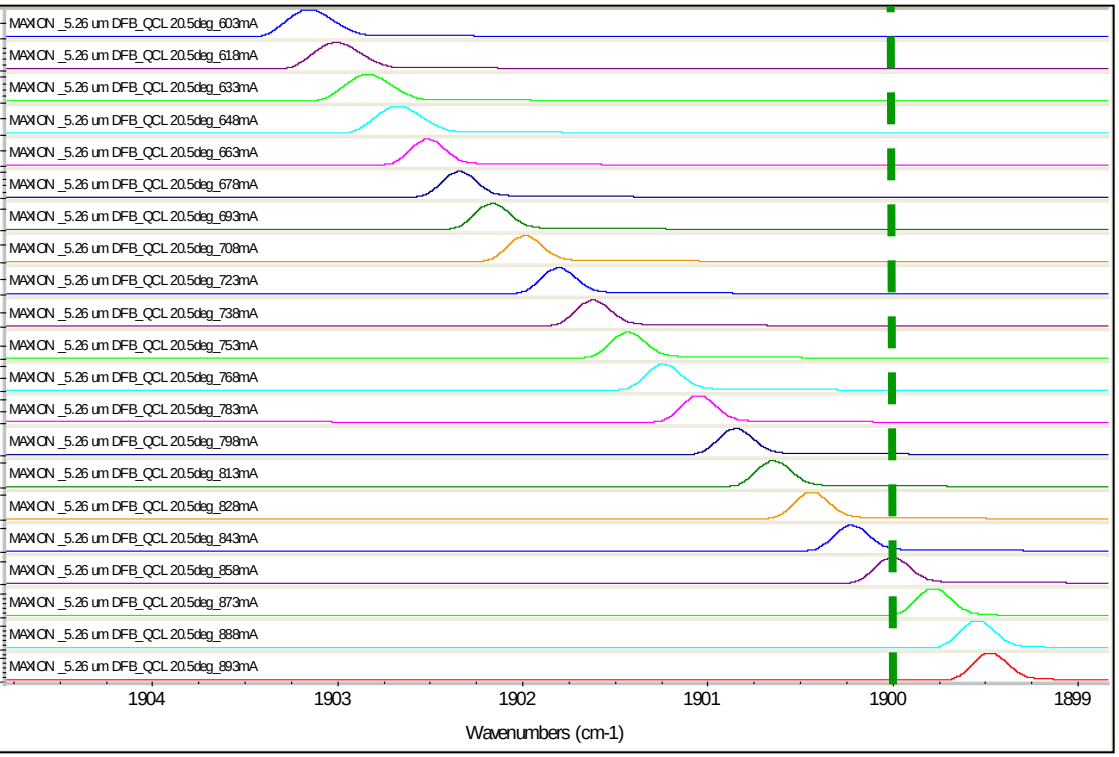

Single frequency QCL radiation recorded with FTIR for different laser current values at a QCL temperature of 20.5°C.

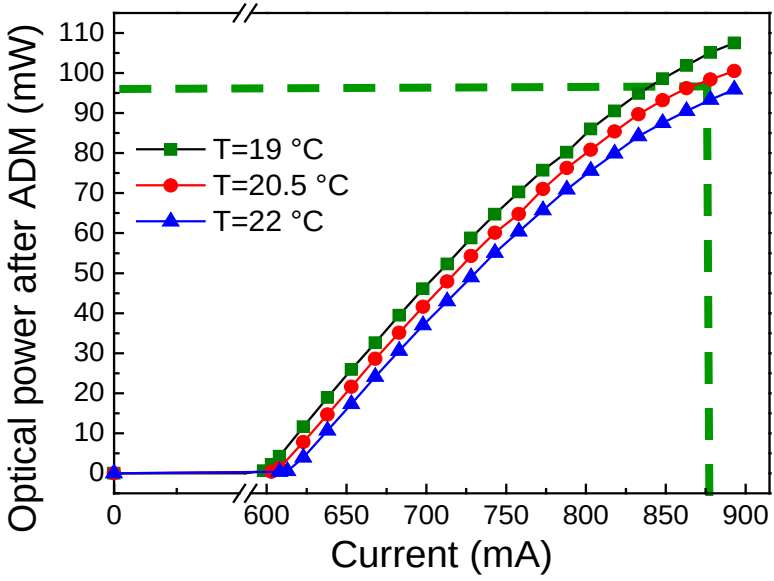

CW DFB-QCL optical power and current tuning at three different temperatures.

RICE

CW TEC DFB QCL based QEPAS NO Gas Sensor

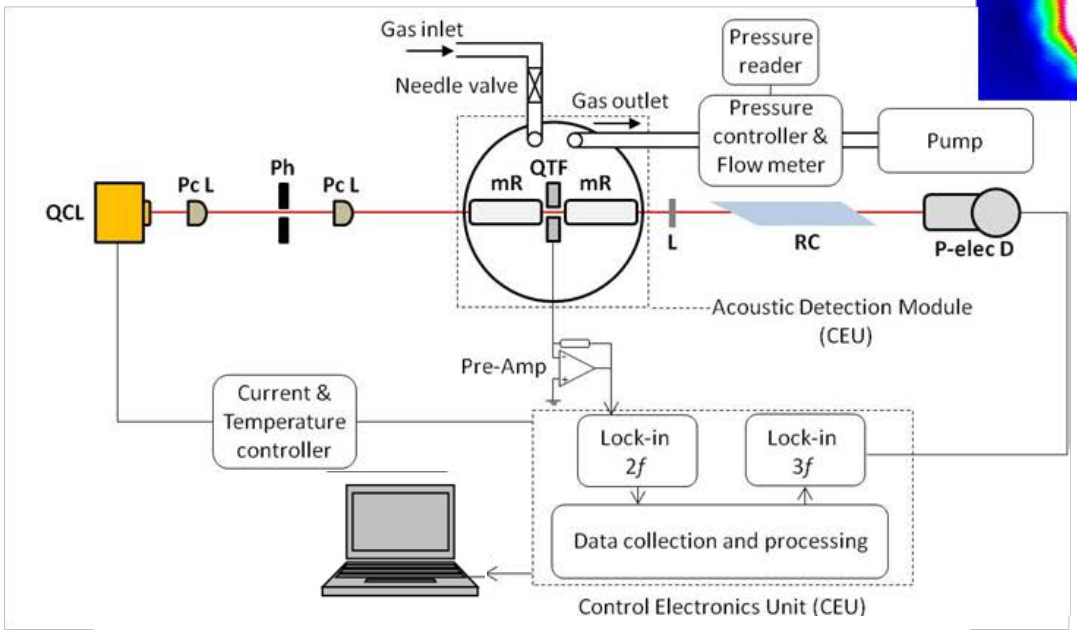

Schematic of a DFB-QCL based Gas Sensor.
PcL – plano-convex lens, Ph – pinhole,
QTF – quartz tuning fork, mR – microresonator,
RC- reference cell, P-elec D – pyro electric detector

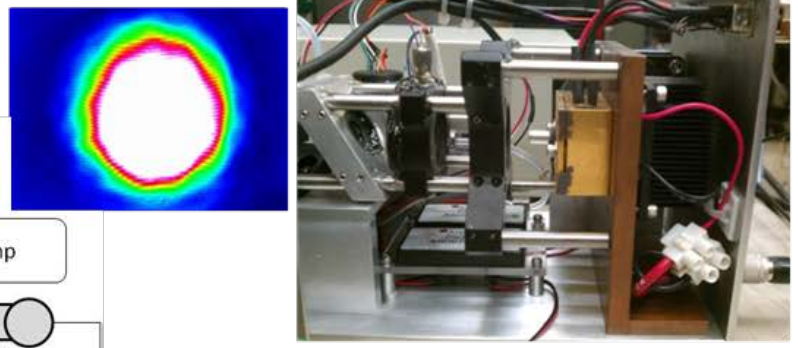

CW HHL TEC DFB-QCL package and IR camera image of the laser beam at 630 mA and 20.5 deg C through tubes after ADM

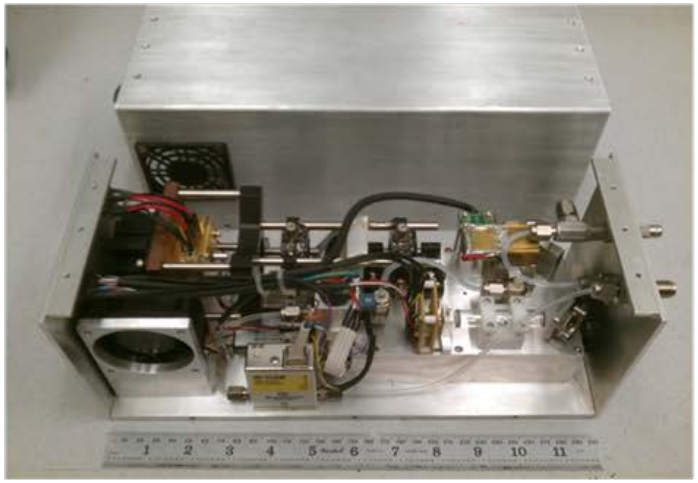

Compact Prototype NO Sensor (September 2012)

RICE

Performance of CW DFB-QCL based WMS QEPAS NO Sensor Platform

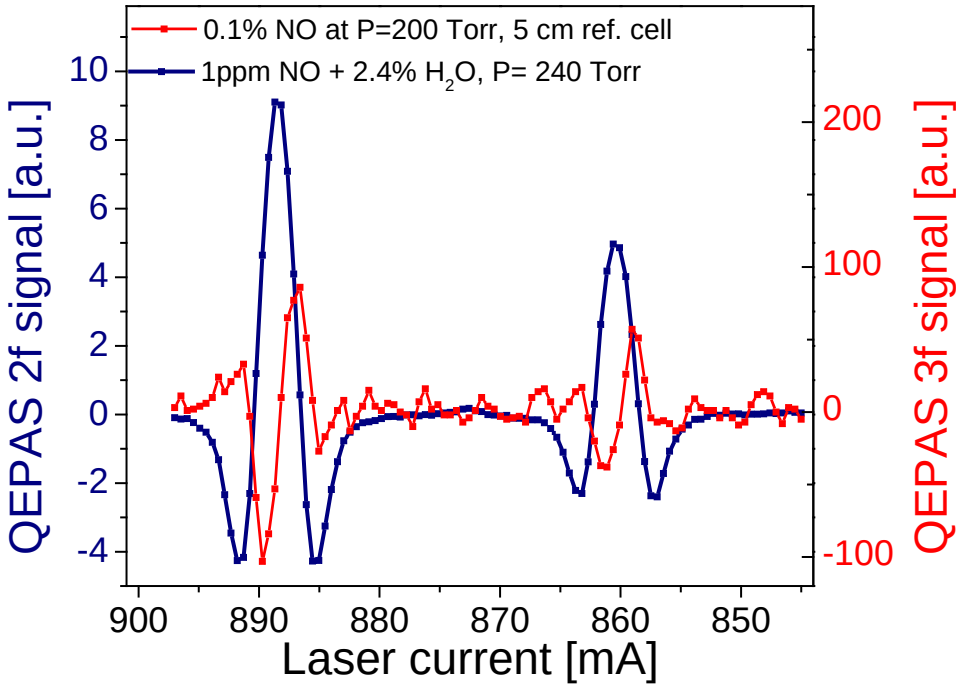

2f QEPAS signal (navy) and reference 3f signal (red) when DFB-QCL was tuned across **1900.08 cm^{-1}** NO line.

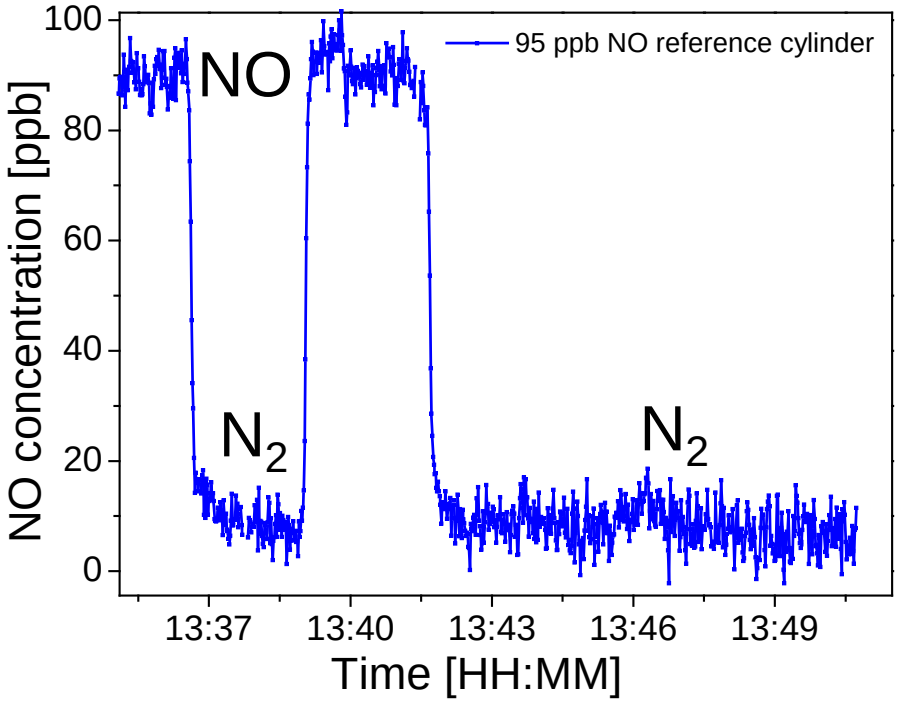

2f QEPAS signal amplitude for 95 ppb NO when DFB-QCL was locked to the **1900.08 cm^{-1}** line.

Minimum detectable NO concentration is:

~ 3 ppbv (1σ; 1 s time resolution)

RICE

Motivation for Carbon Monoxide Detection

- **CO in Medicine and Biology**
  - Hypertension and abnormality in heme metabolism
- **Public Health**
  - Extremely dangerous to human life even at a low concentrations. Therefore CO must be carefully monitored at low concentration levels (<35 ppm).
- **Atmospheric Chemistry**
  - Incomplete combustion of natural gas, fossil fuel and other carbon containing fuels.
  - Impact on atmospheric chemistry through its reaction with hydroxyl (OH) for troposphere ozone formation and changing the level of greenhouse gases (e.g. CH_4).

RICE

Performance of a 4.61μm high power CW TEC DFB QCL

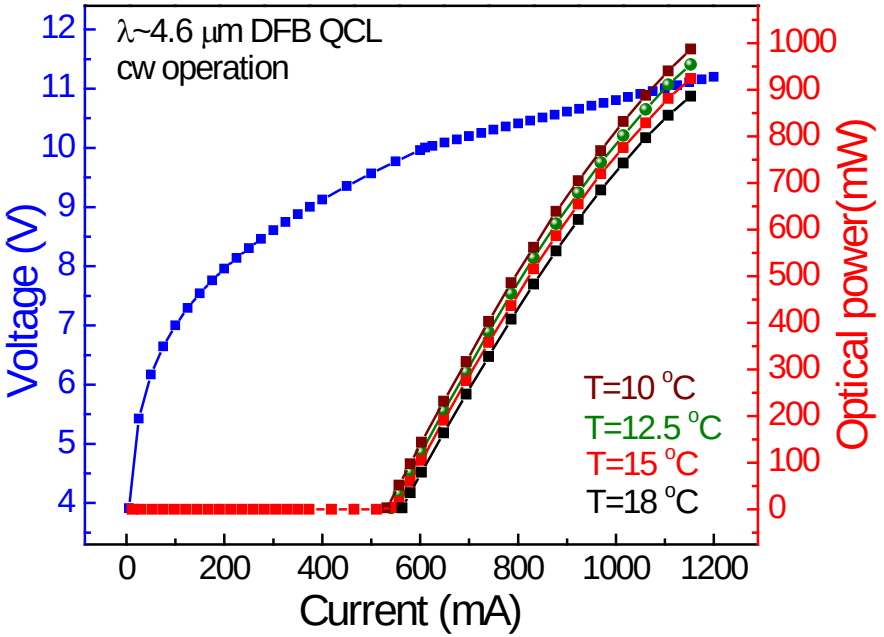

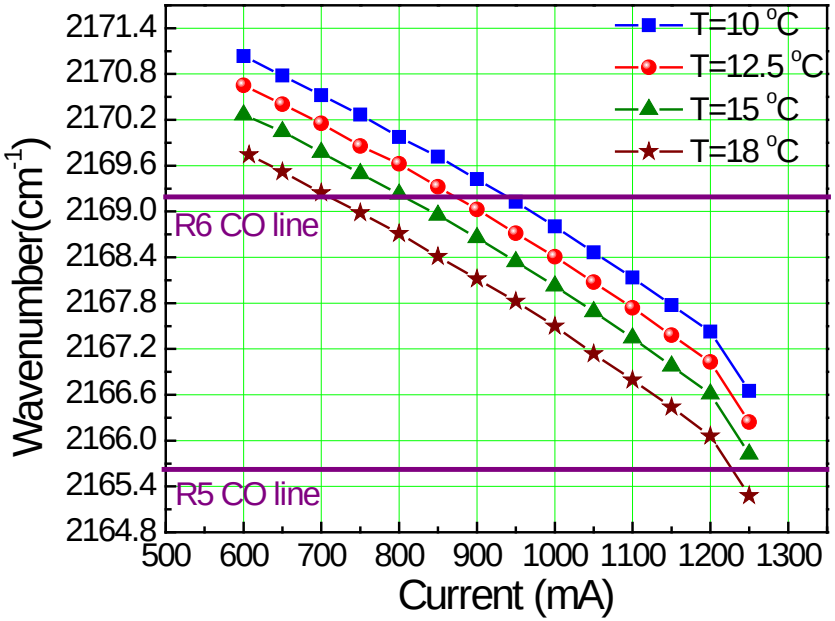

CW DFB-QCL optical power and current tuning at a four different QCL temperatures.

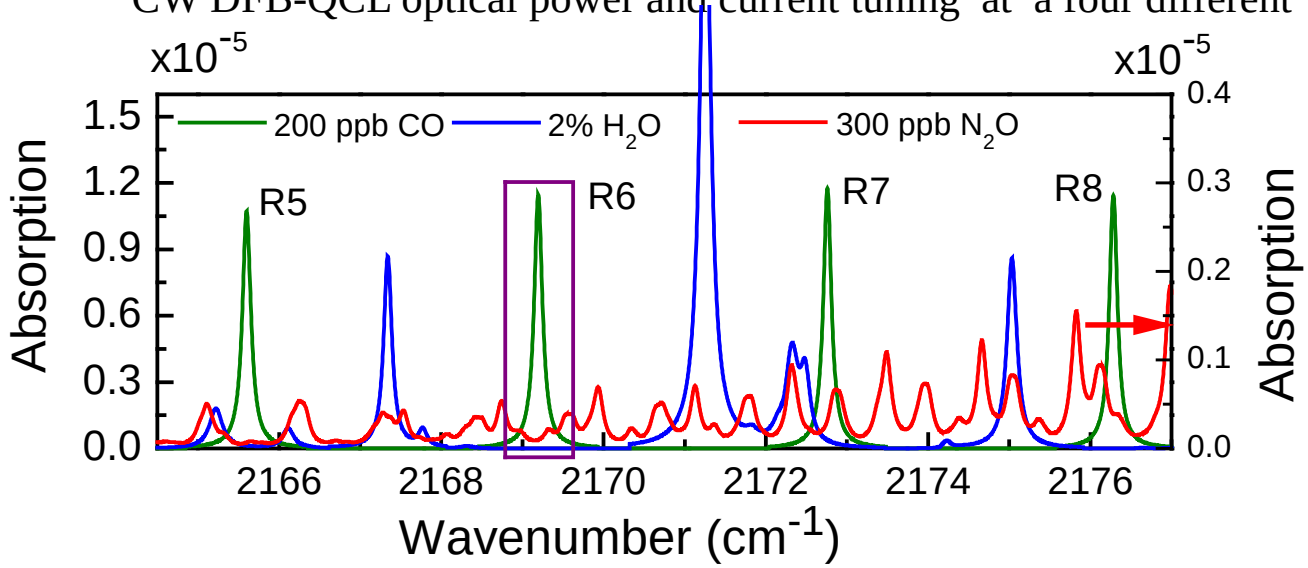

Estimated max wall-plug efficiency (WPE) is ~ 7% at 1.25A QCL drive-current.

RICE

QEPAS Performance in locked Mode and long term Frequency Stability

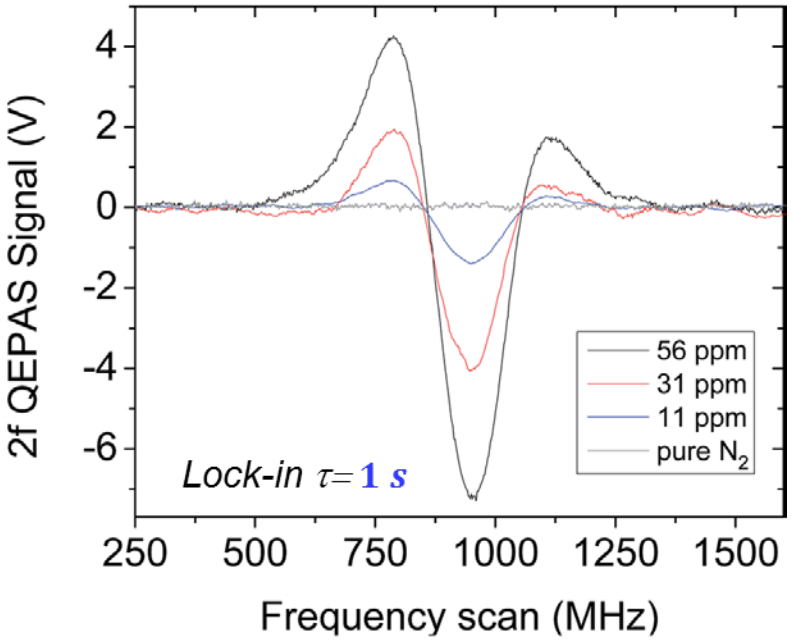

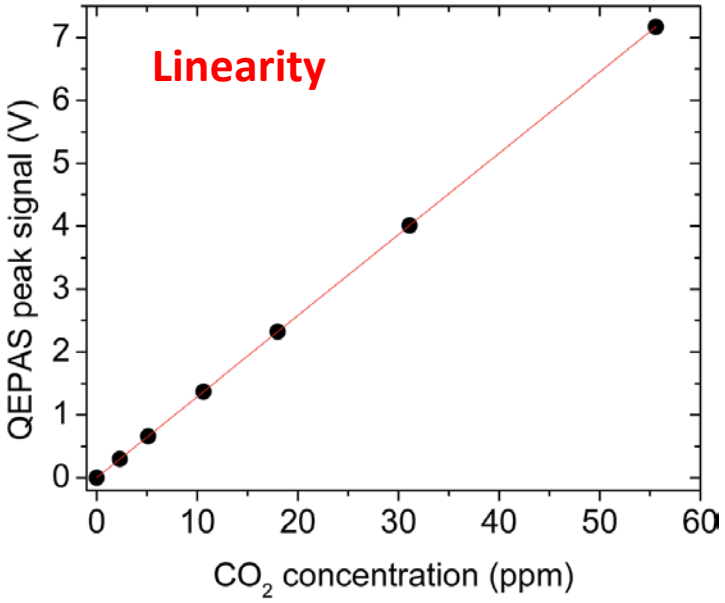

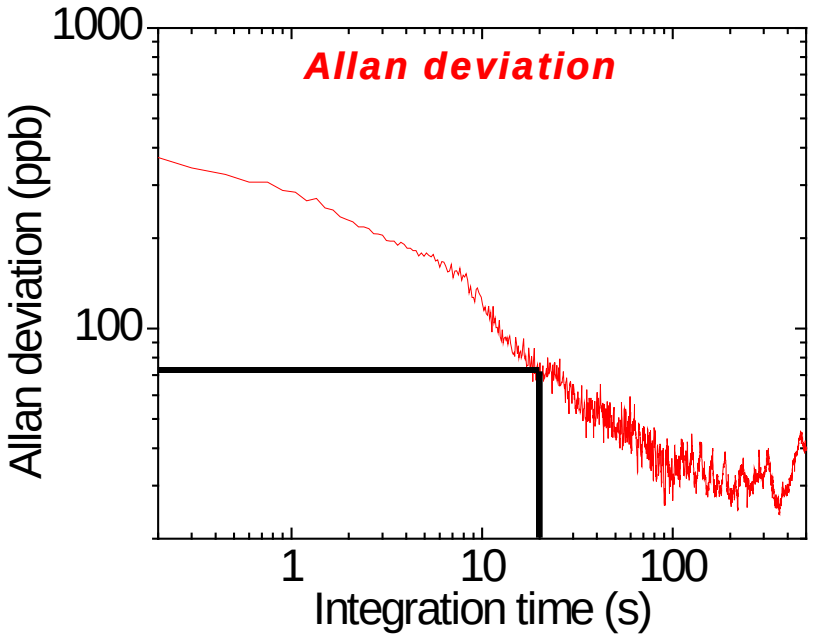

Noise Equivalent Concentration:

NEC = 72 ppb @ 20sec integration time

Normalized Noise Equivalent Absorption:

NNEA = 7.5×10^{-8} $cm^{-1}W(Hz)^{-1/2}$

CW DFB-QCL based CO QEPAS Sensor Results

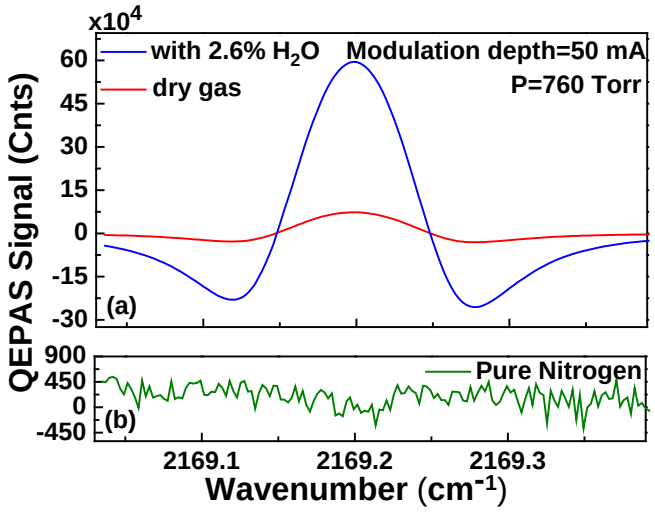

2f QEPAS signal for dry (red) and moisturized (blue) 5 ppm CO:N_2 mixture near **2169.2 cm^{-1}**.

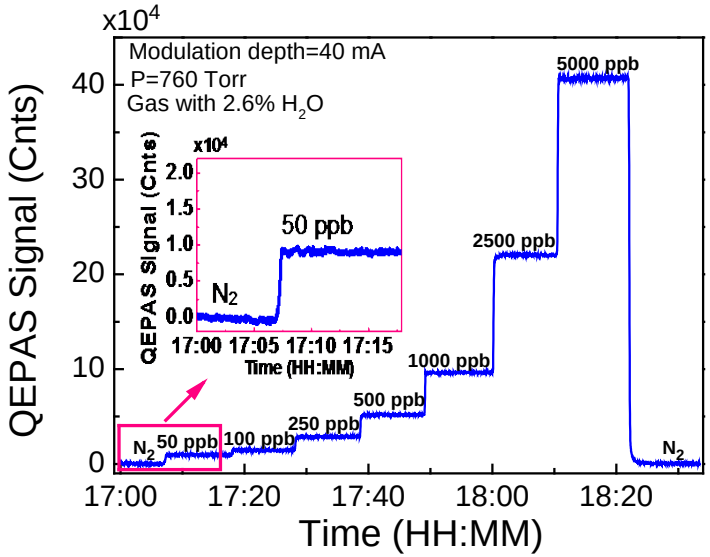

Dilution of a 5 ppm CO reference gas mixture when the CW DFB-QCL is locked to the **2169.2 cm^{-1}** R6 CO line.

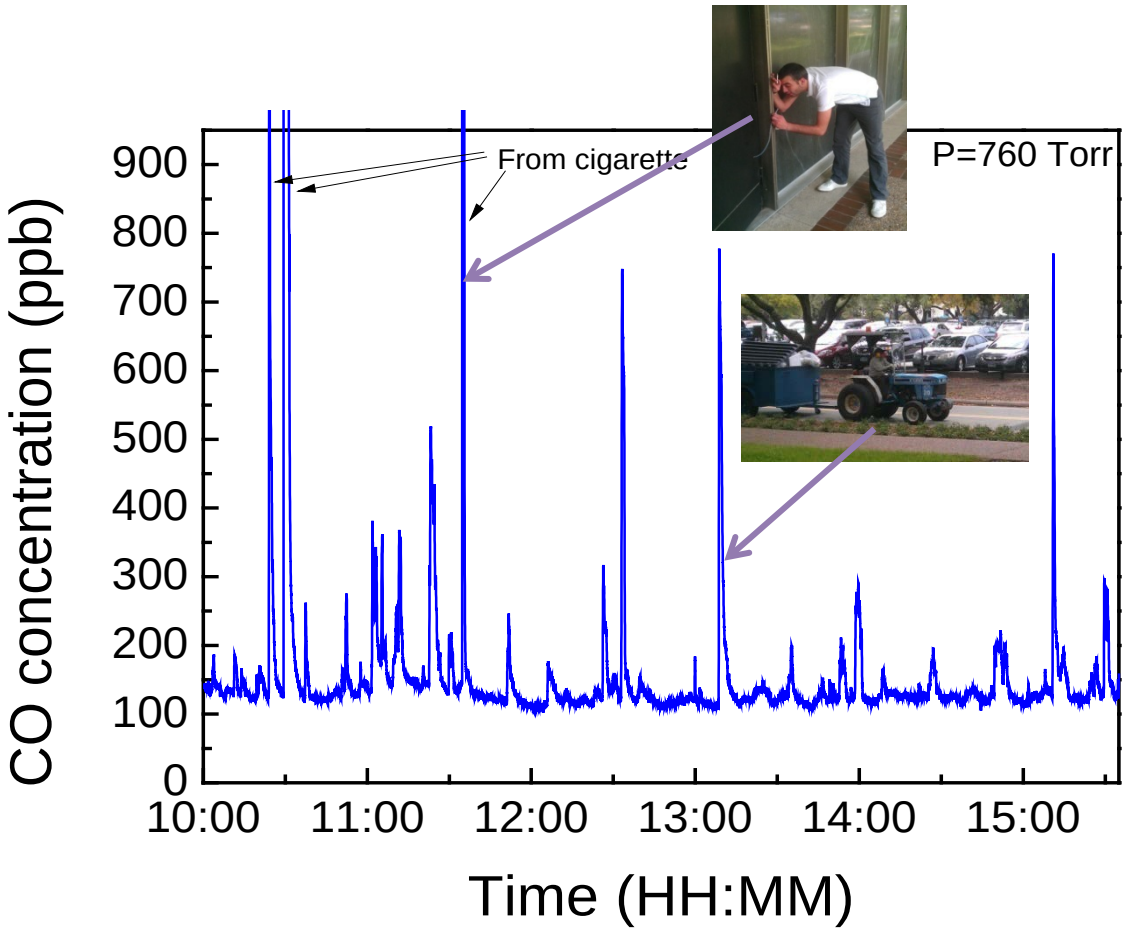

Atmospheric CO concentration levels on Rice University campus, Houston, TX

Minimum detectable CO concentration is:

~ 2 ppbv (1σ; 1 s time resolution)

RICE

Motivation for Carbon Dioxide Detection

- **Environmental Monitoring**
  - CO_2 Exchange Processes in volcanic Emissions which serves as a potential Predictors of increased volcanic activity, in particular of an impending volcanic eruption
- **Medical &Biological Sciences**
  - Monitoring in patients under general Anesthesia during Surgery or in Intensive Care Units
  - Storage & Transportation of Fruit
- **Atmospheric Chemistry**
  - Real time monitoring of atmospheric CO_2 Concentrations, which provides valuable information on the sources and sinks of carbon , which will assist in developing strategies for controlling global warming

RICE

Schematic of a QEPAS CO_2 Detection System

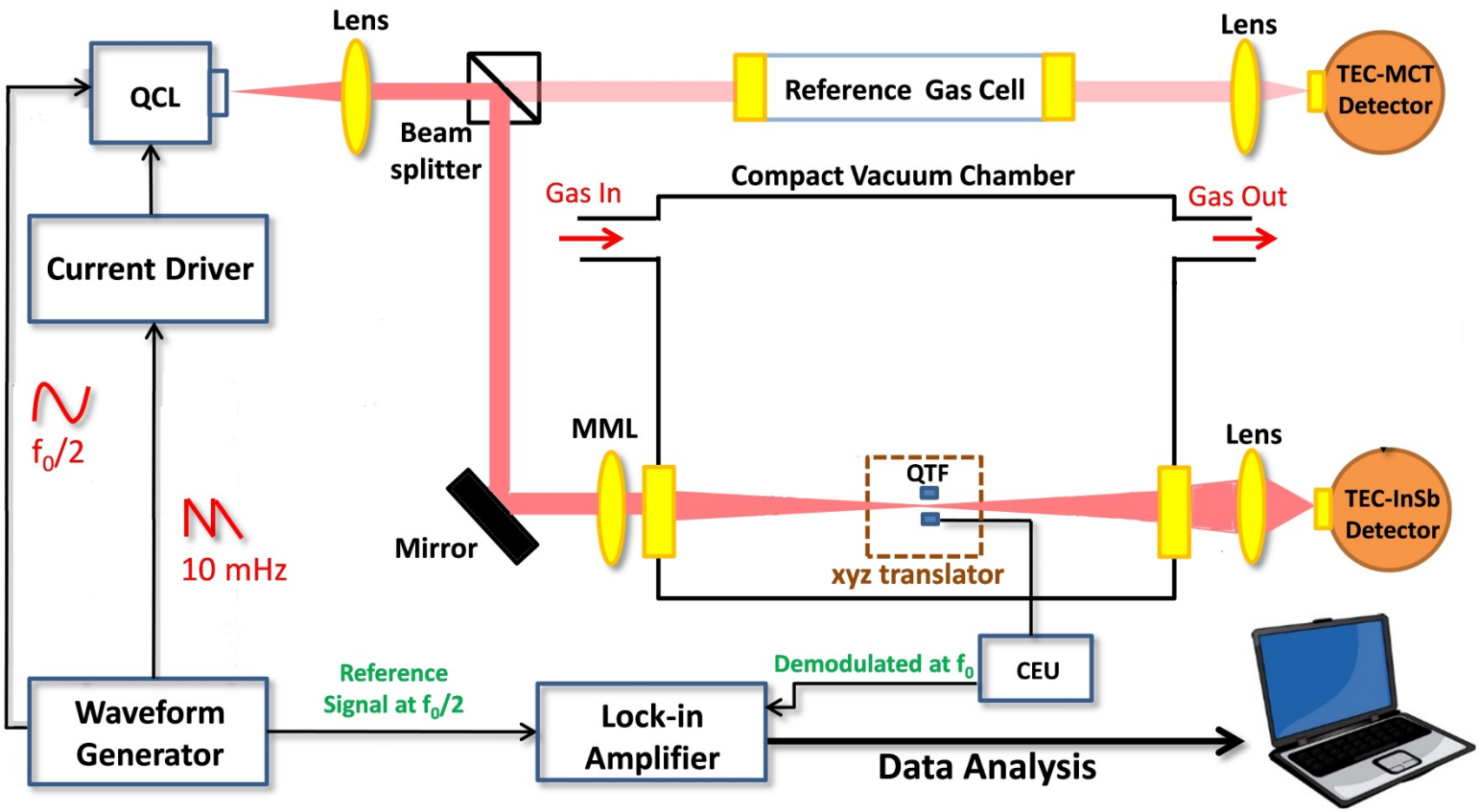

Optical power build up cavity can provide:

Standard single-pass QEPAS platform CO_2 Detection

- **RT CW DFB QCL, λ=4.33 microns**
- **Low noise current driver → narrow QC laser linewidth ~1 MHz**
- **Optical Power of ~3 mW**
- **Gas pressure in the enclosure is 50 mbar**
- **Wavelength modulation approach and f_0 detection**

QEPAS based CH_4 and N_2O Gas Sensor

Motivation for CH_4 and N_2O Detection

- Medical Diagnostics
  - Nausea, blurred vision, vomiting
- Prominent greenhouse gases
- Sources: wetlands, leakage from natural gas systems, fossil fuel production and agriculture

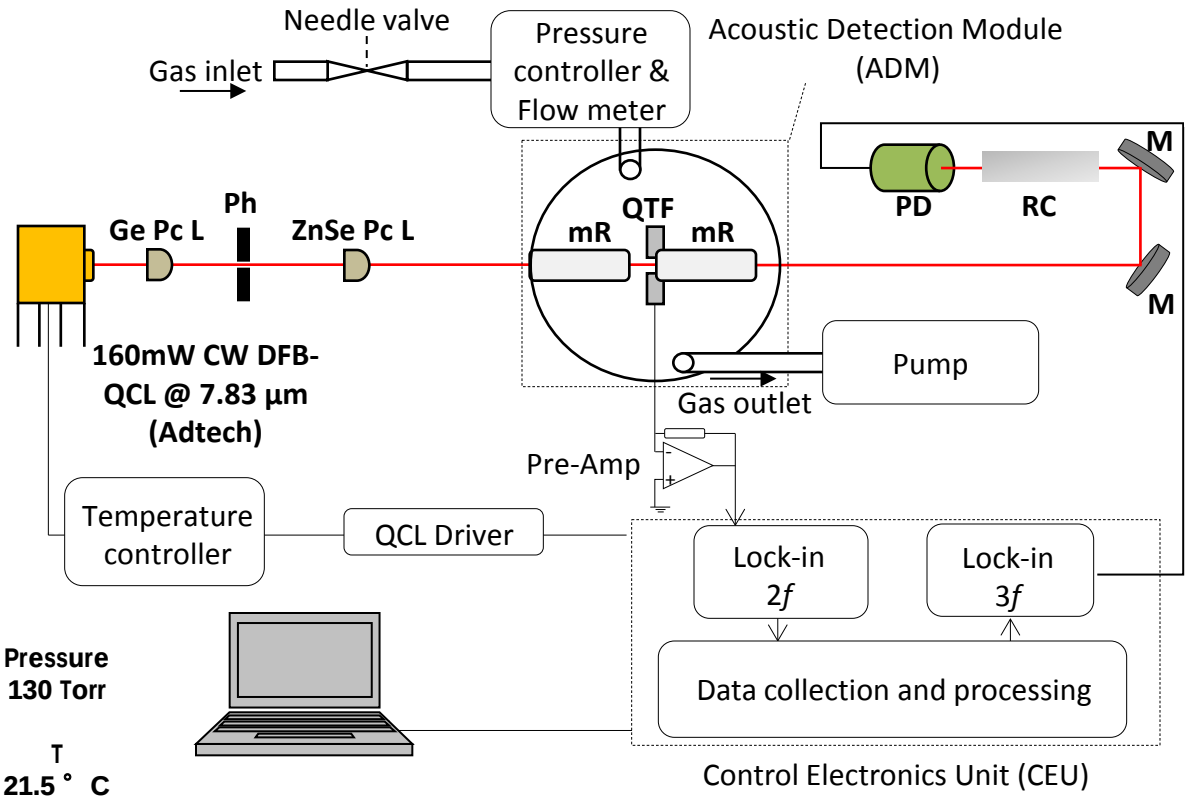

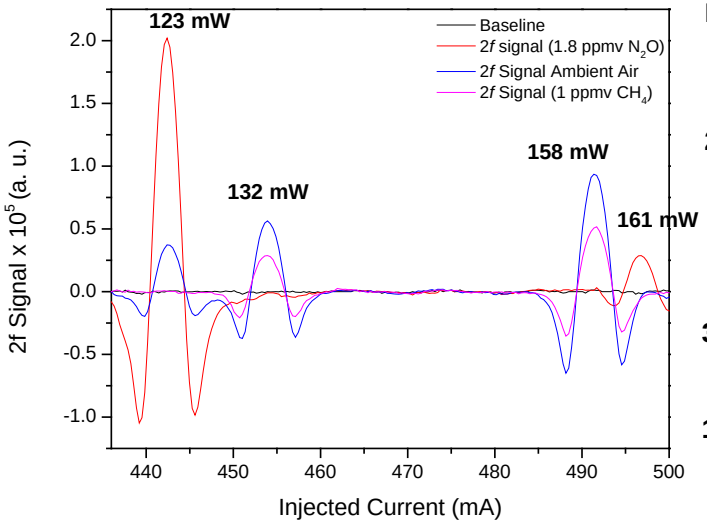

Pressure
130 Torr

T
21.5 ° C

AM
4 mA

f
32760 Hz

f_{mod}
16380 Hz

Detection Limit (1σ) with a **1-sec** averaging time
Methane (CH_4) (1275.04 cm^{-1}) **13 ppbv**
Nitrous Oxide (N_2O) (1275.5 cm^{-1}) **6 ppbv**

Deduced N_2O concentration in the ambient laboratory air: **331 ppbv**

M. Jahjah et al., Analyst, 139, 2063-2069, 2014 & Appl. Lett, 39, 957-960, 2014

RICE

CH_4 Measurements performed with a DFB-QCL based QEPAS Sensor installed in the Aerodyne Mobile Laboratory (Sept 7, 2013)

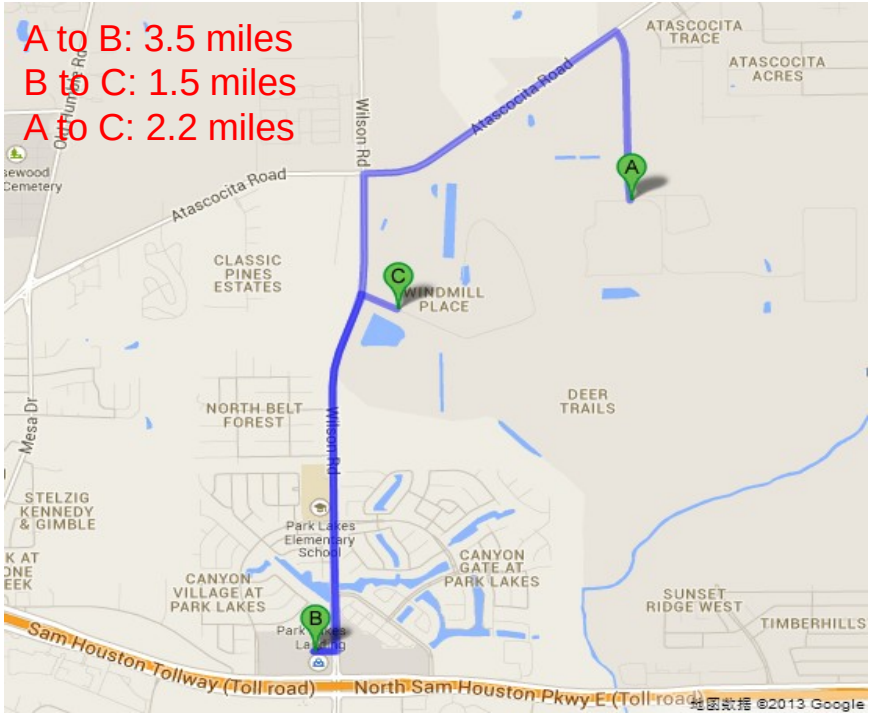

Atascocita Landfill, Humble, TX 77396
CH4 Perimeter Measurements

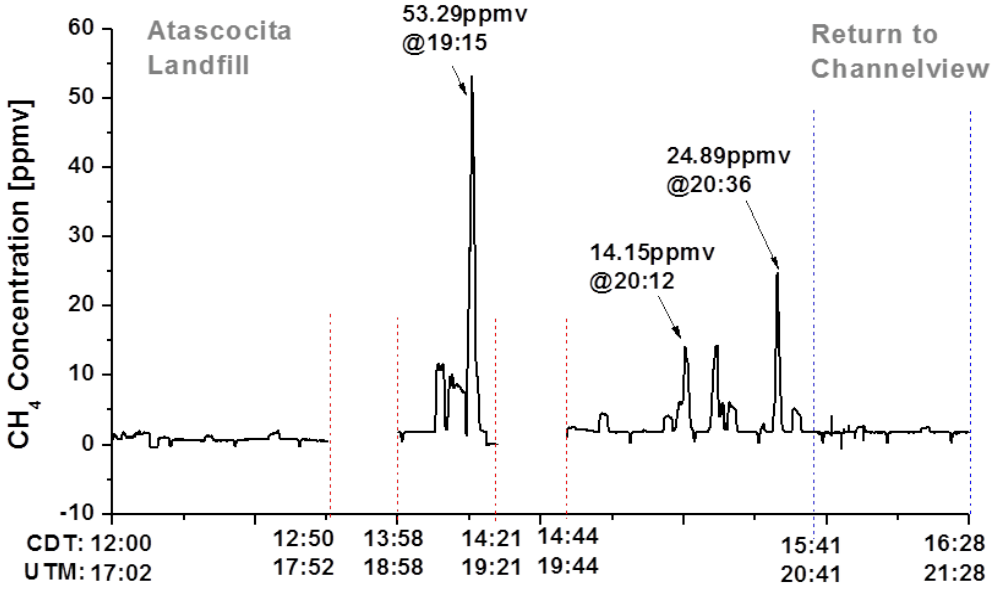

A: 29.9599º North, 95.2334º West
B: 29.9364º North, 95.2508º West
C: 29.9547º North, 95.2462º West (Landfill)

M. Jahjah et. al., Opt. Letters., 39, 957-960, 2014

Comparison of proposed Rice CH_4 Sensor System and current commercially available CH_4 Platforms

Size	Rice	Picarro	ABB-LGR I	ABB-LGR II	Aerodyne
Opt. Path length and method	MIR TDLAS: ~ 9 m	NIR CRDS: >2000m	NIR OA-ICOS: > 1000m	NIR OA-ICOS: > 2000m	MIR TDLAS: 70-100 m
Sensitivity/sec	< 5-10 ppb	1-2 ppb	5 ppb	2 ppb	<1 ppb
Accuracy (drift)	2 ppb stabilized	2 ppb	20 ppb, temp. stabilized	2 ppb	2 ppb
Cell Volume, cc	60	30	500	2000	2000
Pump Size (10 sec flush time)	~ 1 lpm	~ 0.5 lpm	~ 11 lpm	~ 45 lpm	~ 45 lpm
Cavity Mirror Reflectance	98.5%-99%	>99.99%	>99.99%	>99.99%	>99.99%
Power Consumption	2-20 W	200 W	70 W	200 W	400 W
Weight	~ 2-4 kg	~ 20 kg	~ 15 kg	~ 40 kg	~ 40 kg
Cost	~ 20-25K USD	~ 40-50K USD	~ 25K USD	~ 40K USD	~ 100K USD

US Department of Energy Advanced Research Project Agency – Energy (ARPA-E), Methane Observation Networks with Innovative Technology to obtain Reductions (MONITOR)

RICE

Industrial Target Gas: SF_6

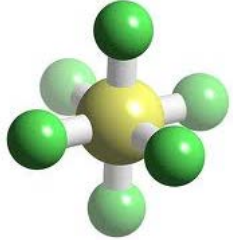

Industrial and semiconductor processes

- In semiconductor manufacturing for plasma etching of metal silicides, nitrides and oxides
- Is an insulating material used as a dielectric in electrical transformers
- SF_6 is a tracer gas for leak detection

Line Selection Criteria for QEPAS:

1. High absorption strength
2. Well resolved spectral absorption features
3. Selected line far from interfering gases such as CO_2 and H_2O

} **Low gas Pressure**

Due to the *fast vibrational-translation relaxation rate* of SF_6, it is possible to work at low pressure (<100 Torr) and take advantage from the typically high quality factor *Q* of the quartz tuning (>20,000) at these conditions

A. Sampaolo et al. SPIE 9755, 97550D-1- 97550D-6 , Quantum Sensing &Nanoelectronics & Photonics XIII, ed M. Razeghi, 2016

Line selection for SF_6

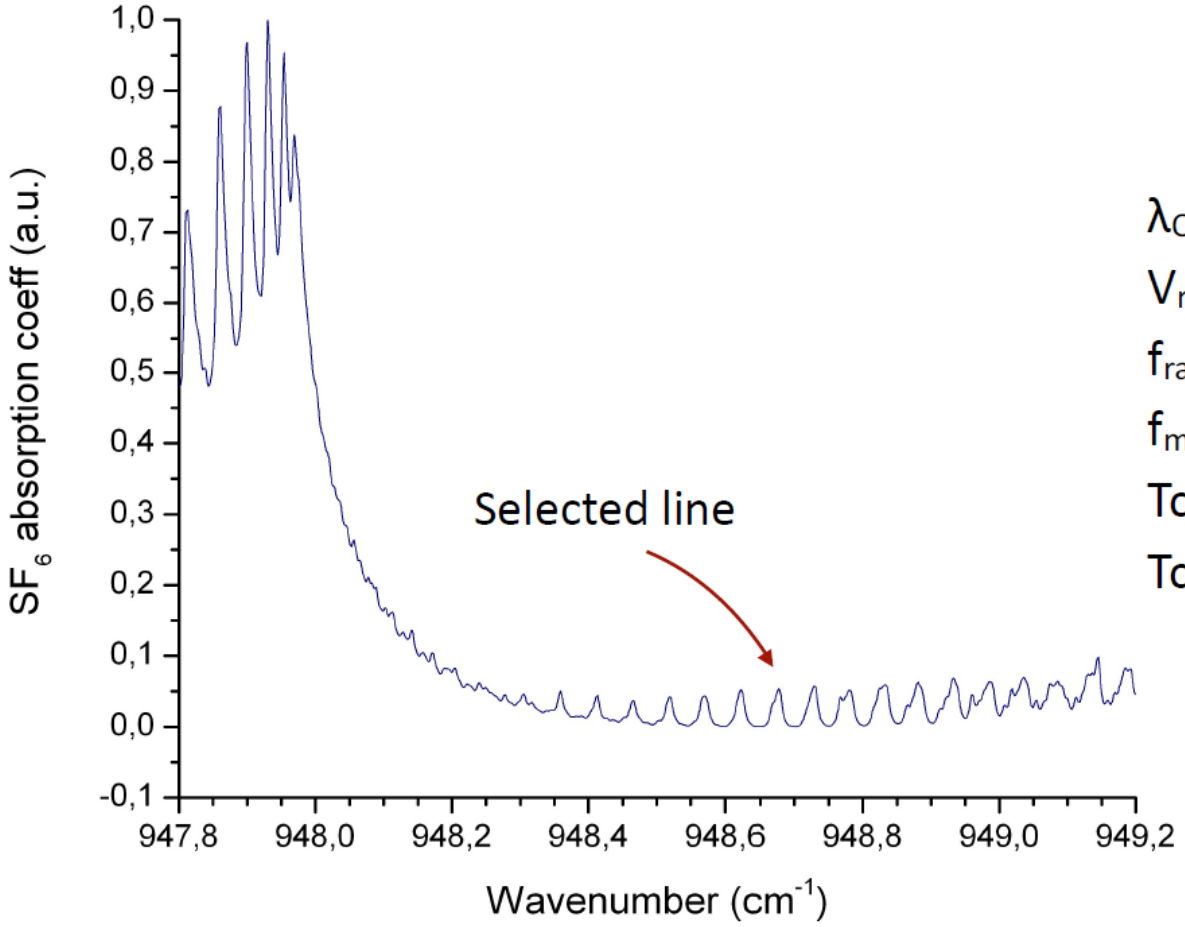

Working Conditions

λ_{QCL} = 948,68 cm^{-1}

V_{ramp} = 26 - 45 V

f_{ramp} = 5 mHz

$f_{modulation}$ = 16,37970 kHz

Tc (lock-in) = 100 ms

Tc (labview) = 300 ms

Selected Line	
Band	Wavelenght (cm^{-1})
ν_3	948.68

Main absorption lines for SF_6 in the range 947cm^{-1}-950cm^{-1} corresponding to the **ν_3 band** (from the HITRAN database).

QEPAS SF_6 Sensor Platform

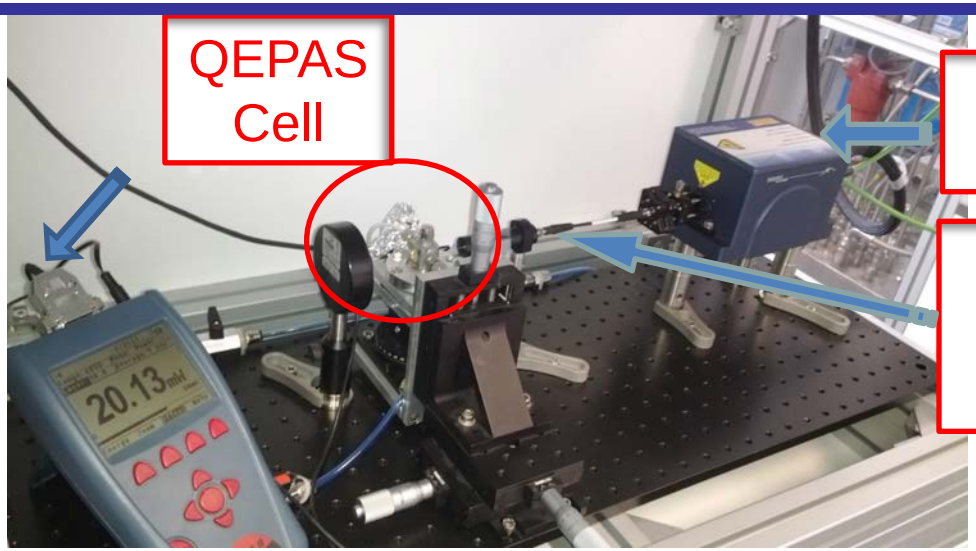

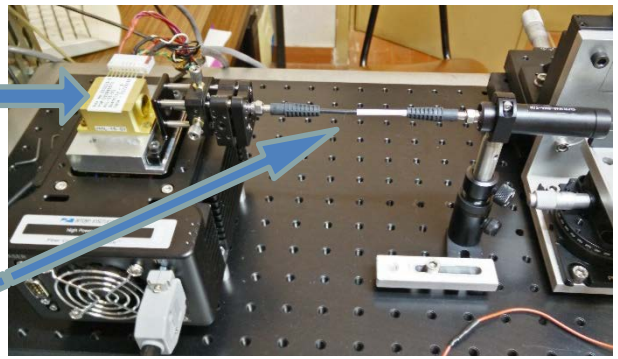

DFB-QCL

- Laser emission @ 10.54µm
- Power: ~ 40 mW
- CW operation @ RT

EC -QCL

- Laser emission 10.15 -10.74 µm
- Power: ~ 25 mW @ 10.54
- CW-MHF operation @ RT

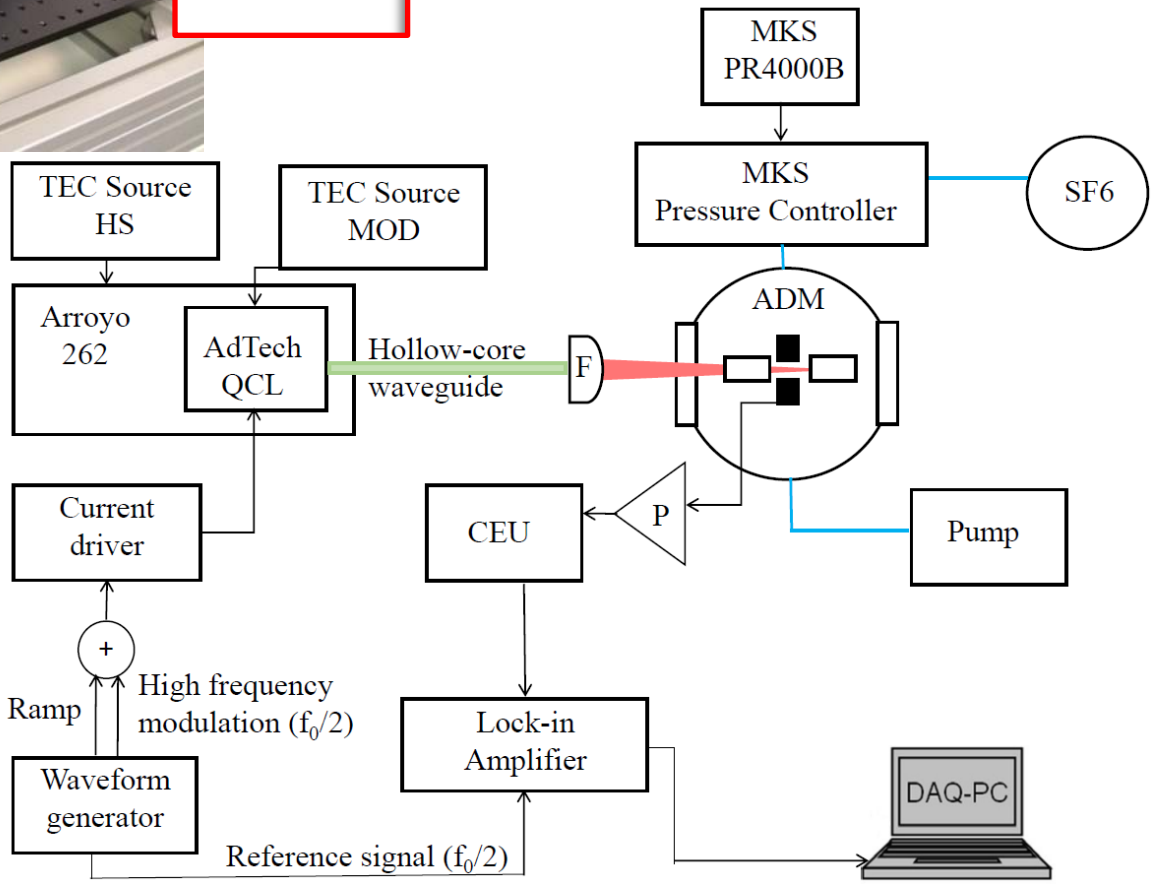

SF_6 QEPAS sensor performance assessment and linearity

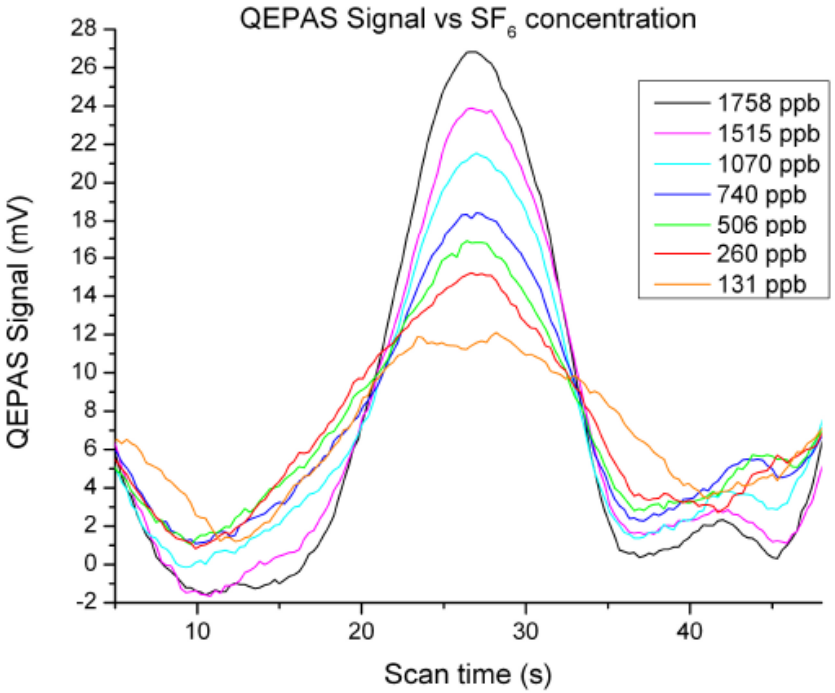

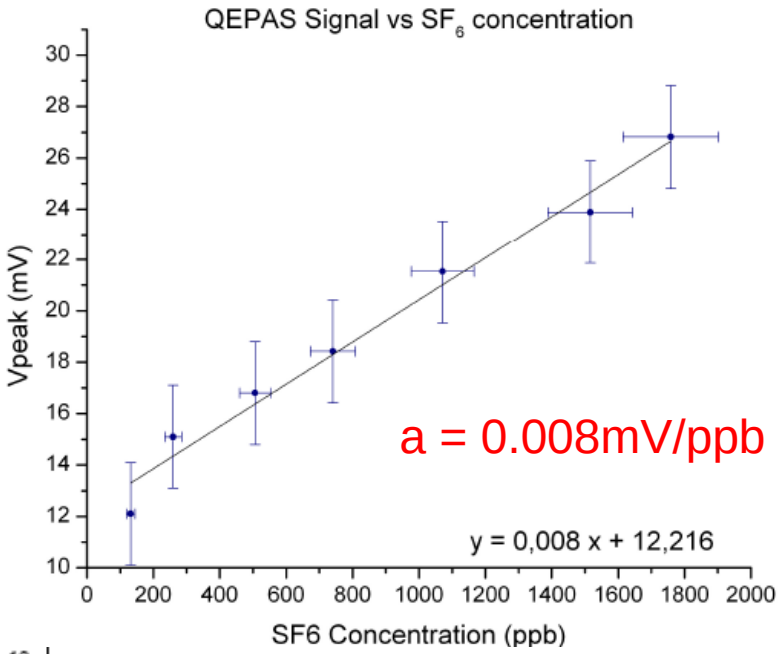

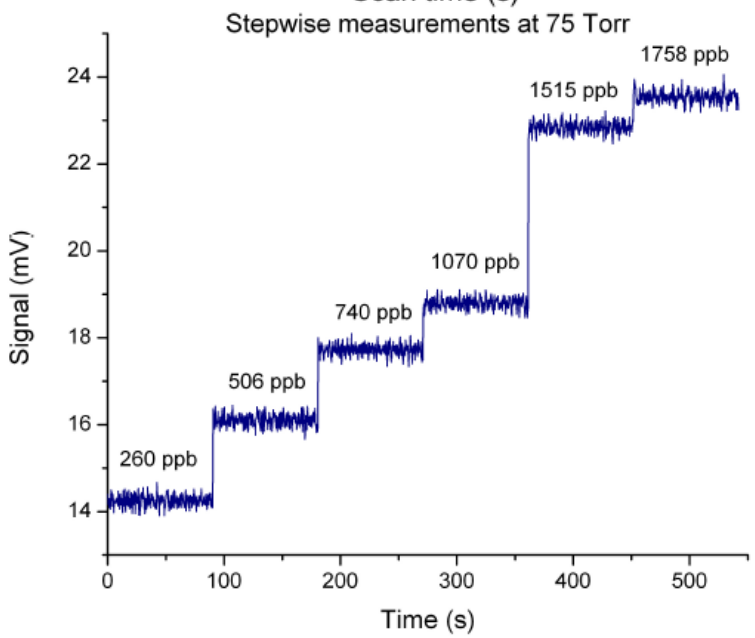

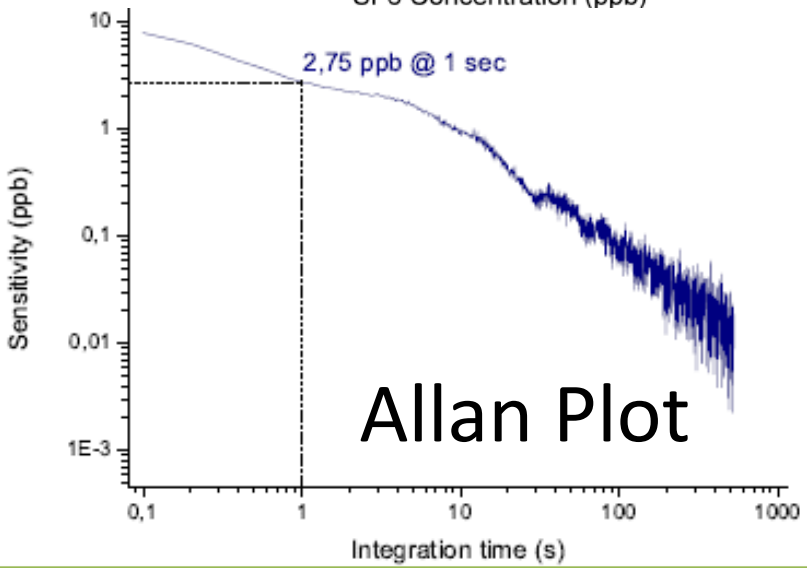

NNEA = 6.7x10^{-11} cm^{-1}W(Hz)$^{-1/2}$

15 cm-long single mode HWG with 200 µm-Core

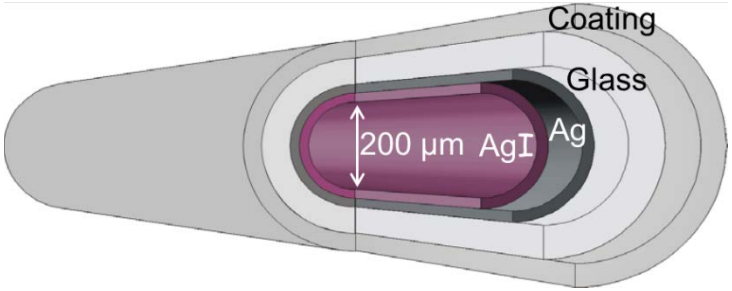

DFB-QCL Laser beam output

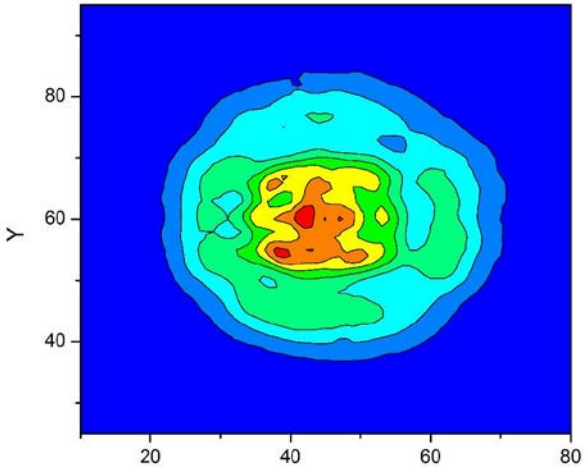

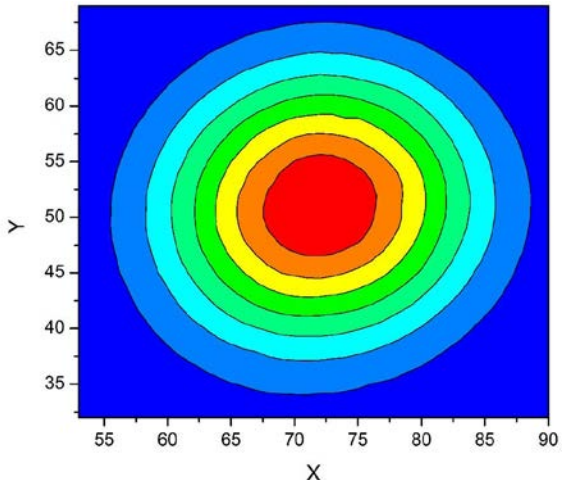

Laser beam exiting the Hollow Waveguide

One-dimensional profile on a log scale measured by a pyroelectric camera at the focusing plane

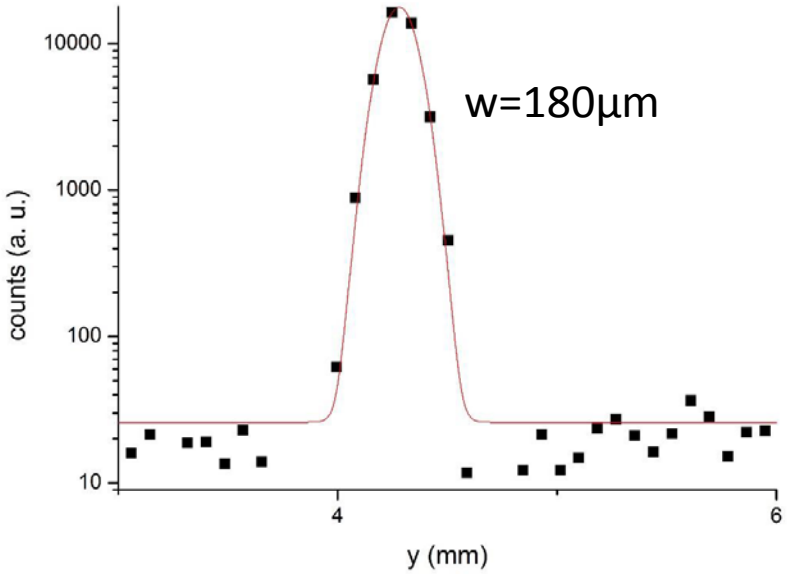

Leak detector platform & performance evaluation

1. A certified gas mixture wase used to calibrate & check SF_6 Sensor
2. SF_6-Sensor system was validated using a certified leak

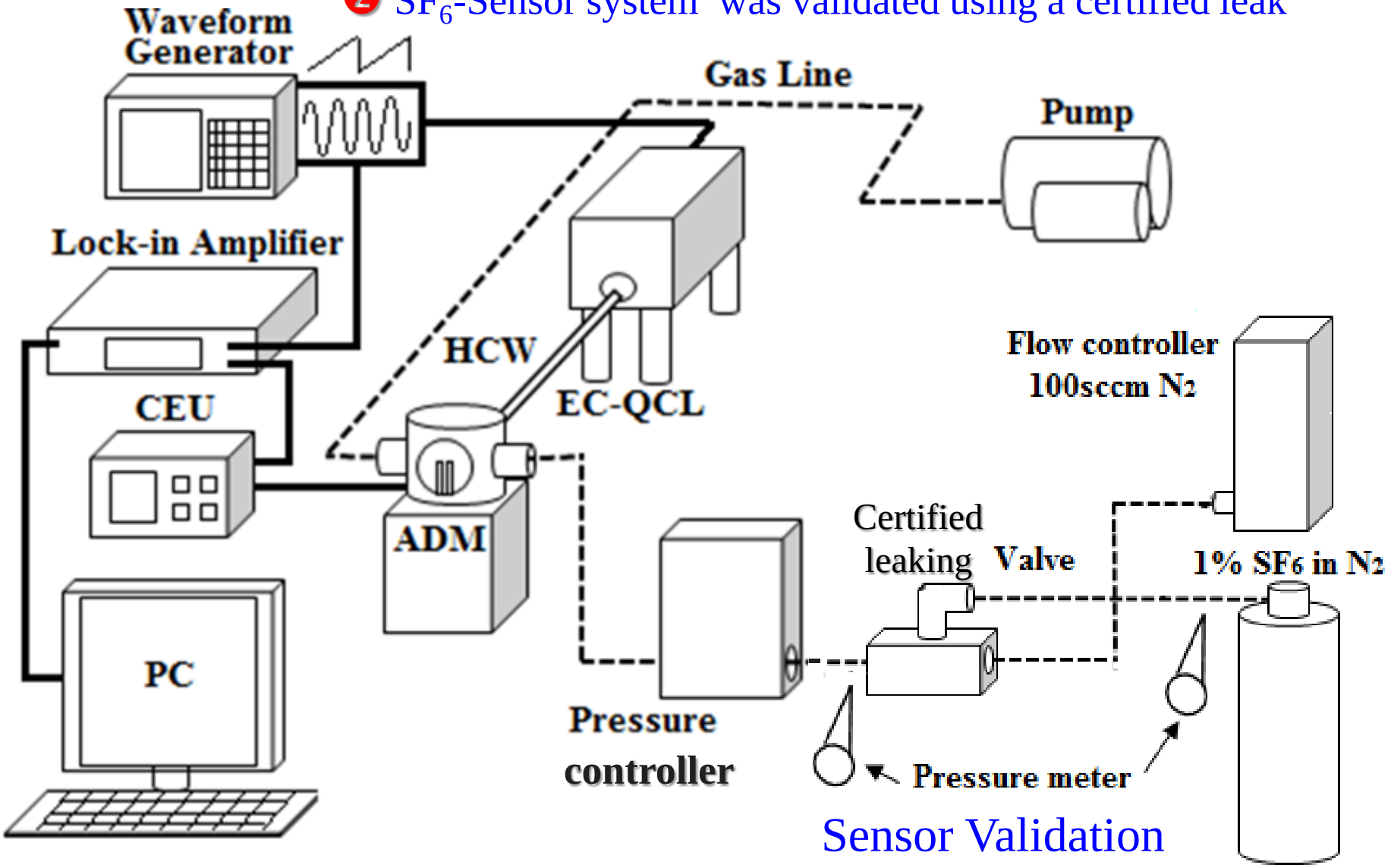

Sensor Validation

Leak detector measurements

❶ Flux N_2 in the ADM ❷ Overpressure 1% SF_6:N_2 mixing at the test valve

❸ Valve leak level was measured by extracting SF_6 concentration

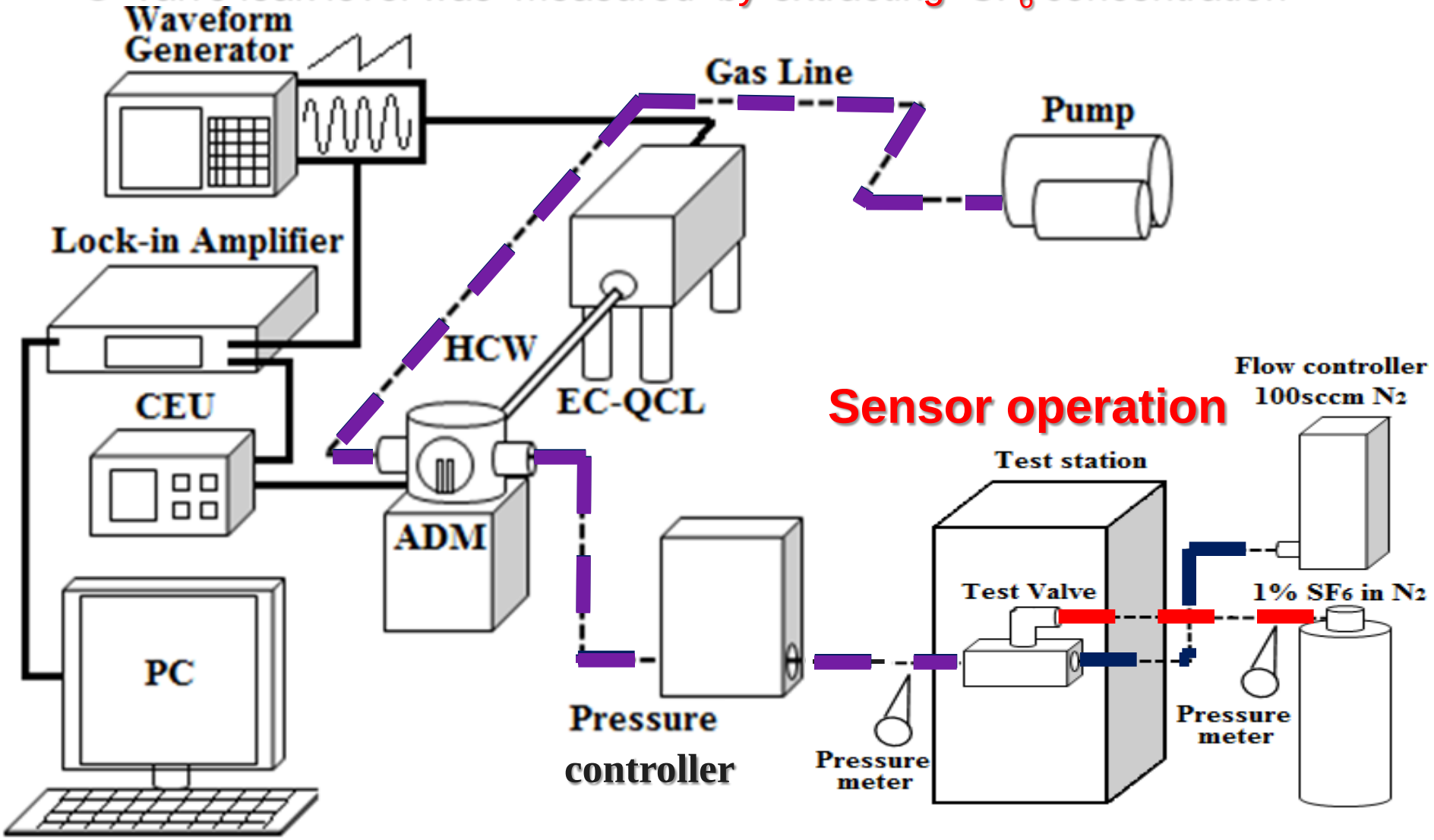

Leak detection Test Station

The leak flow F_L can be calculated by:

$$F_L = \frac{F_C \cdot S}{a \cdot C_{SF_6} - S}$$

F_C is the N_2 gas carrier flow (in sccm)
S is the QEPAS peak signal after background subtraction
C_{SF6} is the SF_6 concentration in N_2 (1% in our test)
a is the sensor linearity slope (8μV/ppb)

Certified Valve Sample

Test chamber

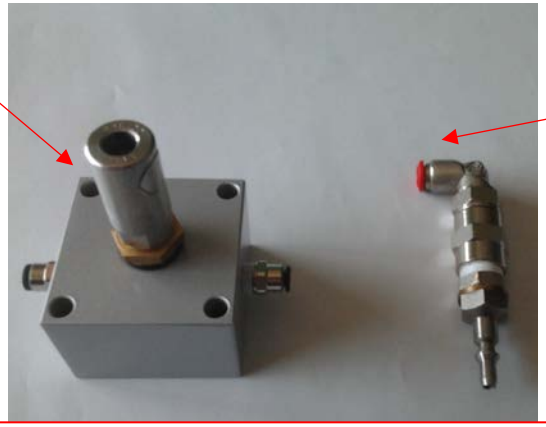

Certified Leak

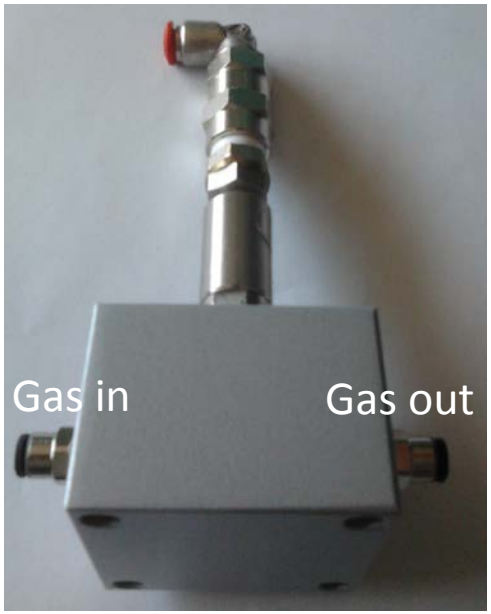

At constant ΔP of 100 kPa

1 std cc/s ⟹ 1 mbar l/s

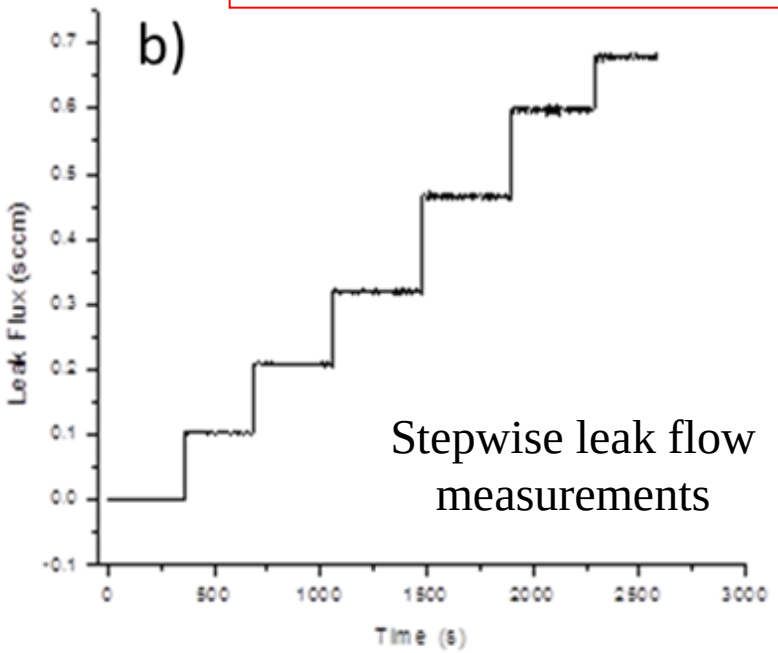

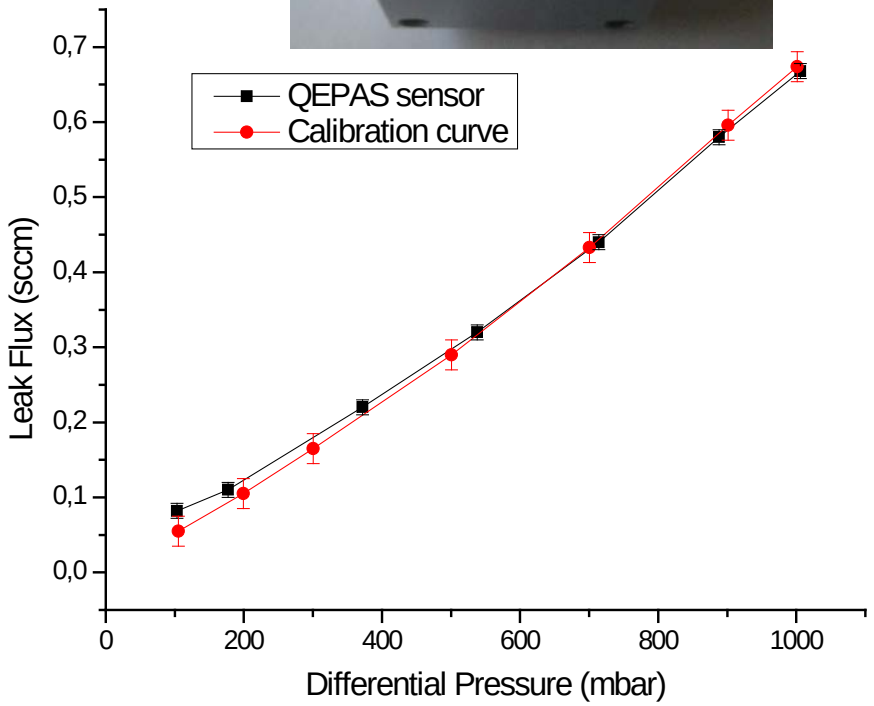

QEPAS spectral scan vs defects

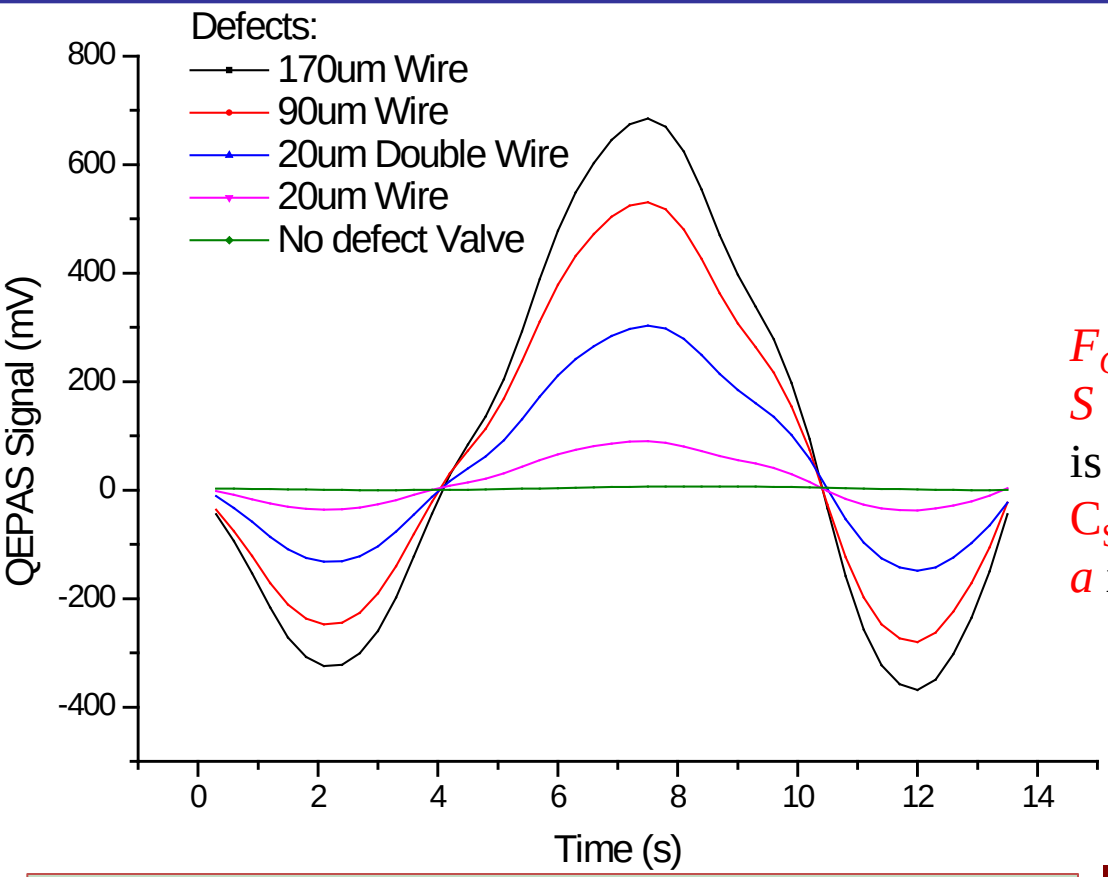

The leak flow F_L can be calculated by:

$$F_L = \frac{F_C \cdot S}{a \cdot C_{SF_6} - S}$$

F_C is the gas carrier flow,
S is the QEPAS peak signal if background is removed
C_{SF6} is the SF_6 concentration in N_2
a is the sensor linearity slope

ΔP between the chamber containing 1% SF_6:N_2 and the chamber filled with pure N_2 fixed at 400 mbar

Starting with a QEPAS sensor minimum detectable concentration of 2.8 ppb for a 1 s integration time and considering a N_2 gas carrier flow of 40 sccm/min, **the minimum detectable leak is ~ 1x10^{-5} sccm/min**, which can be decreased to **~ 1x10^{-7} sccm/min = 1.7x10^{-9} sccm/sec if pure SF_6 is used as as a gas leak tester**.

Valve (*defect*)	QEPAS Signal (V)	Leak Flows (sccm/min)
Valve1 *(unmodified)*	noise	0
Valve2 *(20 μm wire)*	0.09	0.04
Valve3 *(20 μm double-wire)*	0.30	0.18
Valve4 *(90 μm wire)*	0.53	0.26
Valve5 *(170 μm wire)*	0.69	0.34

Chemicals of Interest in Defense & Security Applications

- **Chemical warfare agents**
  - Nerve agents
  - Blister agents
  - Pulmonary agents
  - Blood agents
- **Explosives**
  - TNT, RDX, PETN, RTN
- **High Threat Toxic Industrial Chemicals (TICs)**
  - Formaldehyde, Sulphur dioxide, Hydrogen sulphide Carbon disulphide, Chlorine, Ethylene oxide, Fluorine, Hydrogen bromide, Hydrogen chloride, Hydrogen cyanide, Hydrogen fluoride, Nitrogen dioxide, Phosgene and Ammonia
- **CWA and TIC monitoring platforms**
  - Naval vessels in particular submarines
  - Aircraft and drones
  - Exposure to combat personnel in battle field
  - Ultra-low power chemical analysis system for remote site detection (DOD IARPA-MAEGLIN)

RICE

QEPAS Performance for Trace Gas Species (May 2016)

	Molecule (Host)	Frequency, cm^{-1}	Pressure, Torr	NNEA, $cm^{-1}W/Hz^{1/2}$	Power, mW	NEC (τ=1s), ppbv
VIS	O_3 (air)	35087.70	700	3.0×10^{-8}	0.8	1,270
	O_2 (N_2)	13099.30	158	4.74×10^{-7}	1228	13,000
NIR	C_2H_2 (N_2)*	6523.88	720	4.1×10^{-9}	57	30
	NH_3 (N_2)*	6528.76	575	3.1×10^{-9}	60	60
	C_2H_4 (N_2)*	6177.07	715	5.4×10^{-9}	15	1,700
	CH_4 (N_2+1.2% H_2O)*	6057.09	760	3.7×10^{-9}	16	240
	N_2H_4	6470.00	700	4.1×10^{-9}	16	1,000
	H_2S (N_2)*	6357.63	780	5.6×10^{-9}	45	5,000
	HCl (N_2 dry)	5739.26	760	5.2×10^{-8}	15	700
	CO_2 (N_2+1.5% H2O) *	4991.26	50	1.4×10^{-8}	4.4	18,000
Mid-IR	C_2H_6	2976.8	200	4.2×10^{-8}	1.8	.74
	CH_2O (N_2:75% RH)*	2804.90	75	8.7×10^{-9}	7.2	120
	CO (N_2 +2.2% H_2O)	2176.28	100	1.4×10^{-7}	71	2
	CO (propylene)	2196.66	50	7.4×10^{-8}	6.5	140
	N_2O (air+5%SF_6)	2195.63	50	1.5×10^{-8}	19	7
	C_2H_5OH (N_2)**	1934.2	770	2.2×10^{-7}	10	90,000
	NO (N_2+H_2O)	1900.07	250	7.5×10^{-9}	100	3
	H_2O_2	1295.6	150	4.6×10^{-9}	100	12
	C_2HF_5 (N_2)***	1208.62	770	7.8×10^{-9}	6.6	9
	NH_3 (N_2)*	1046.39	110	1.6×10^{-8}	20	6
	SF_6	948.62	75	2.7×10^{-10}	18	0.05 (50 ppt)

** - Improved microresonator and double optical pass through ADM

*** - With amplitude modulation and metal microresonator

NNEA – normalized noise equivalent absorption coefficient.

NEC – noise equivalent concentration for available laser power and τ=1s time constant, 18 dB/oct filter slope.

RICE

For comparison: conventional PAS 2.2 $\times10^{-9}$ $cm^{-1}W/\sqrt{Hz}$ for NH_3

Development of a novel I-QEPAS based Sensor Design:

Performance Evaluation of I-QEPAS based on CO_2 Detection

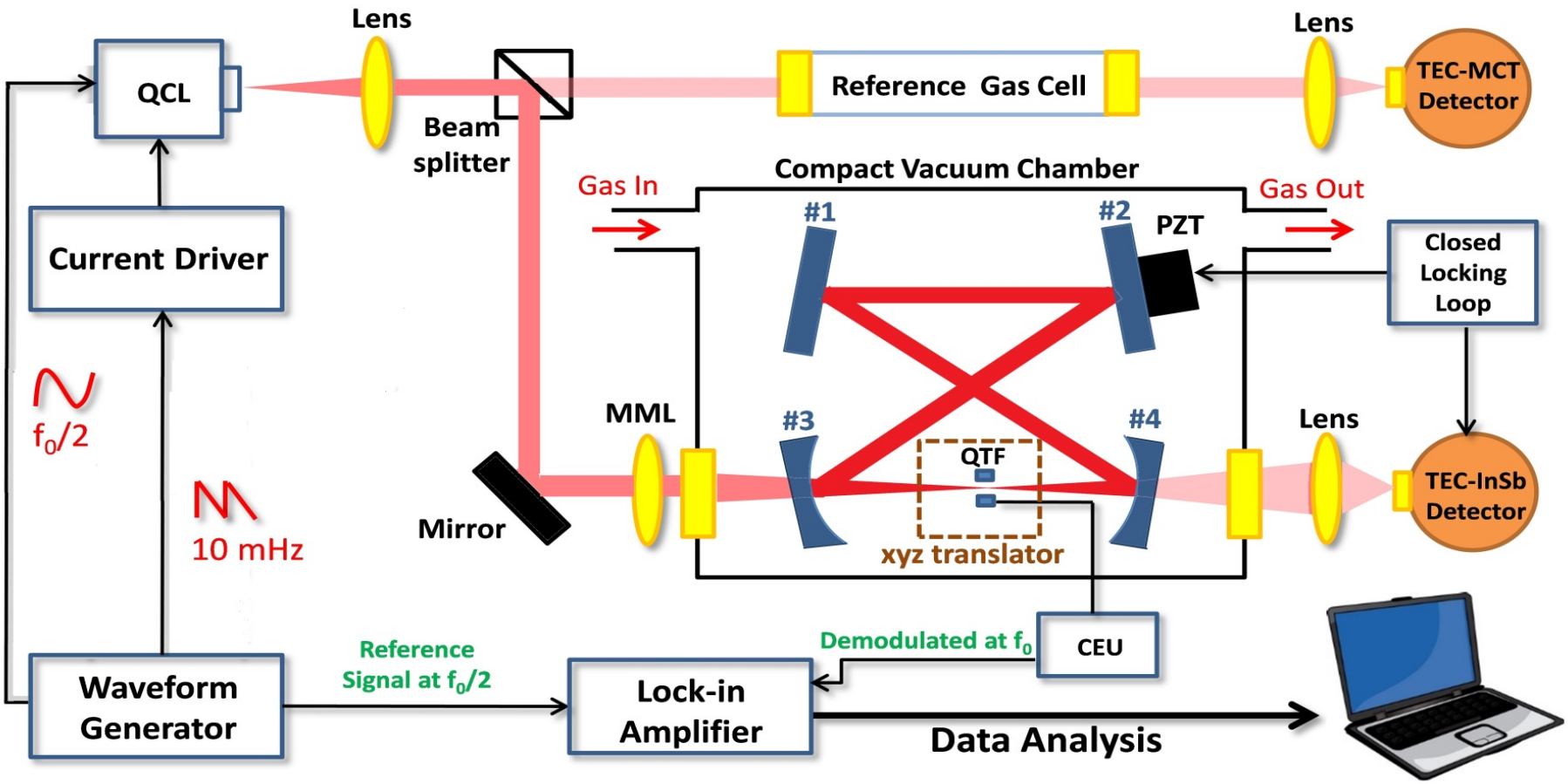

- **Bow-tie cavity consisting of 4 high reflectivity mirrors, R=99.9%**
- **Electronic Control Loop + PZT driver for locking of the cavity resonant frequency to QCL frequency**

P. Patimisco, G. Scamarcio, F.K. Tittel & V. Spagnolo, "Quartz-enhanced photoacoustic spectroscopy: a review", Sensors, 14, 6165-6206 (2014)

Optical properties of a bow-tie cavity

Cavity response:

- Voltage ramp + **modulation dither** applied to QCL
- under vacuum
- locking loop **ON**

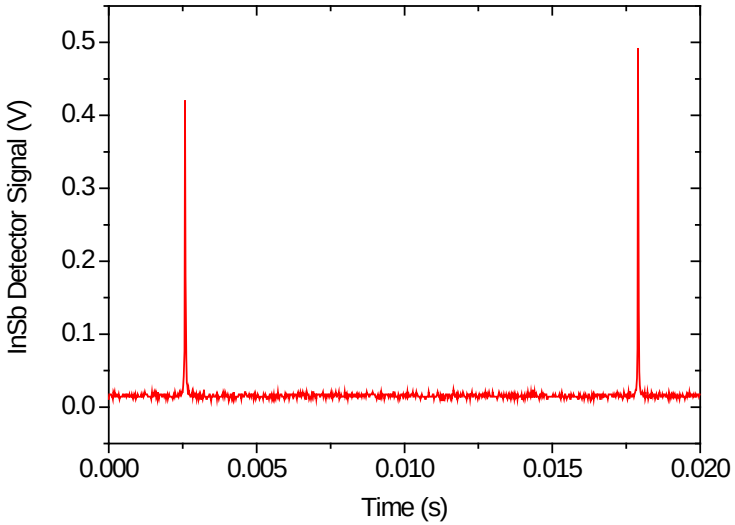

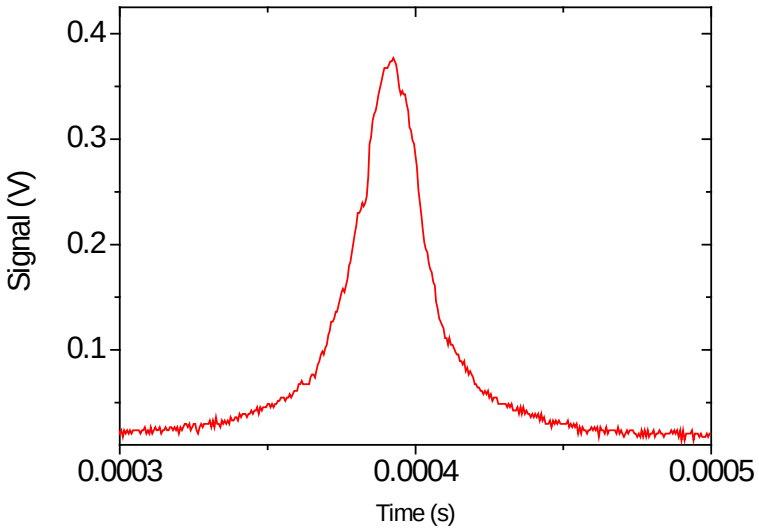

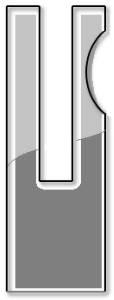

Cavity length L = 174mm

FSR = c/L = 1.725 GHz

Δν(FWHM)= 1.15 MHz

F = FSR/ Δν = 1505

G = F/π= 480

Mode matching 50%

Intracavity optical power enhancement factor = 240

Optical properties of the bow-tie cavity

Cavity response:

- Voltage ramp + **modulation dither** applied to QCL
- under vacuum
- locking loop **ON**

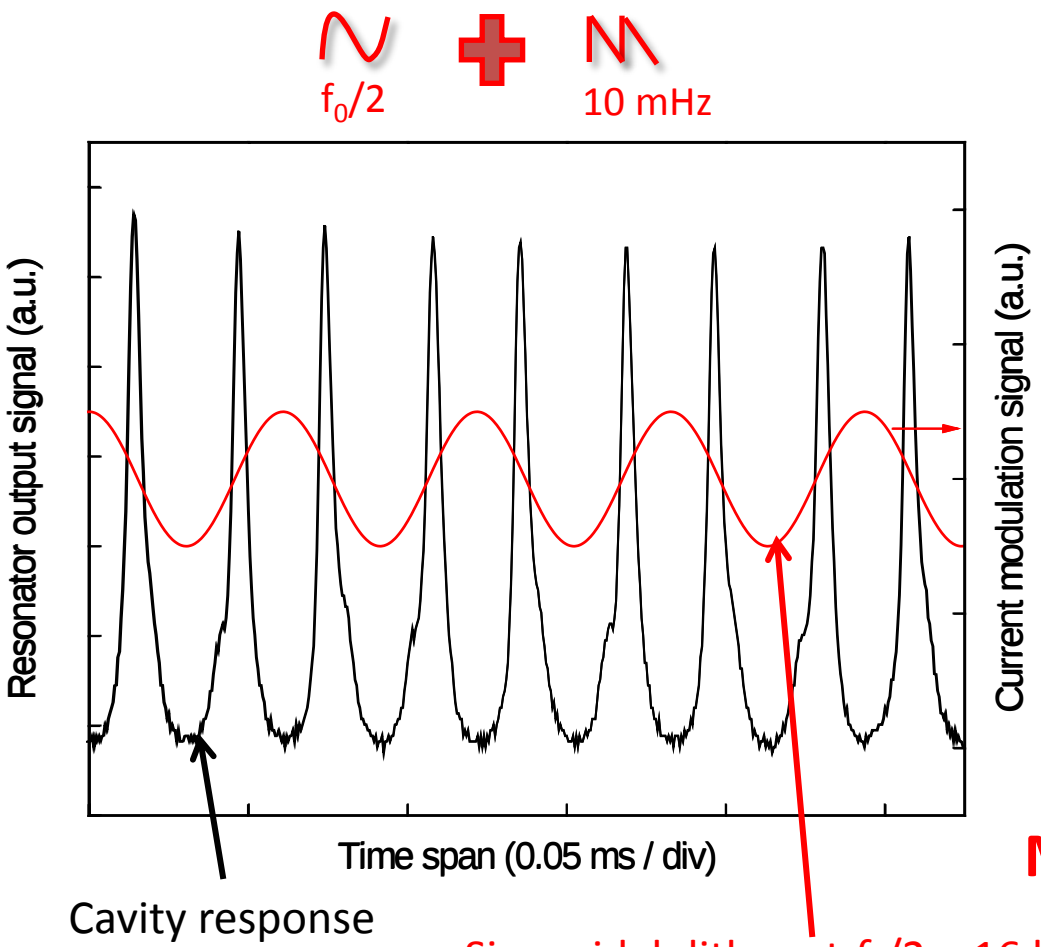

- The close-locked loop acts on the PZT tuning the cavity length
- It was not fast enough to follow the fast dither at $f_0/2$ = 16 kHz
- It maintains the optical cavity resonant with the laser frequency at the center of the fast dither

Mechanical chopper at f_0

I-QEPAS CO_2 Performance in locked Mode & long term Frequency Stability

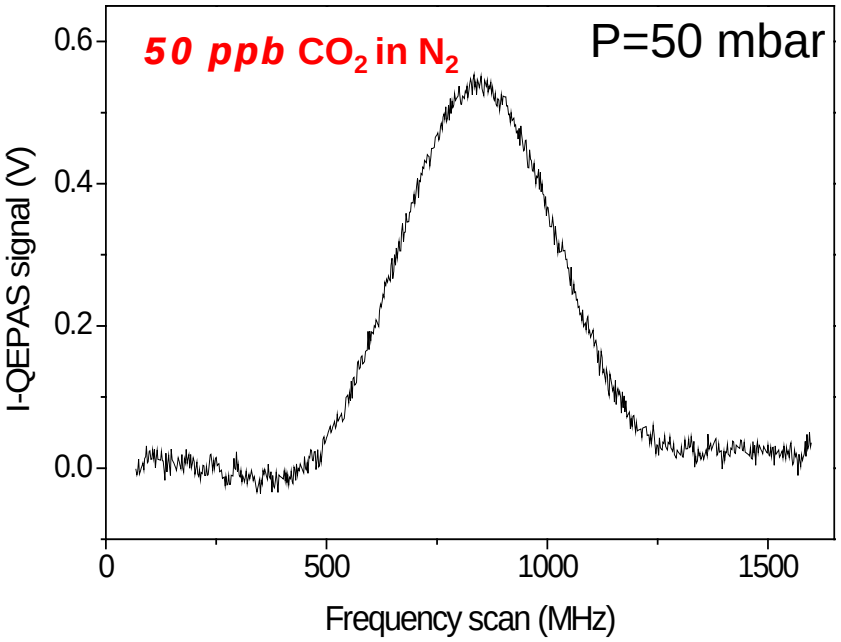

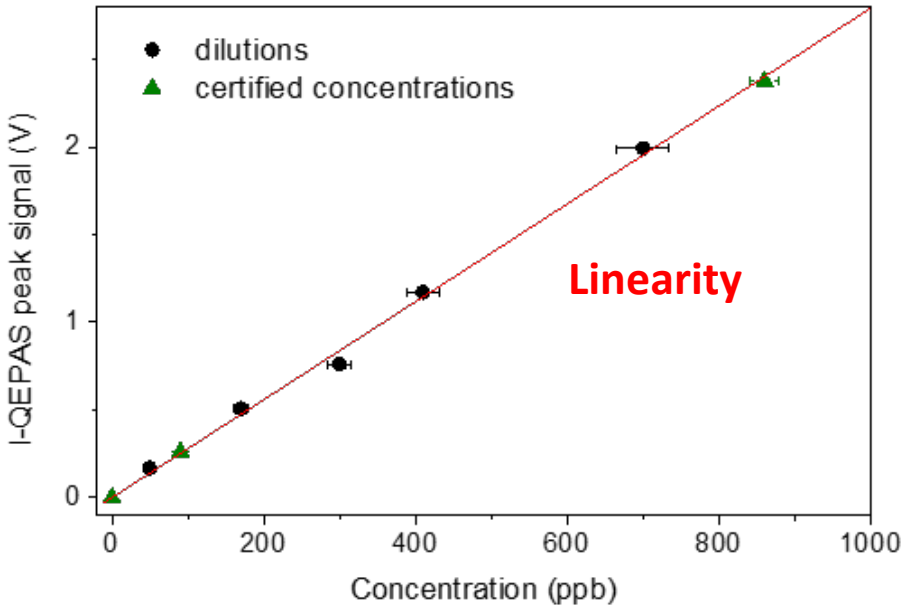

NEC = 300 ppt @ 20sec integration time
(4sec lock-in time constant)

NNEA = 3.2×10^{-10} $cm^{-1}W(Hz)^{-1/2}$

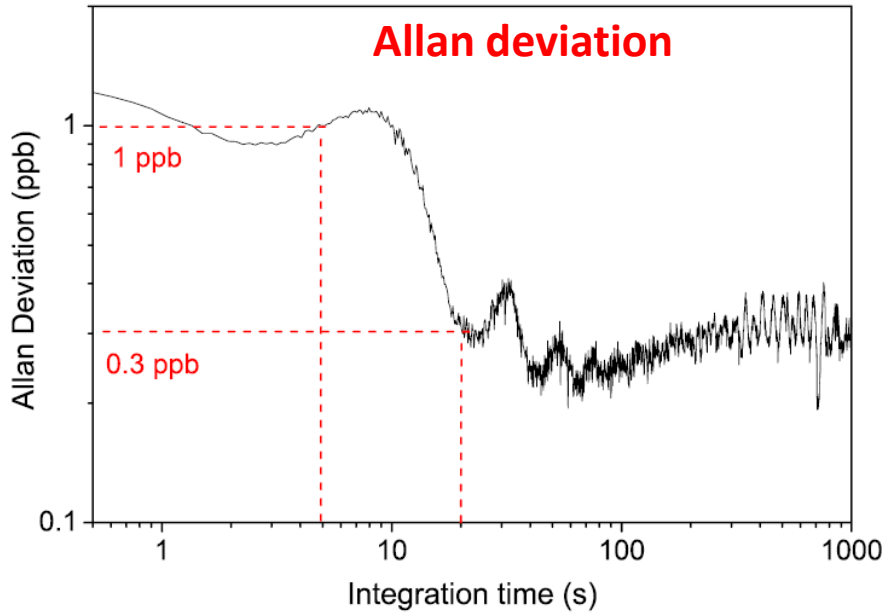

I-QEPAS results in an intracavity optical power enhancement factor of 240

S. Borri et al., Applied Physics Letters, 104, 091114 (2014)

Further Development of a novel I-QEPAS based Sensor Design

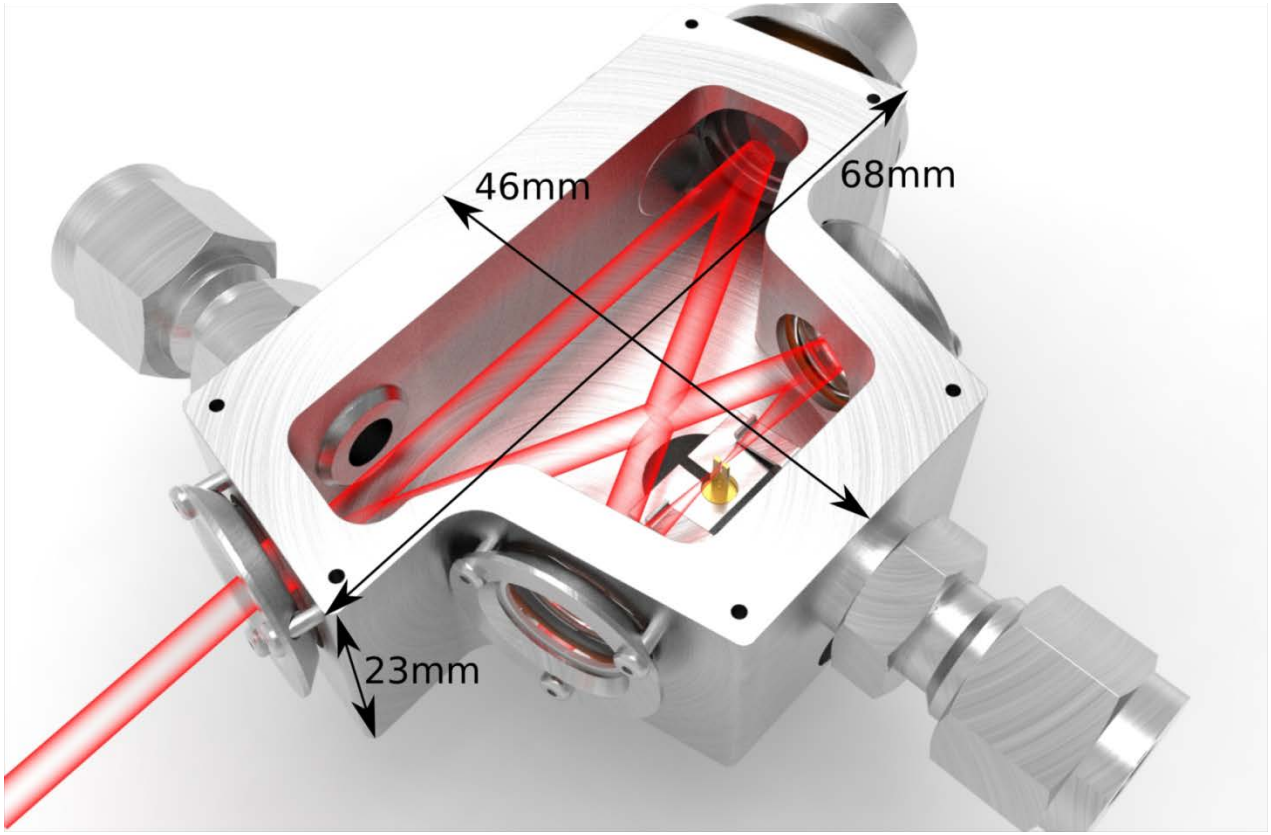

Computer Visuaization of an Intra-Cavity Quartz Enhanced Photoacoustic Spectroscopy Optical Resonator

Bow-tie cavity resonator consists of 4 high reflectivity mirrors, R=99.9%

Electronic Control Loop + PZT driver for locking of the cavity resonant frequency to the frequency of the frequency Laser excitation source

Comparison of I-QEPAS with Other Trace Gas Sensing Techniques

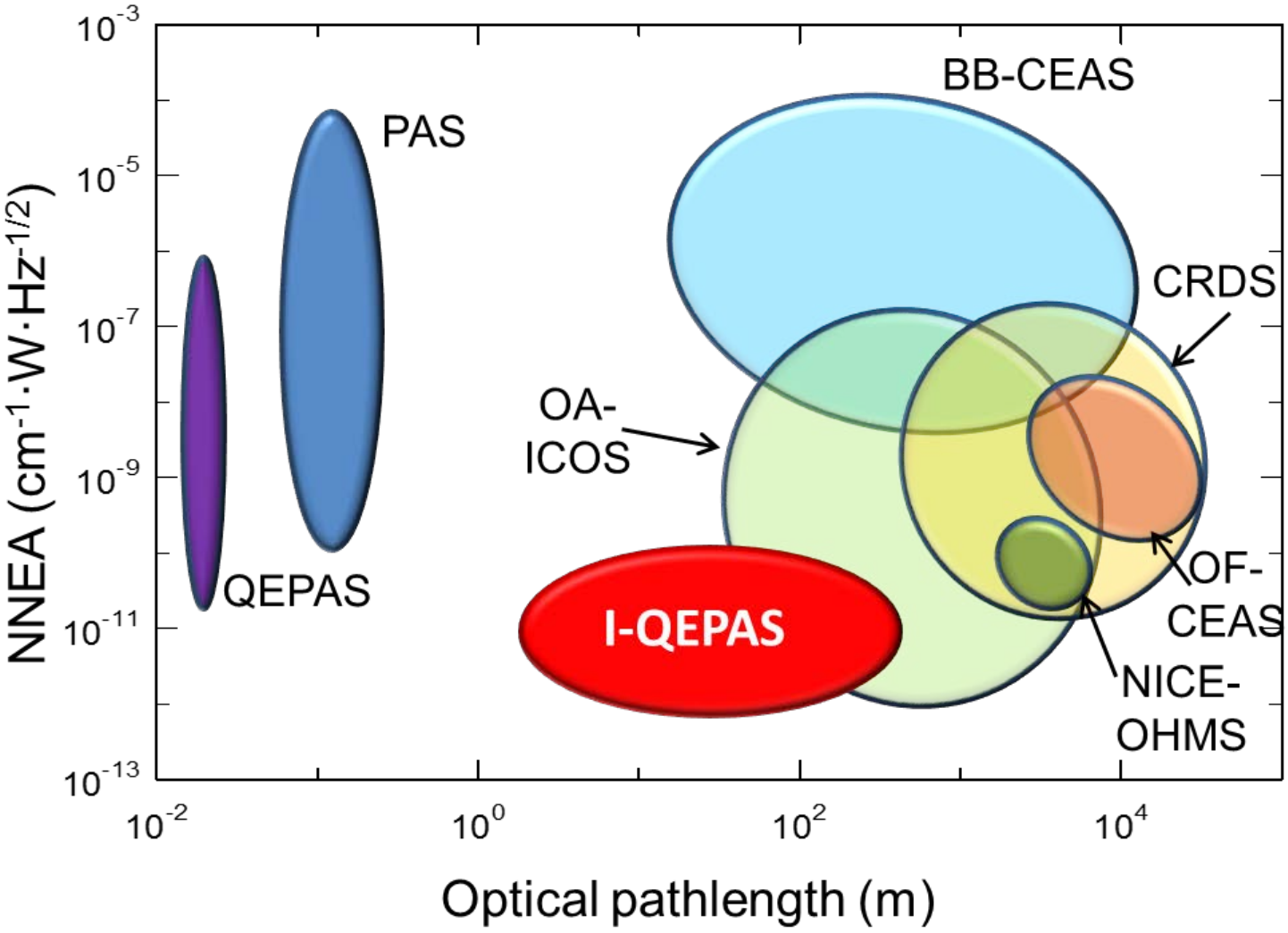

P. Patimisco, G. Scamarcio, F.K. Tittel & V. Spagnolo, "Quartz-enhanced photoacoustic spectroscopy: a review", Sensors, 14, 6165-6206 (2014)

Photograph of a PMMA microwire modified QTF taken with an optical microscope.

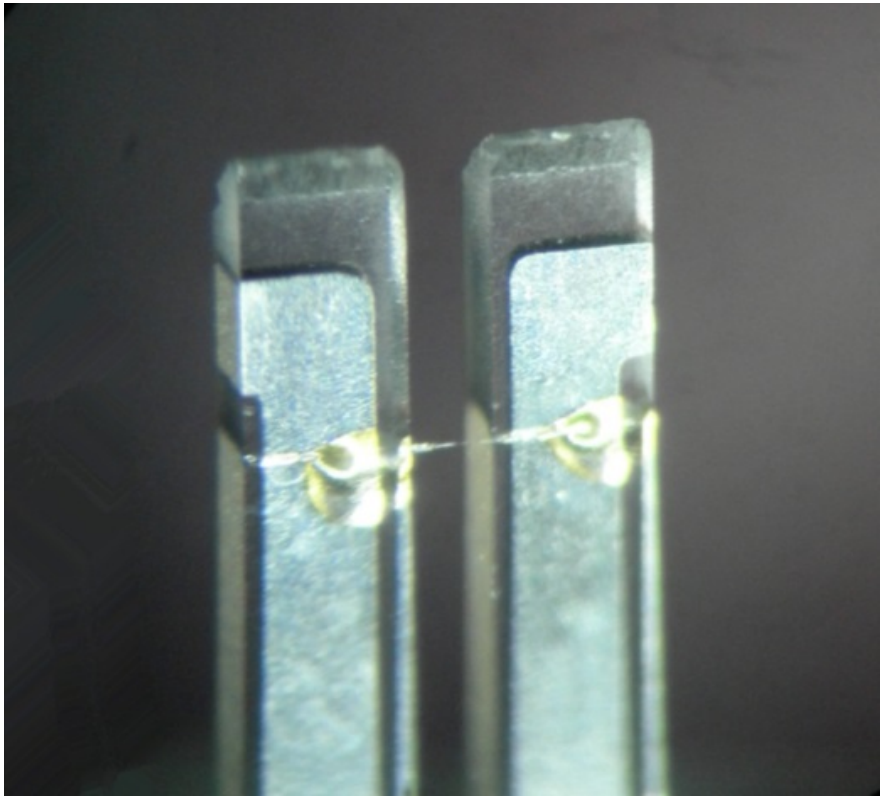

H. Zheng, X. Yin, G. Zhang, L. Dong, H. Wu, X. Yui, W. Ma, L. Zhang, W. Yin, L. Xiao, S. Jia, F. K. Tittel; Quartz-enhanced conductance spectroscopy for nanomechanical analysis of polymer wire"; APL 107, 221903, 2015

Schematic of the experimental setup

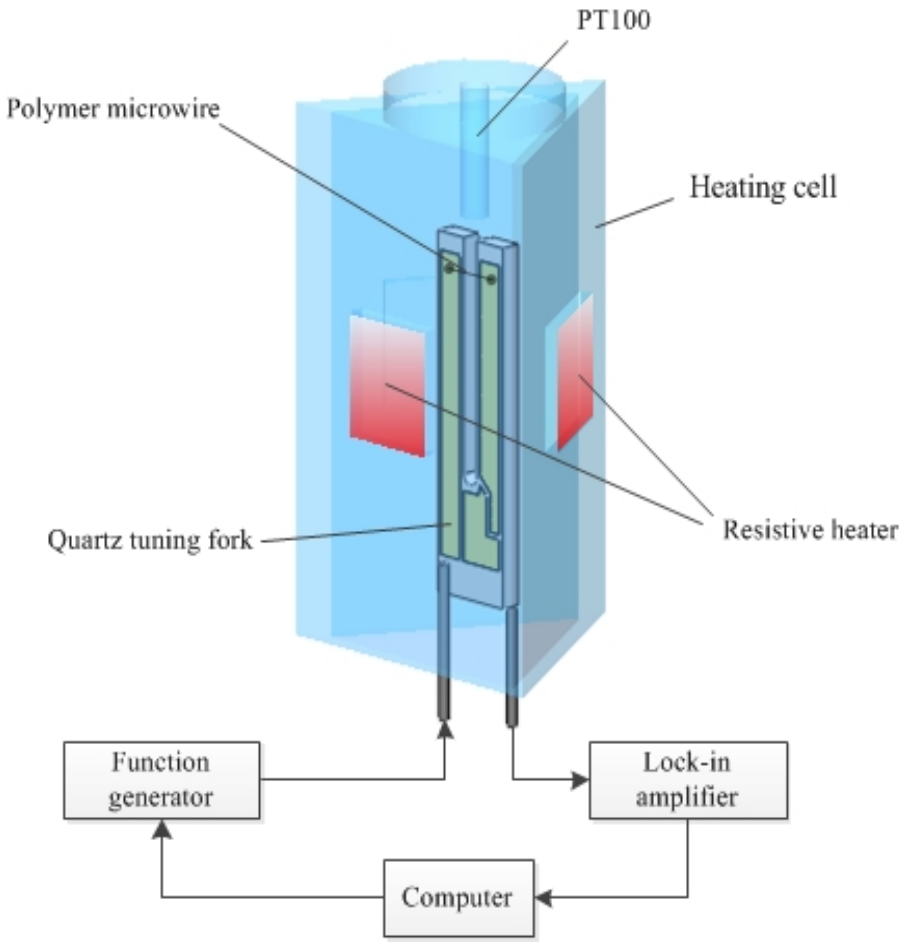

Conductance spectra of a QTF before (black) and after (red) modification by the PMMA microwire

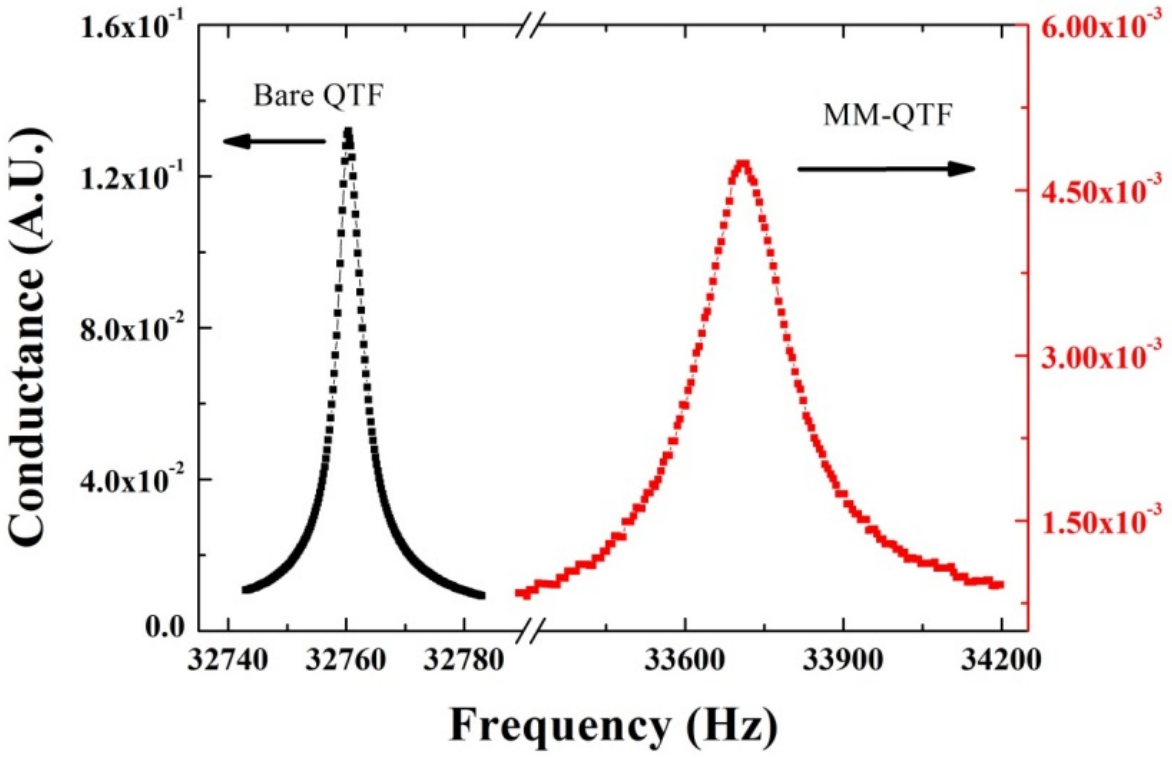

Resonance frequency variations of a PMMA microwire modified QTF as a function of temperature. The figure inset shows the resonance frequency variations of an unmodified QTF

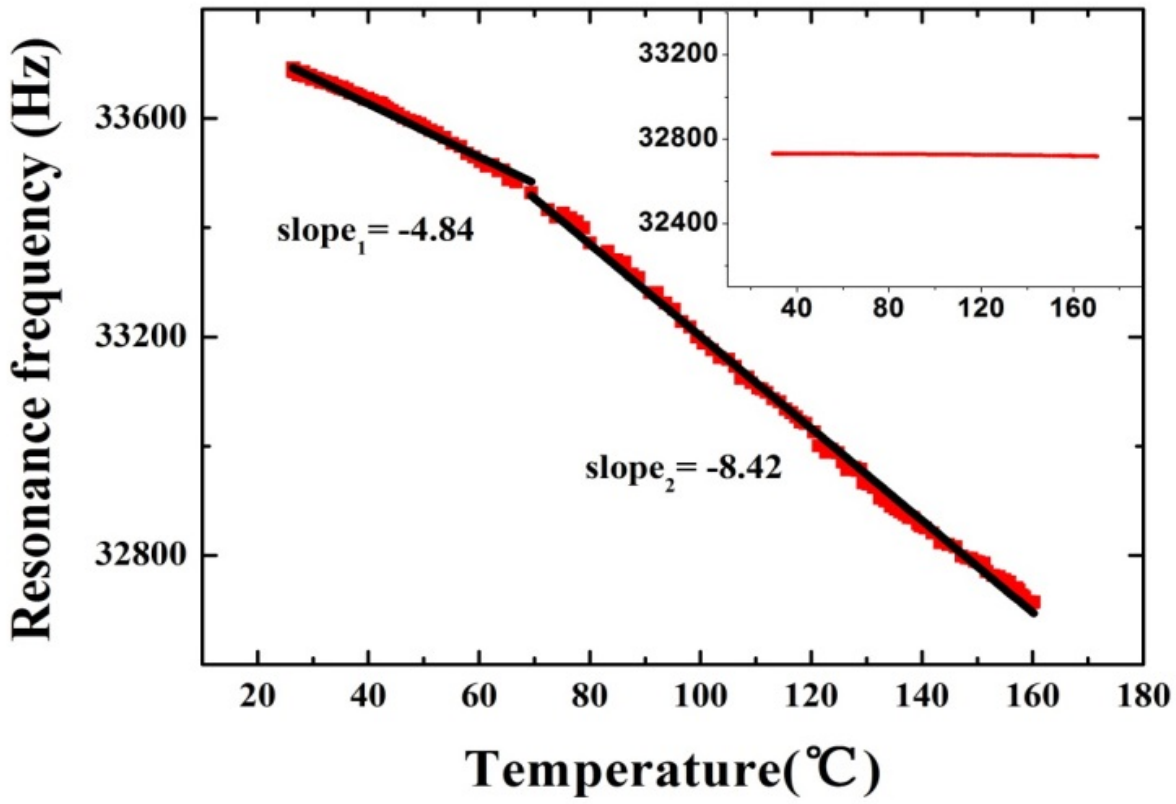

Q factor variations of a PMMA microwire modified QTF as a function of temperature. The inset shows the Q factor variations of an unmodified QTF

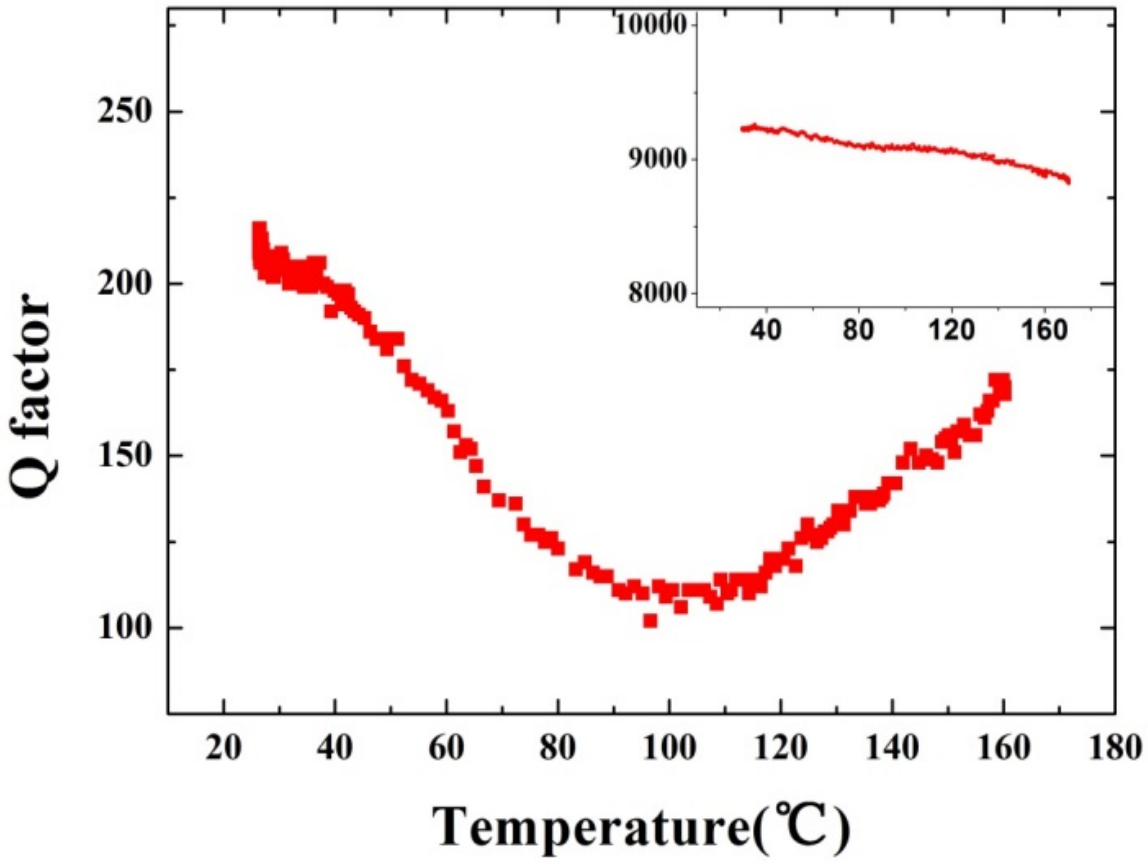

(a) (b) and (c) corresponds to resonance frequency, Q factors, and loss modulus variations of a PMMA microwire modified QTF as a function of temperature in the heating and cooling process (d) loss modulus variations as a function of time.

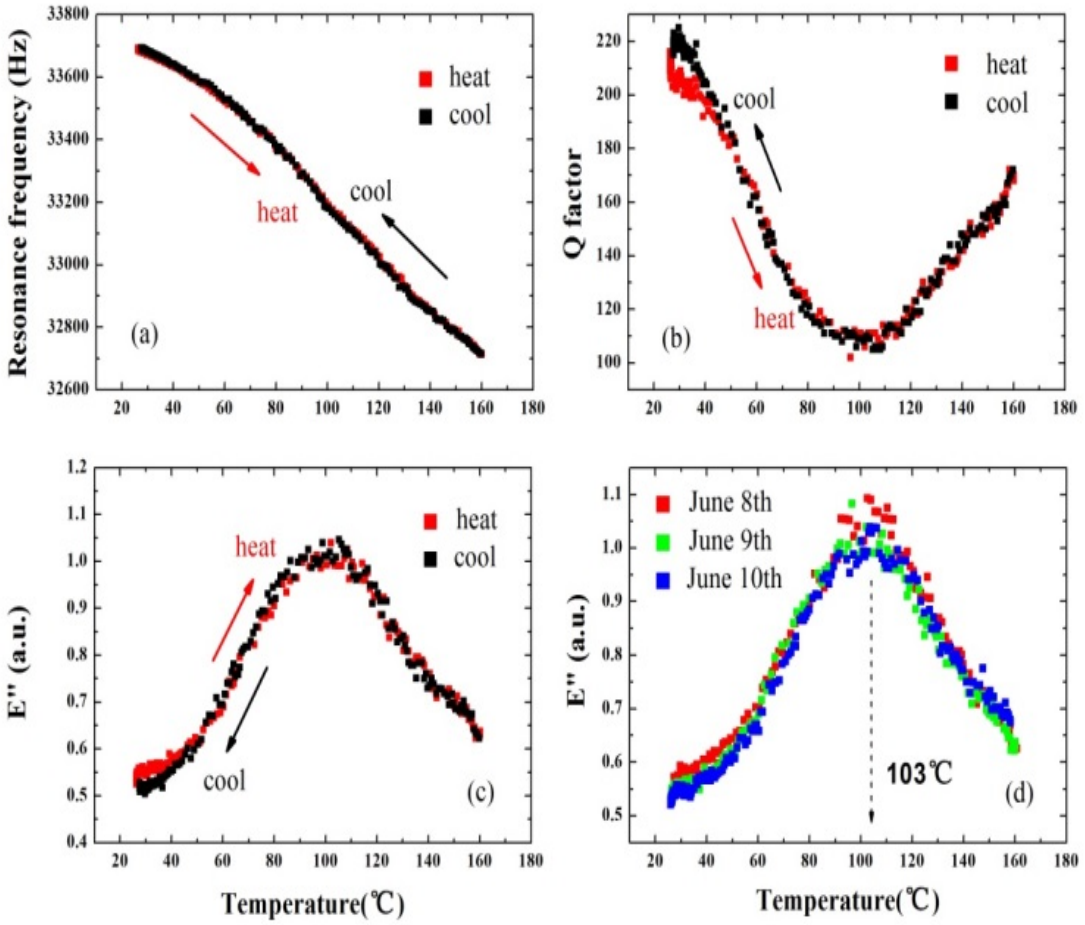

Why have QEPAS sensors not been developed in the THz spectral range so far?

Standard QTFs have a very small volume ($\sim 0.3 \times 0.3 \times 3\ mm^3$)

In QEPAS sensor systems , it is critical to avoid laser illumination of the QTF, since the radiation blocked by the QTF prongs results in an undesirable non-zero background as well as a shifting fringe-like interference pattern.

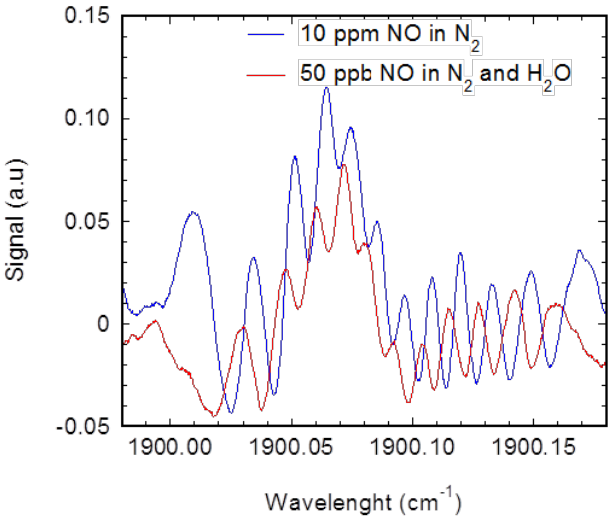

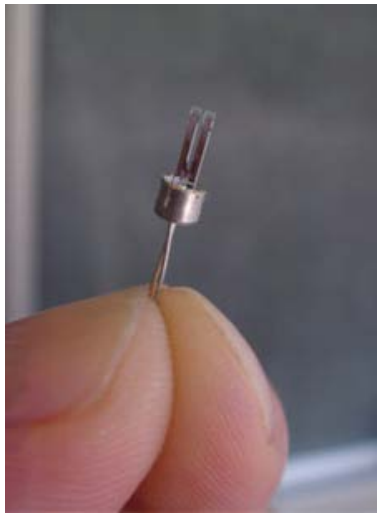

Standard QTF

The standard QTF prong separation of 330 µm is comparable with the THz wavelength which prevents the use of a QEPAS sensor architecture in the THz range unless we use large sized QTFs .

Custom fabricated QTFs with new Shapes and Dimensions optimized for mid-IR and THz QEPAS

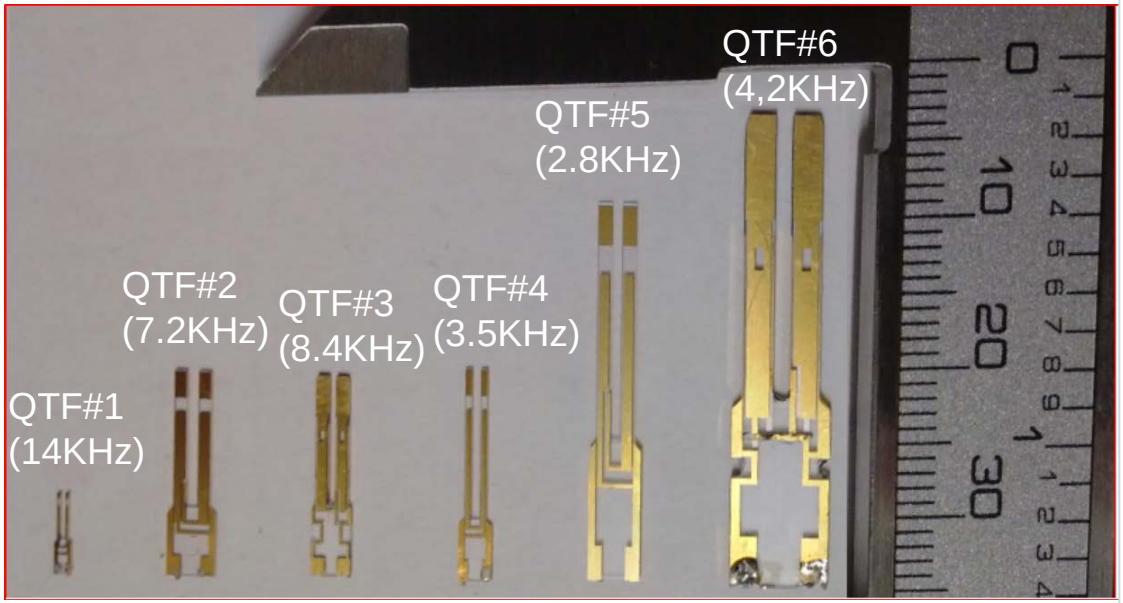

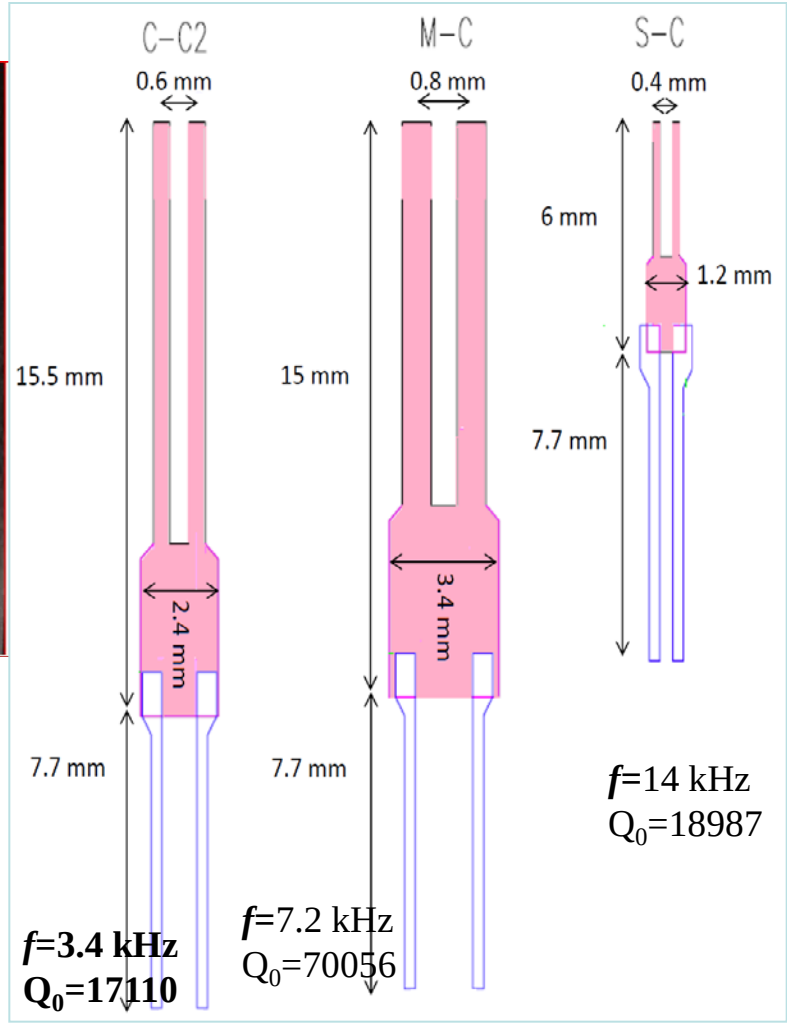

- Standard photolithographic techniques were used to etch custom QTFs. Chromium/gold layer was deposited on both sides of the custom QTFs for electrical contacts.
- New generation of custom QTFs behave similar to "standard" QTFs in terms of their vibrational mode(s).

Why is THz based Trace Gas Sensing useful ?

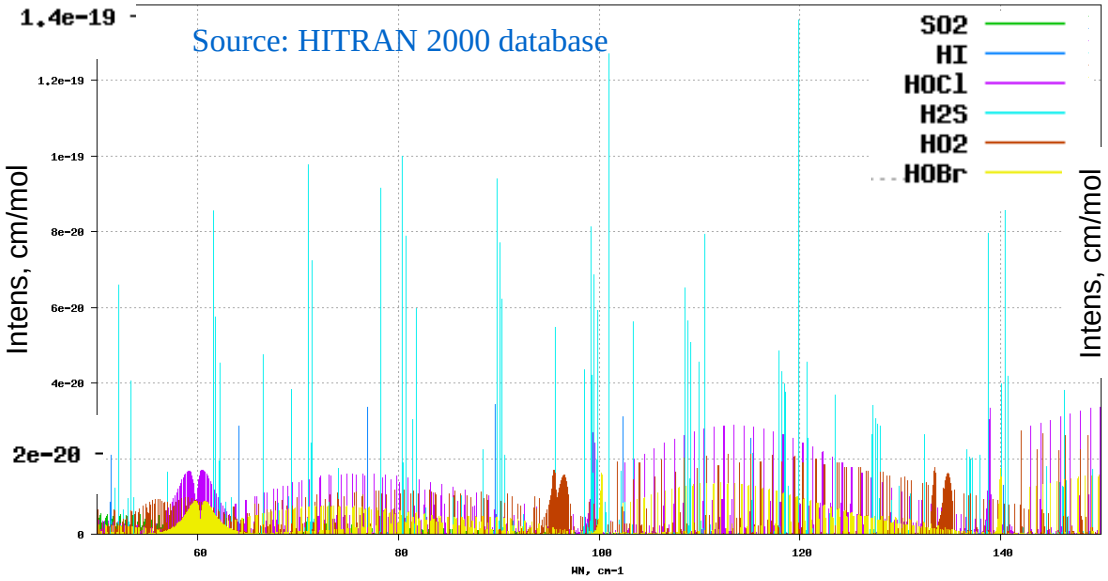

1.6 e-18

Several gas species such as HF, OH, HCN, HCl, HBr, NH_3, H_2O_2, H_2S, H_2O & explosives (in the vapor phase) show strong absorption bands in the THz spectral range.

Mainly rotational levels are involved in THz absorption processes and rotational-translational (R-T) relaxation rates are **up to three order of magnitude faster** with respect to vibrational-translational (V-T) in the mid-infrared

Recently realized a THz QEPAS sensor for H_2S trace gas detection using a 1mW CW QCL emitting 2.91 THz (~ 97.11 cm^{-1}) operating at 15 K. Achieved a MDL of 170 ppm in 10 sec to date .

(Optics Express in press 2015)

THz QCL Sources via Nonlinear Optics

Use intra-cavity DFG in mid-IR QCLs

$$W(\omega_{THz}) \propto \left|\chi^{(2)}\right|^2 W(\omega_1) W(\omega_2) \times l_{eff}^2$$

THz QCL source based on intra-cavity DFG

- *Same fabrication/user operation as regular QCLs*
- *Room temperature operation*
- *Broadband THz tuning*

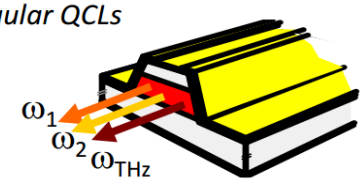

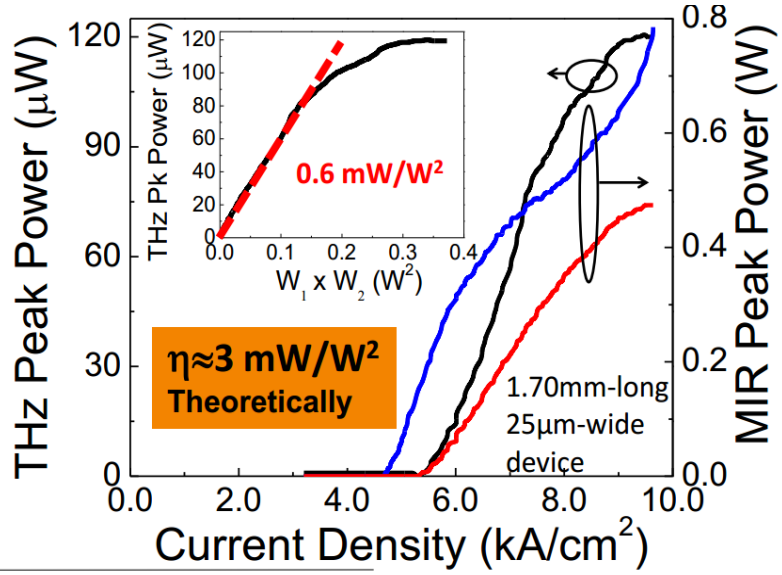

Vijayraghavan *et al., Nature Comm.* ***4,*** *2021* (2013)

2.3-mm-long, 22-μm-wide device @ room temperature

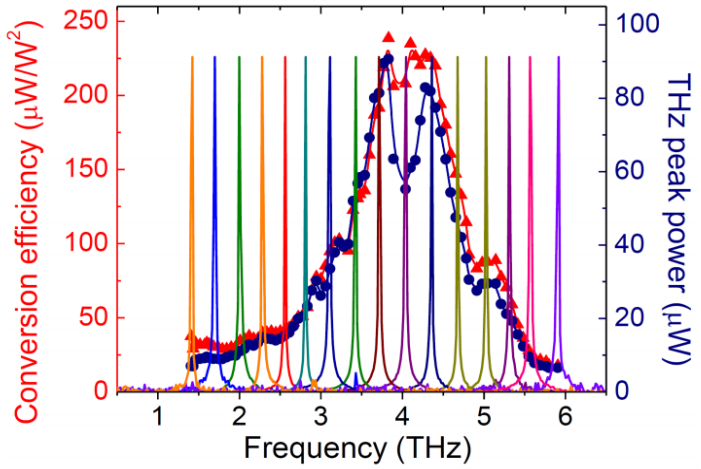

Vijayraghavan *et al., Nature Comm.* ***4,****2021* (2013); Jiang *et al., J. Opt.* **16,**094002 (2014)

Monolithic tuners: 0.58 THz of tuning – Jung *et. al., Nature Comm.* ***5,*** *4267* (2014)

IQCLSW 2014, Policore, Italy: M.A. Belkin et al, UT Austin, USA
Photonics West 2015, San Francisco: M. Rhazeghi et al, NWU, USA

In-plane view of designs of three types of tuning forks realized in this work. The size scale is shown on the right bottom.

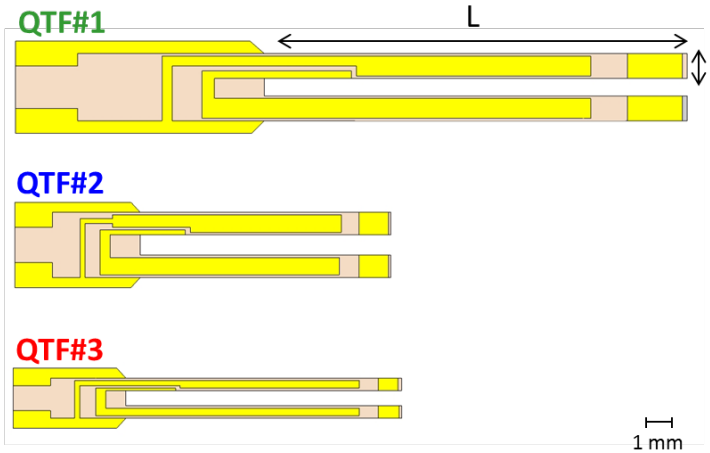

	QTF#1		QTF#2		QTF#3	
L (mm)	17		10		11	
T (mm)	1		0.9		0.5	
w (mm)	0.25		0.25		0.25	
	n =1	n = 2	n =1	n = 2	n =1	n = 2
f_n (Hz)	2,913.42	18,245.49	7,577.81	47,456.54	3,479.25	21,789.04
node points (mm)	17	3.717	10	2.210	11	2.411
antinode points (mm)	0	09	0	05.3	0	05.8

F. K. Tittel, A. Sampaolo, P. Patimisco, L. Dong, A. Geras, T. Starecki, V. Spagnolo, Optics Express, 24, A683-A692, 2016

QTFs resonance curves measured at a fixed excitation level V = 3.46 mV and at a pressure of 75 Torr in standard air for QTF#3 (a), QTF#2 (b) and QTF#1(c), for the fundamental and first overtone mode

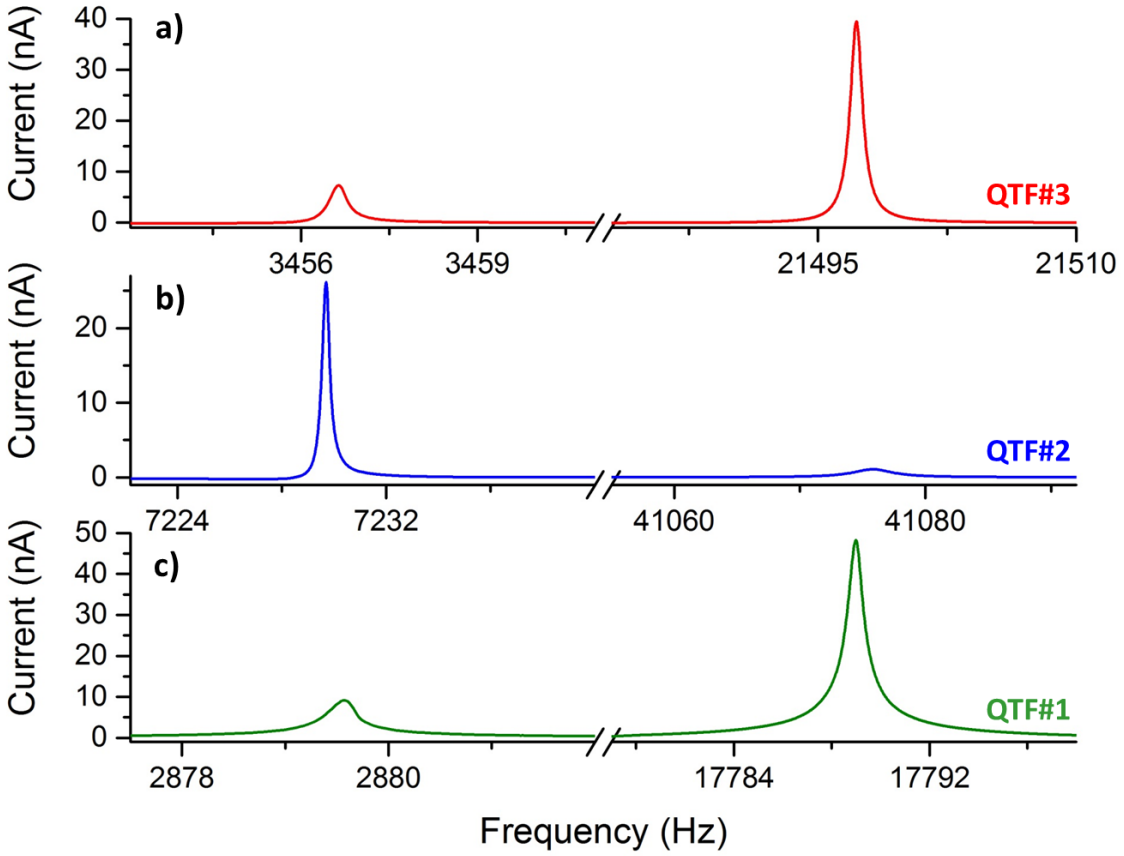

Quality factors of the fundamental and the first overtone resonance frequency measured for QTF#1 (■), QTF#2 (●) and QTF#3 (▲).

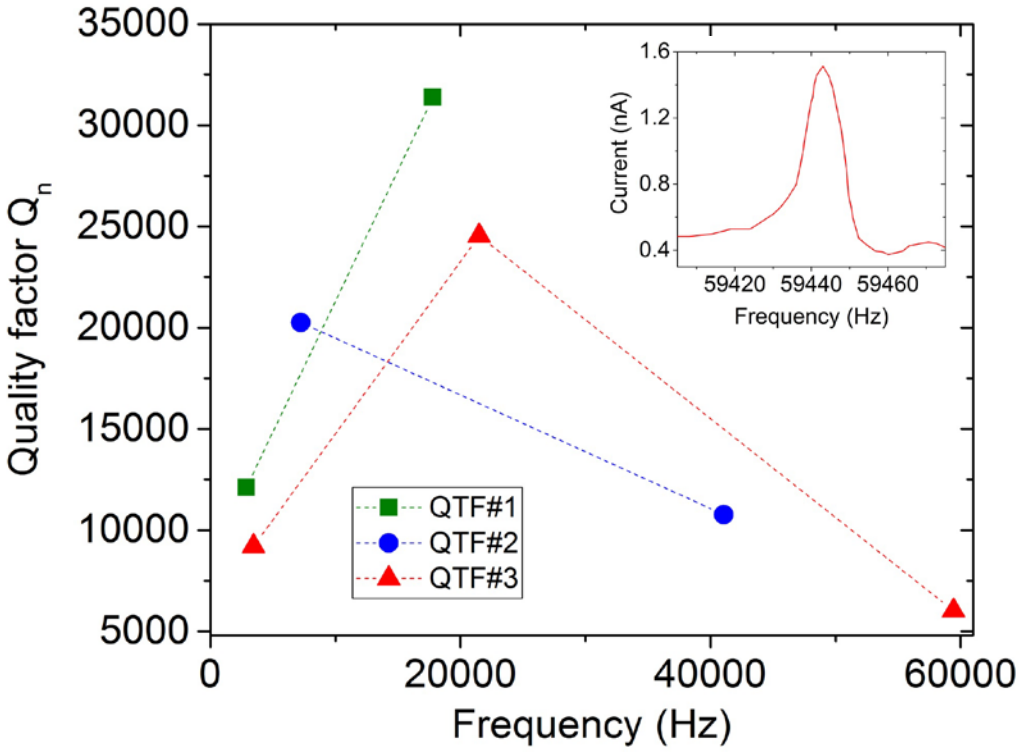

For QTF#3, the quality factor of the second overtone mode is also reported. Dashed lines serve as a visual guide. Inset: resonance profile measured for the QTF#3 second overtone mode (*n*=3) at an excitation level V = 3.46 mV and at a pressure of 75 Torr in standard air.

Schematic of the QEPAS trace gas sensor using a diode laser as the excitation source. A housing was imlemented in order to allow easy interchange of the custom QTFs. PC: Personal Computer

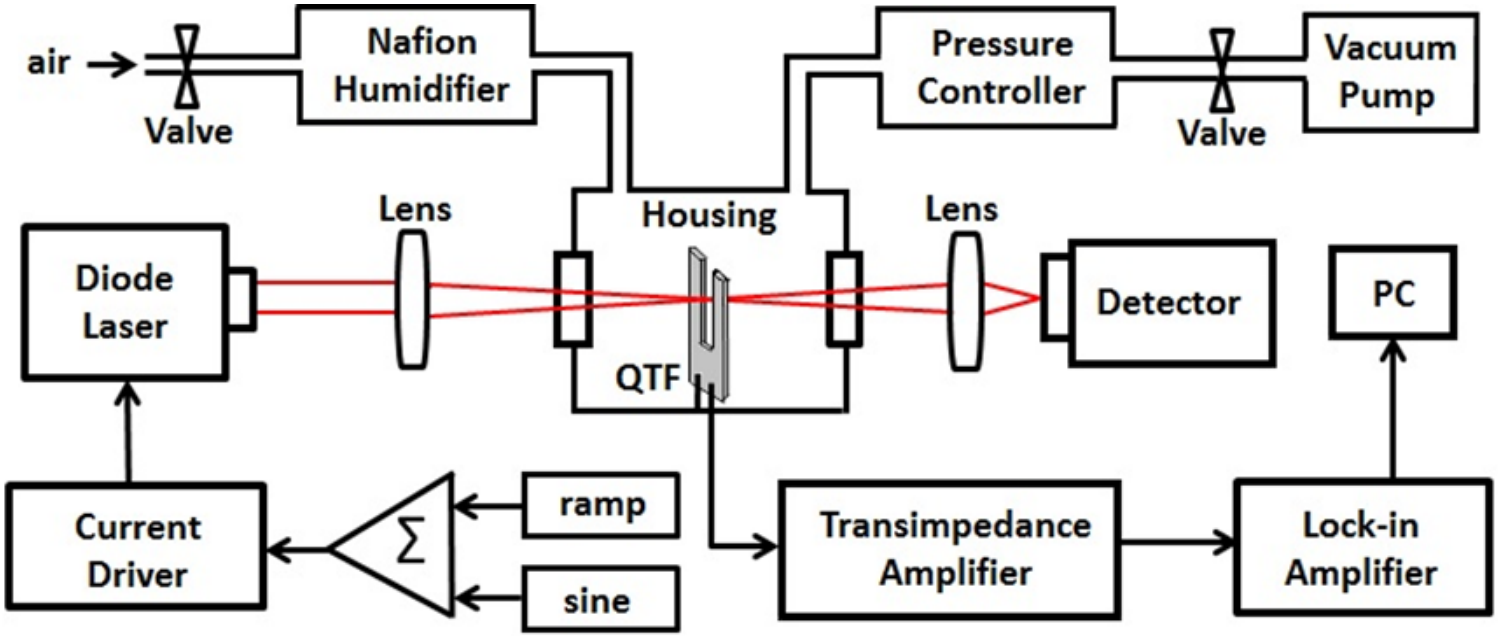

(a, c) Normalized transverse displacement of the prong for QTF#1 calculated as a function of the distance from the QTF top

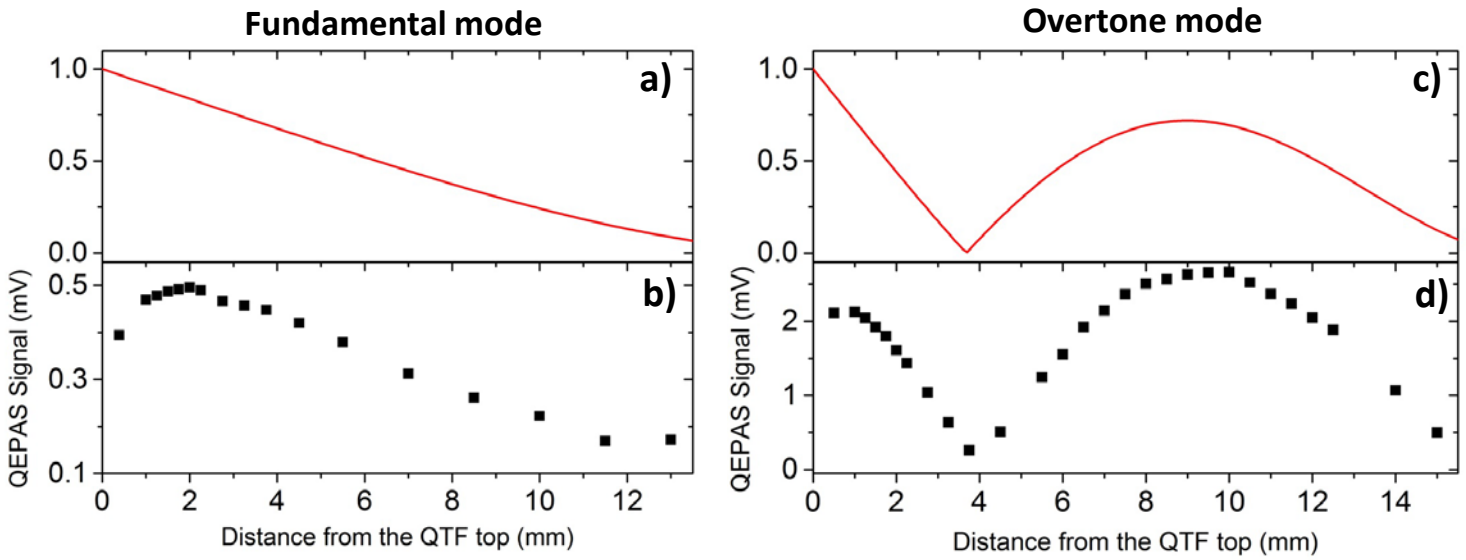

for the fundamental (a) and overtone (c) mode. (b, d) QEPAS signals as a function of the laser beam distance from the QTF#1 support measured for the fundamental (b) and first overtone mode (d), at a pressure of 75 Torr. The laser beam position was scanned along the symmetry axis of the QTF#1.

Normalized QEPAS peak signals as a function of the air pressure acquired for the fundamental at 7.2 kHz

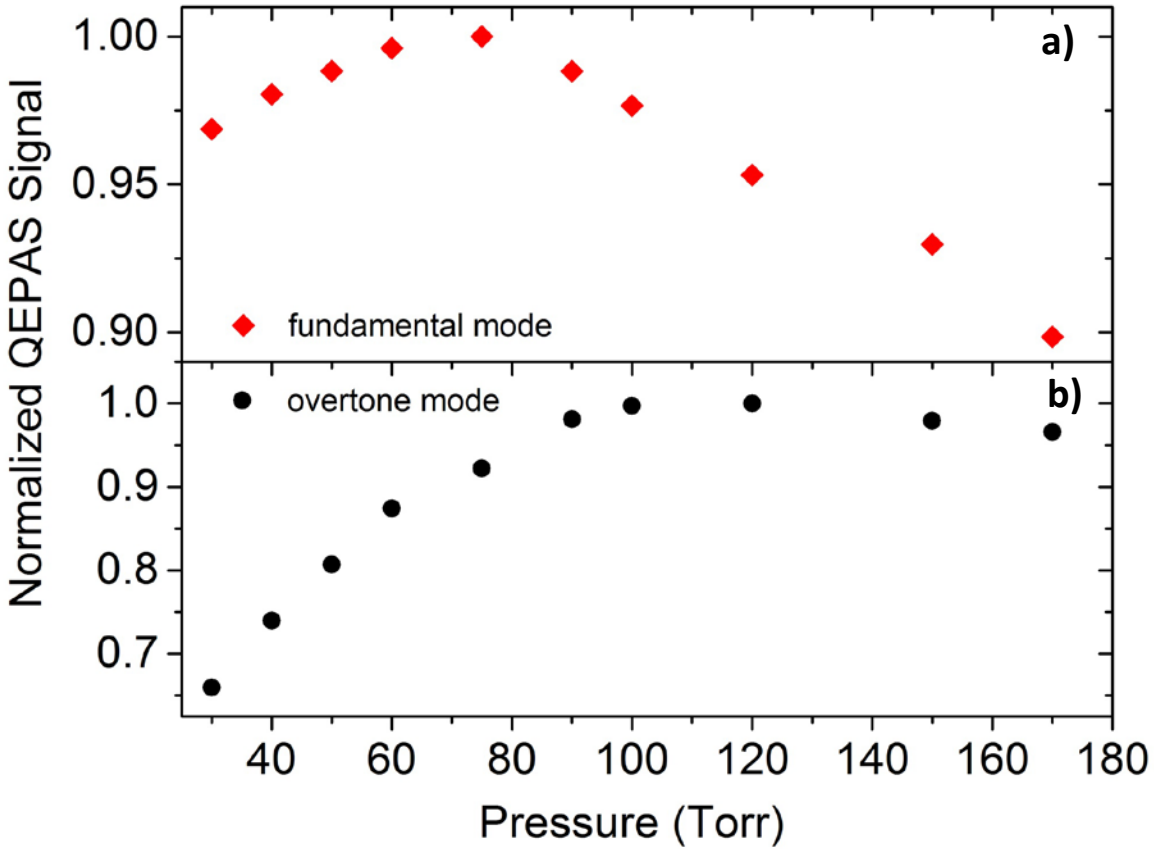

(a) and first overtone (b) at 41.0 kHz mode of QTF#2.

QEPAS spectral scans of a gas mixture containing air with a 1.7% water concentration for the fundamental mode (black solid line) and for the first overtone one (red solid line) of the QTF#1 (a), QTF#2 (b) and QTF#3 (c).

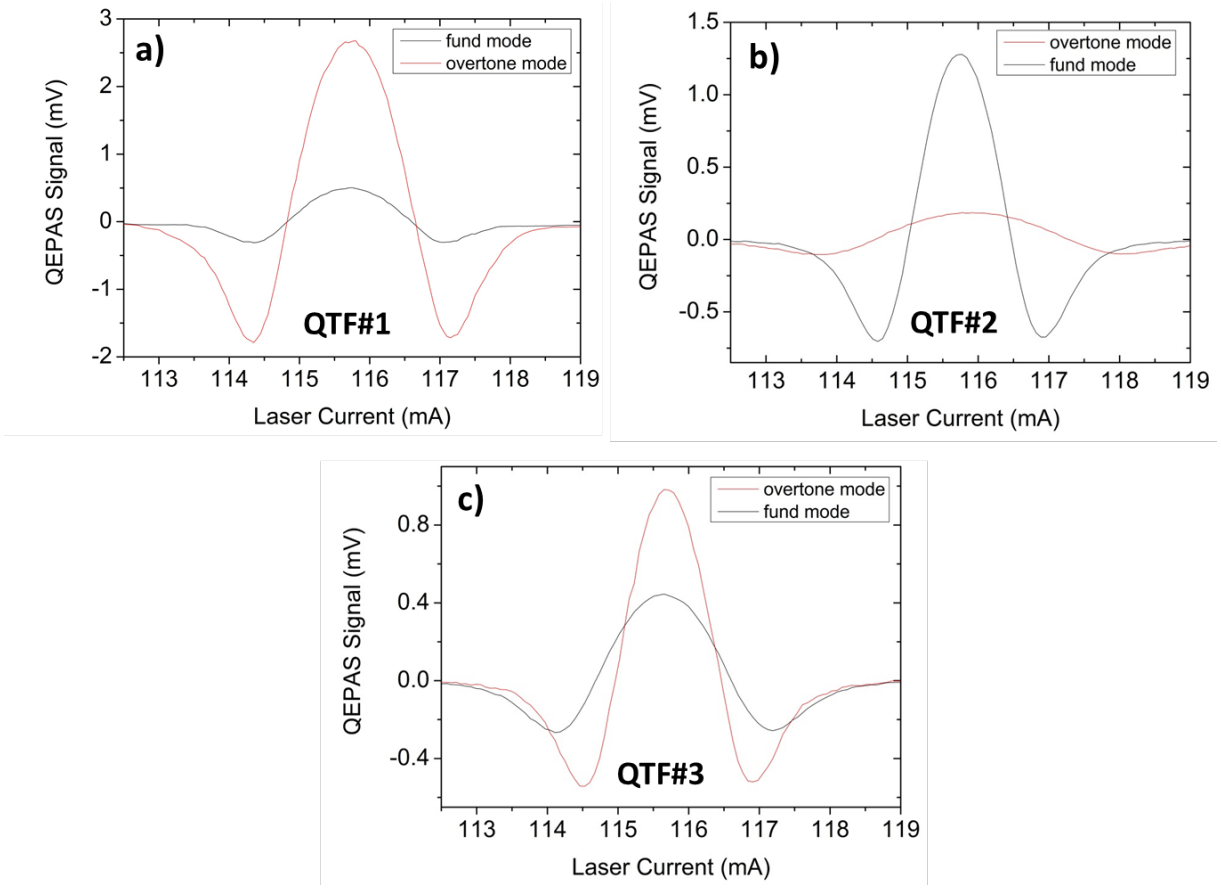

All scans were acquired at the laser modulation depth of 0.05 cm^{-1} and recorded with a 100 ms lock-in integration time.

Schematic view of QTF dimensions

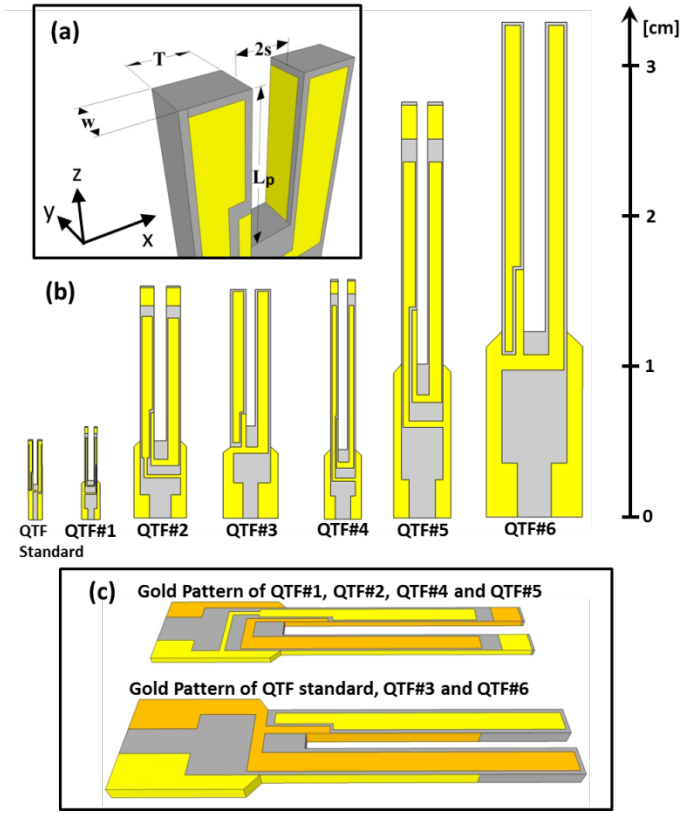

(a) Schematic view of QTF dimensions. (b) x-z plane view of standard and custom designed tuning forks. The size scale is shown on the right. (c) Surface and side view of the two different designed gold patterns for electrical charge collection. The grey areas stand for uncovered quartz, while the yellow and gold-yellow area represent the two electrodes of each pattern.

Picture showing realized custom tuning forks.

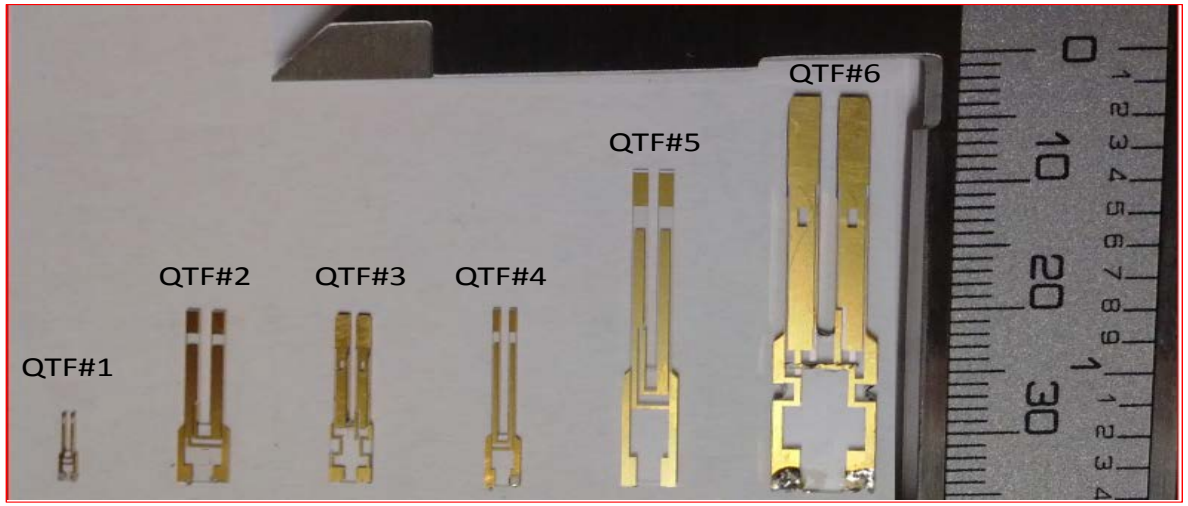

The size scale in mm is shown on the right

Parameters	QTF standard	QTF #1	QTF #2	QTF #3	QTF #4	QTF #5	QTF #6
L_p (mm)	3.0	3.5	10.0	10.0	11.0	17.0	16.8
w (mm)	0.34	0.25	0.25	0.5	0.25	0.25	0.8
T (mm)	0.35	0.2	0.9	1.0	0.5	1.0	1.4
Prong spacing, 2s (mm)	0.3	0.4	0.8	0.5	0.6	0.7	0.8
m_e (mg)	0.230	0.113	1.447	3.216	0.884	2.733	12.102

Dimensions and prong effective mass me of the standard and custom tuning forks: Lp (QTF prong length), T (thickness of the prong), w (thickness of the quartz crystal) and 2s (spacing between prongs).

Circuit diagram for QTF characterization

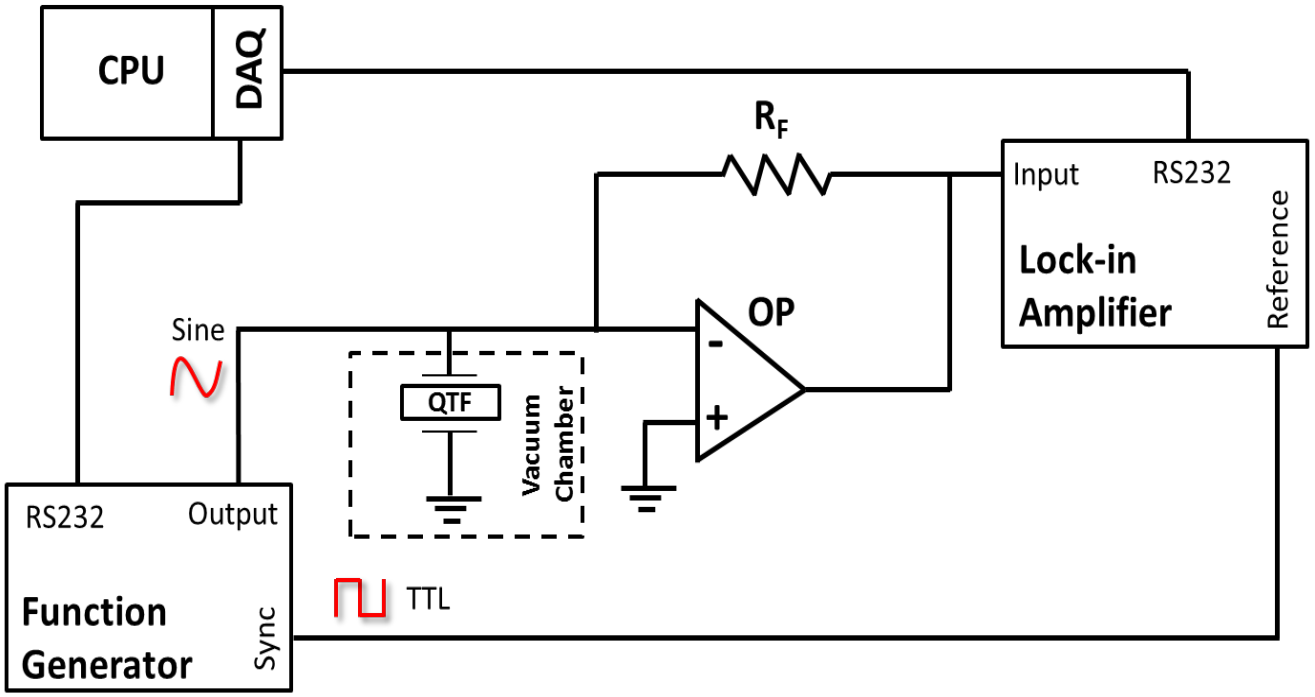

The excitation sine voltage is supplied by a high-resolution waveform generator, which also provides the reference TTL signal for the lock-in amplifier. The QTF current output is converted to a voltage by means of a transimpedance amplifier with a feedback resistor of R_F = 10 MΩ. The QTF is mounted inside a vacuum chamber allowing low gas pressure measurements. OP: operational amplifier.

Resonance curves for in-phase I_a (black dots) and out-of-phase I_b (red dots) components of the QTF current

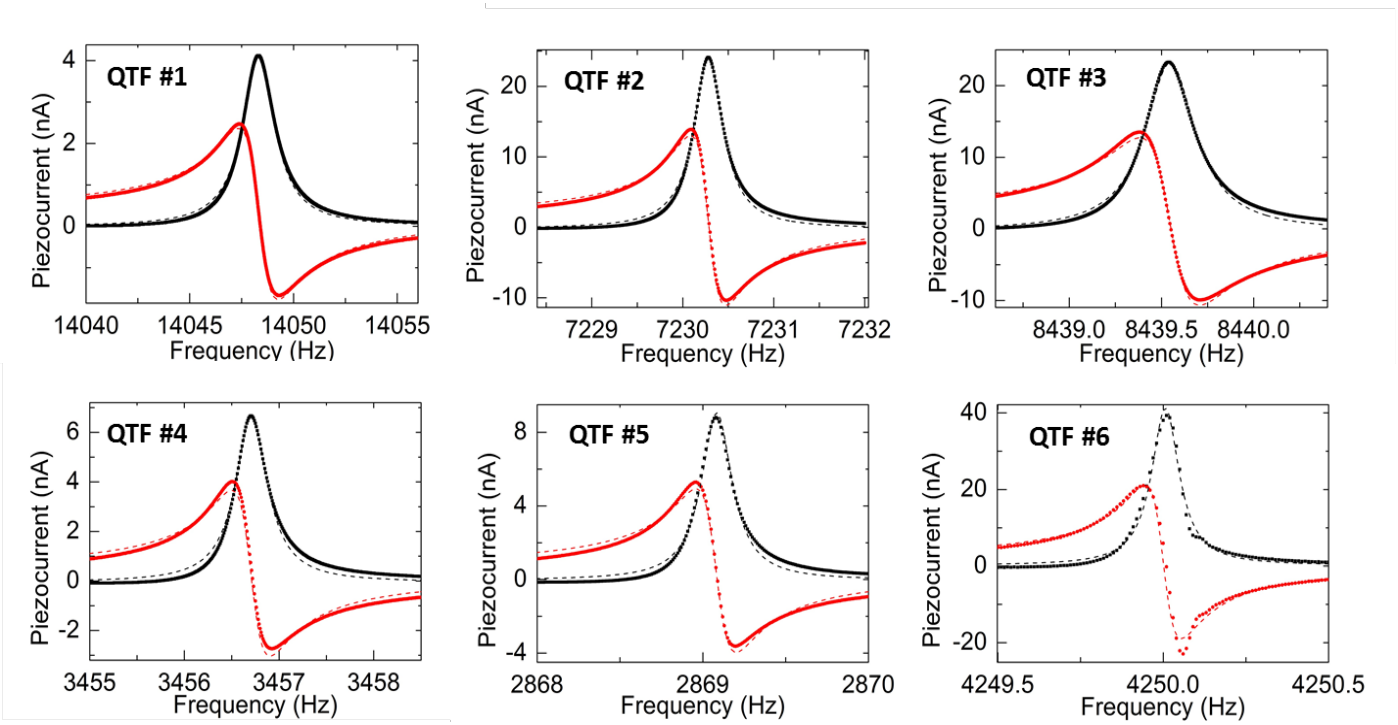

Resonance curves for in-phase I_a (black dots) and out-of-phase I_b (red dots) components of the QTF current measured at a fixed excitation level $V_0 = 0.5$ mV and at a pressure of 50 Torr in standard air for custom QTFs near the fundamental oscillation mode. The dashed lines indicate the best-fit curves using **Eq. (7) .**

Quality factor Q (● symbols) measured as a function of the standard air pressure for the six custom QTFs.

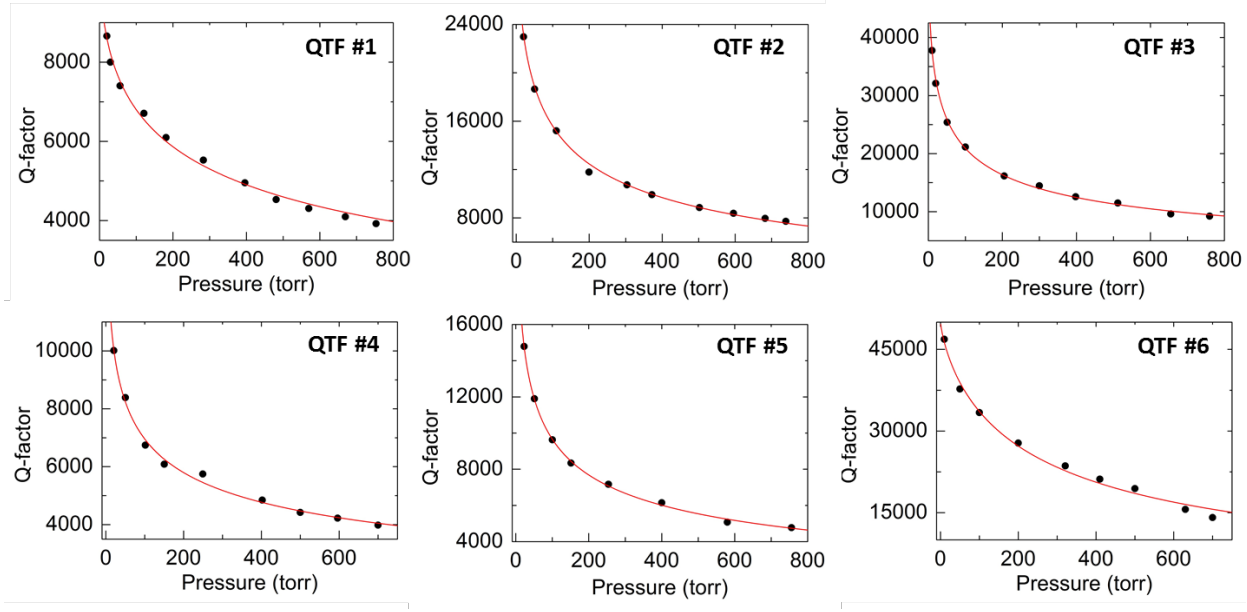

Quality factor Q (● symbols) measured as a function of the standard air pressure for the six custom QTFs. Solid curves are the best fit obtained using $Q(P)= Q_0/(1+ Q_0\, bP^c)$. The related fit parameters are reported in Table IV, where Q_0 is the quality factor of the QTF under vacuum, including all the intrinsic losses mechanisms, and b and c are parameters related to the QTF geometry and surrounding fluid viscosity. In fact, QTFs are used for density, viscosity and velocity measurement of fluids [14,17]. In order to

Comparison between fundamental and the first overtone QTF flexural modes for QTF#5 - *Electrical Characterization*

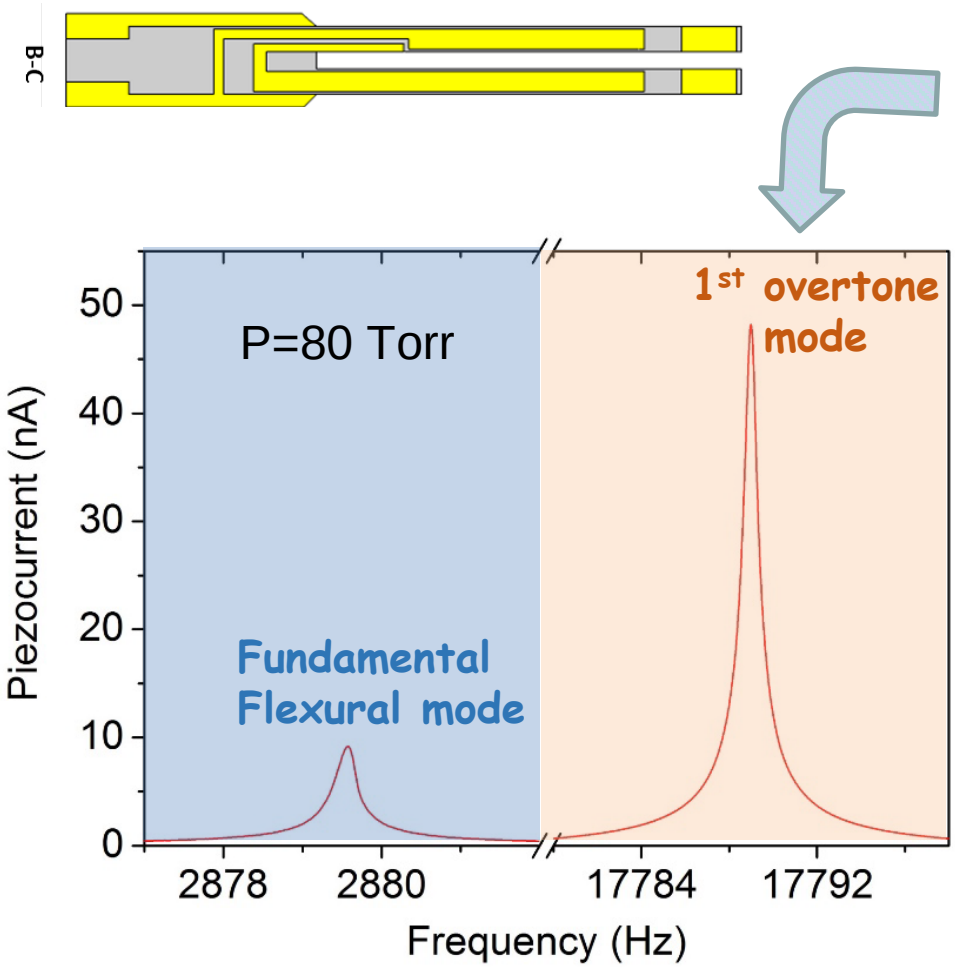

Comparison between the QTF fundamental and 1st overtone flexural modes

@ 760 torr	fundamental n = 0	1st overtone n = 1
Frequency (Hz)	2,879.5	17,788.9
Quality factor Q	12,099	31,374

A ~ 5.3 higher piezocurrent is measured when operating with the first overtone flexural mode instead of the fundamental mode.

Gold coated electrode pattern was optimized for the fundamental vibrational mode, resulting in an enhanced piezo-charge collection for the 1st overtone flexural mode

Schematic of the QEPAS trace gas sensor using a THz Quantum Cascade Laser (THz QCL) as the excitation source

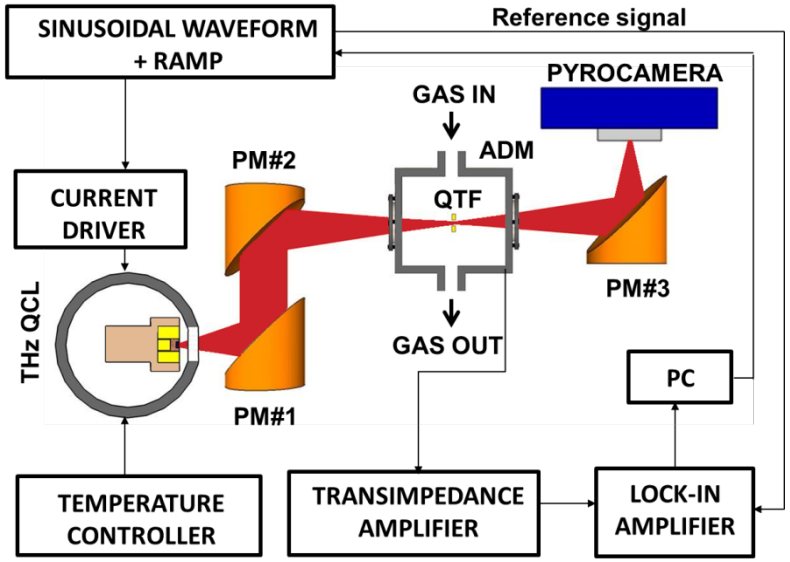

PM – Parabolic Mirror; ADM – Acoustic Detection Module; QTF – Quartz Tuning Fork; PC – Personal Computer.

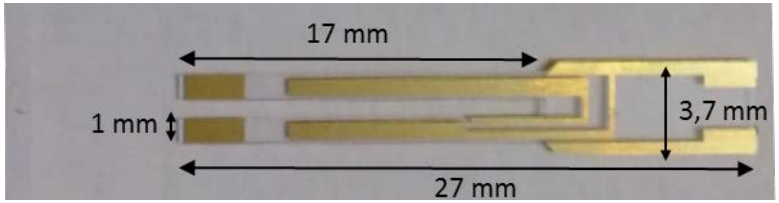

Picture of the N-QTF including the size of the main geometrical parameters.

A. Sampaolo, P. Patimisco, M. Giglio, M. S. Vitiello, H. E. Beere, D. A .Ritchie, G. Scamarcio, F. K. Tittel, V. Spagnolo; "Improved tuning fork for terahertz quartz-enhanced photoacoustic spectroscopy"; Sensors, 16, 439, 2016

Two-dimensional beam profile of the THz-QCL acquired by means of an IR pyrocamera after mirror PM#3 (see Fig. 2) when the beam is focused out the N-QTF

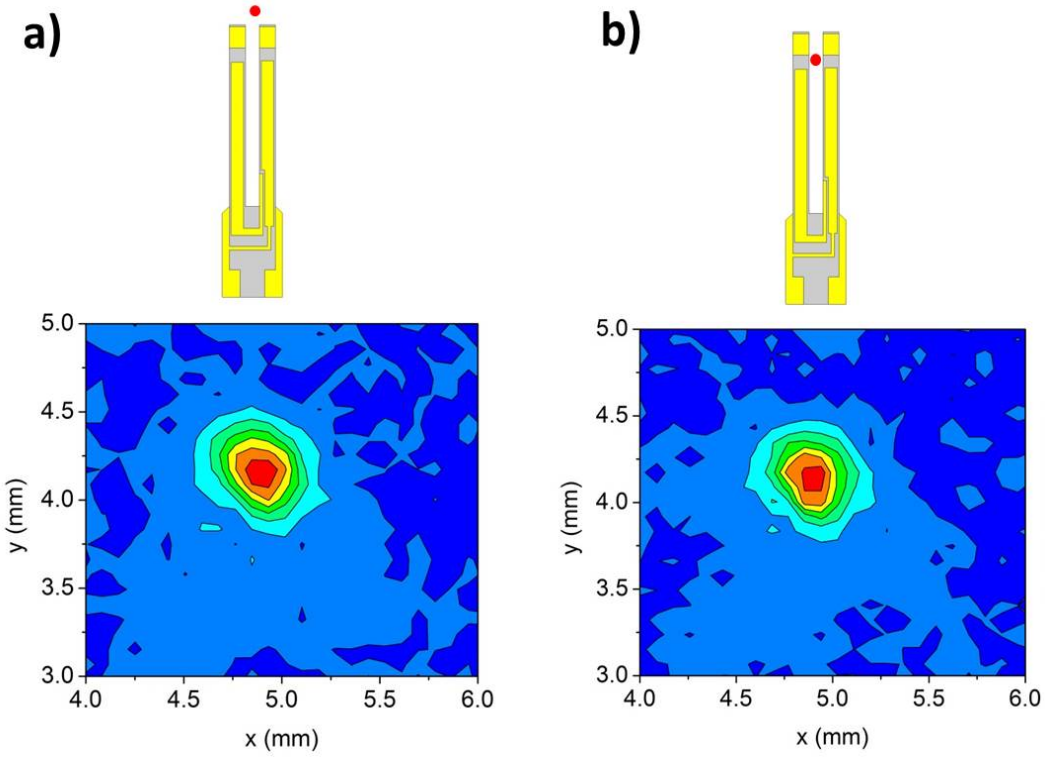

(a) or between the two prongs (b). Both beam profiles are shown together with an illustration representing the position of the focused THz beam (red spot) with respect the N-QTF.

(a) QEPAS spectral scans of gas mixture containing different concentrations of methanol in N_2 at gas pressure of 10 Torr acquired with 3 seconds lock-in integration time.

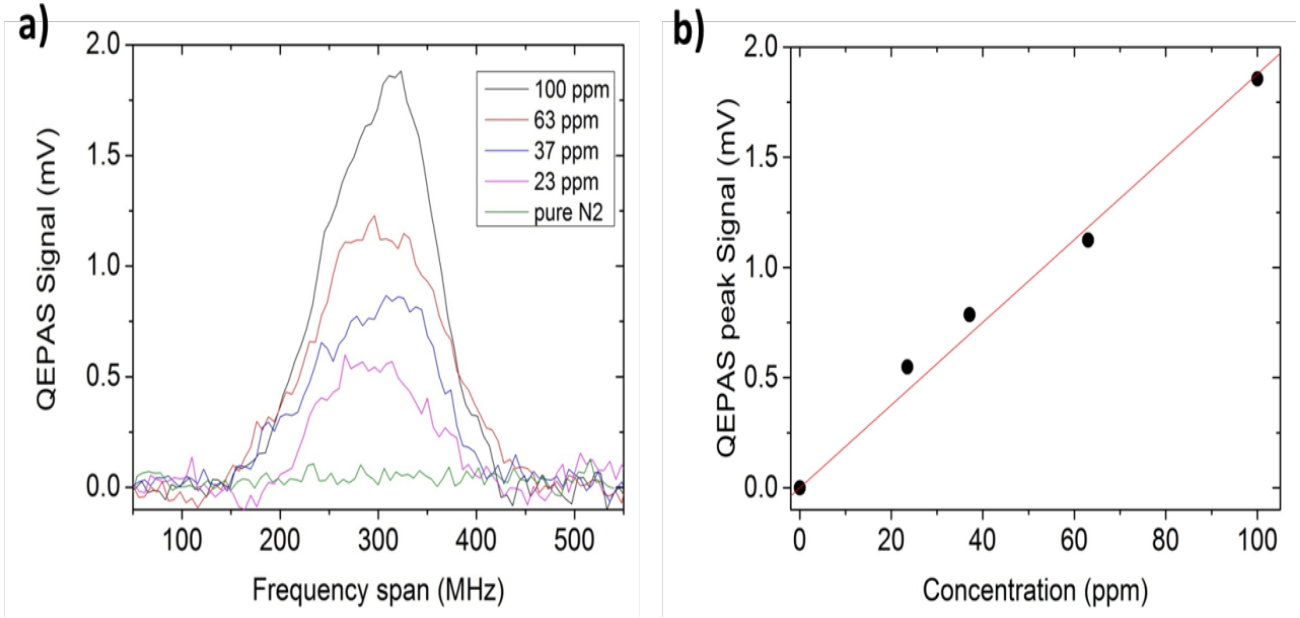

The spectral scan obtained for pure N_2 under the same operating conditions is also depicted. (b) Calibration curve (solid red line) obtained from the linear fit of measured QEPAS peak signals (•) vs methanol concentrations.

NNEA results obtained with QEPAS sensor for the gas species reported versus employed laser wavelength, in the UV-Vis, near-IR, mid-IR and THz spectral ranges

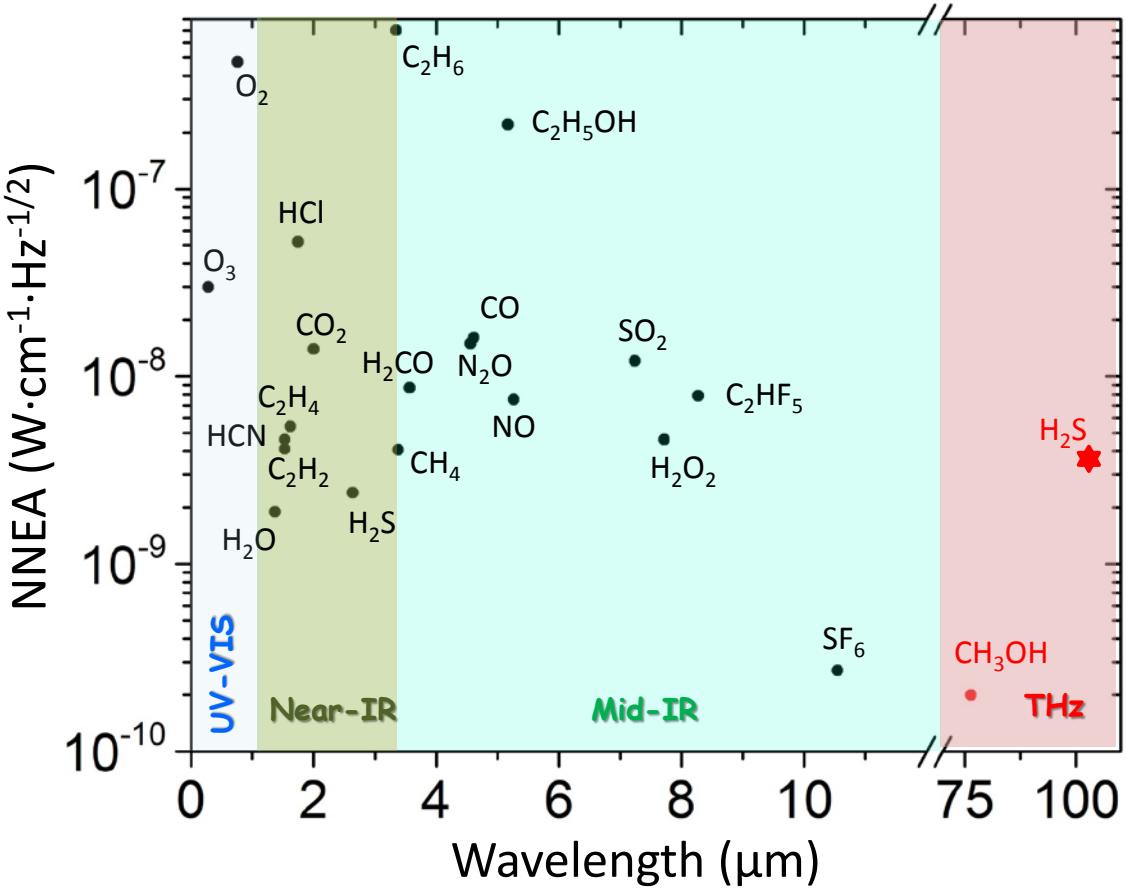

Red symbol (*) marks the result of present work.

Vincenzo Spagnolo, Pietro Patimisco,Riccardo Pennetta,Angelo Sampaolo,Gaetano Scamarcio,Miriam S. Vitiello,and Frank K. Tittel; 'THz Quartz-enhanced photoacoustic sensor for H_2S trace gas detection"; 23, 7574-7582, (2015)

THz QEPAS H_2S Sensor employing QTF#5

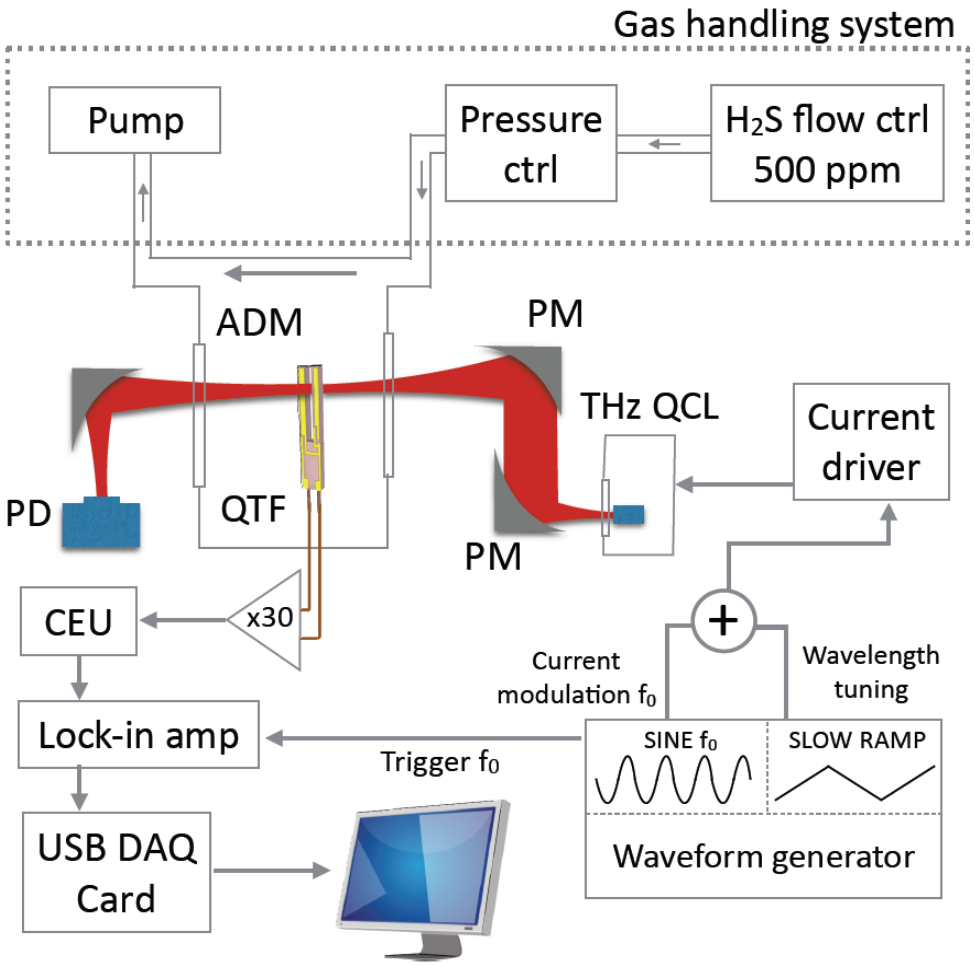

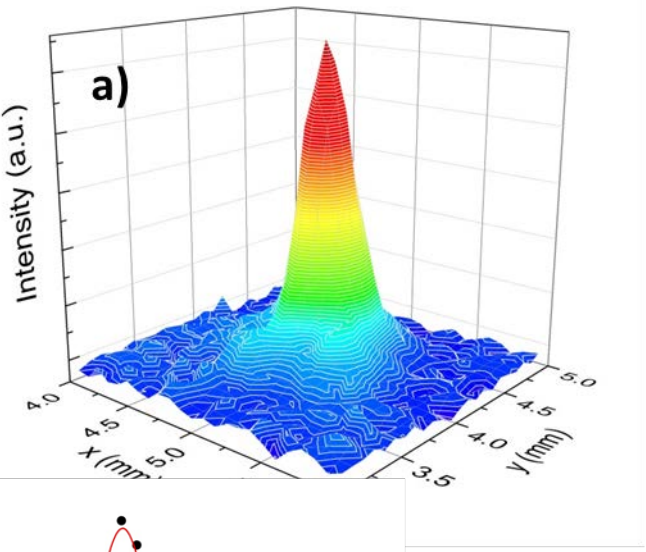

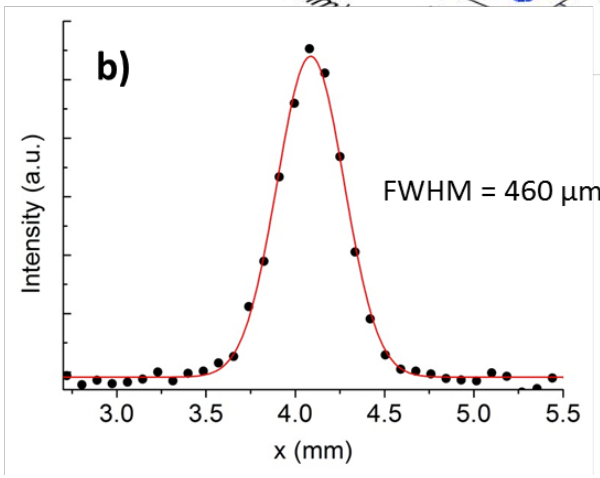

Selected Line			
Transition		Wavelenght (cm^{-1})	Line-strength
(15 5 10-15 4 11)	rotational	97,114 (2.913 THz)	1.15×10^{-22} cm/mol

THz QEPAS H_2S Sensor Performance Assessment and Linearity

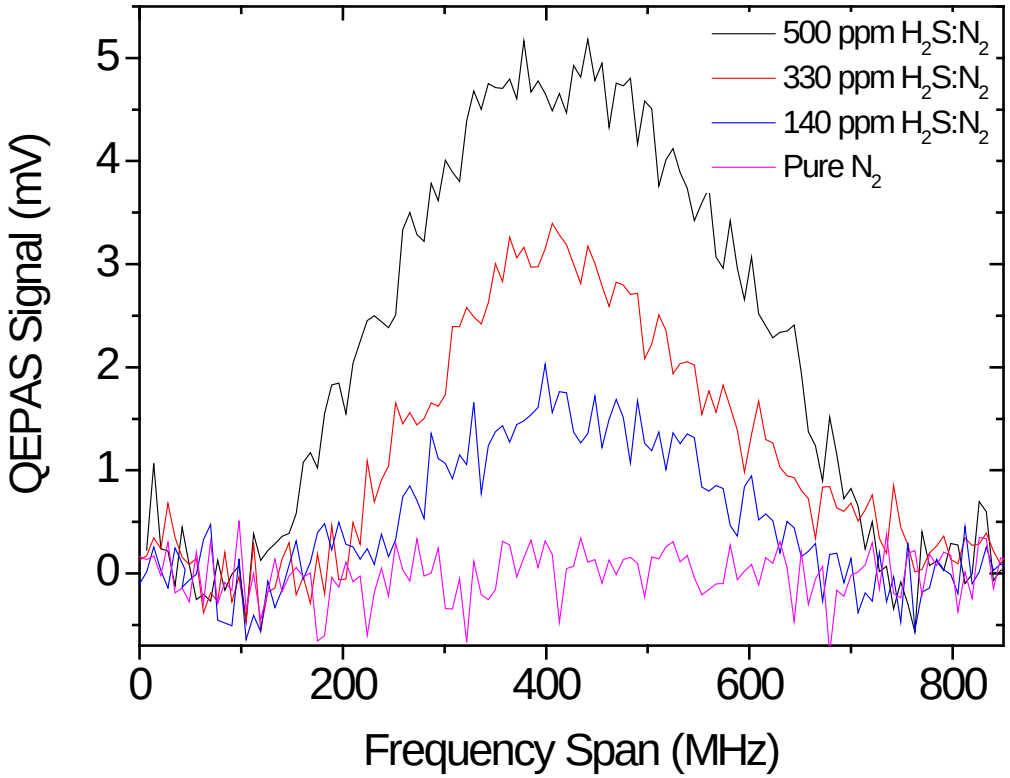

No signal changes with a few % of H_2O

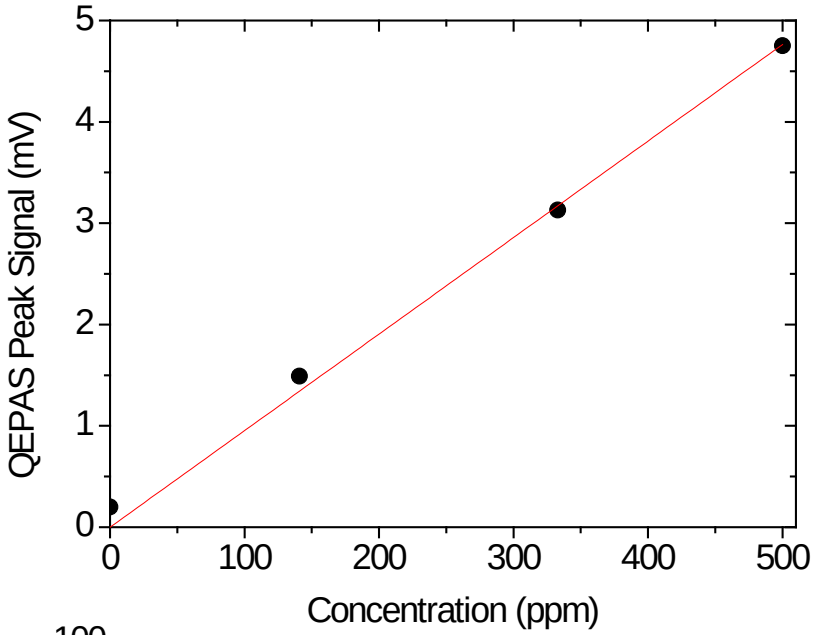

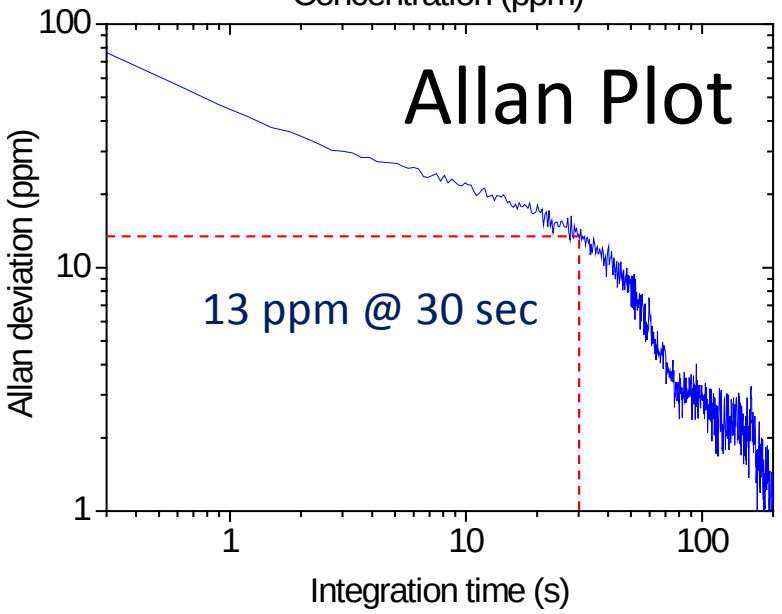

Absorption coefficient normalized to a detection bandwidth (*0.00556 Hz*) and an optical power (*240 μW*):

NNEA = 4.05×10^{-10} $cm^{-1}W(Hz)^{-1/2}$

Comparison of three QEPAS based sensors for H_2S detection operating in the near-IR, mid-IR and THz spectral ranges.

	Near-IR	Mid-IR	THz
Frequency (cm^{-1})	3788.56	1266.93	97.113
Laser power (mW)	3	45	0.24
Line strength (cm/mol)	$1.67 \cdot 10^{-21}$	$1.51 \cdot 10^{-21}$	$1.13 \cdot 10^{-22}$
NNEA ($cm^{-1} \cdot W/\sqrt{Hz}$)	$2.4 \cdot 10^{-9}$	$7.3 \cdot 10^{-9}$	$3.6 \cdot 10^{-9}$
Detection sensitivity @ 30s lock-in integration time	750 ppb	330 ppb	107 ppm

(a) Spectral scan of 100 ppm of methanol in N_2 at a gas pressure of 10 Torr acquired with a 3 sec lock-in integration time using the N-QTF.

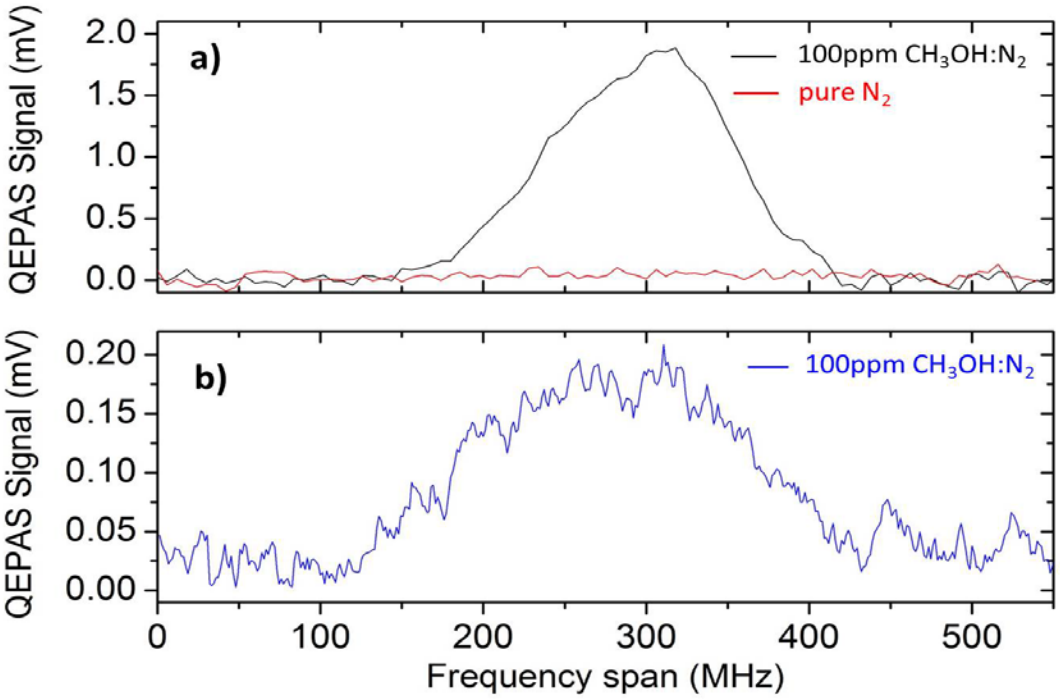

(b) Spectral scan of 100 ppm of methanol in N_2 obtained for the same experimental conditions using the C-QTF with a standard geometry. The lower data sampling in panel (a) is due to a faster voltage ramp employed in this work with respect to the measurements reported in [11].

Allan-Werle deviation in ppm as a function of the lock-in integration time for the QEPAS sensor. The curve was calculated by analyzing 120 minutes-long acquisition periods of the signal measured for pure N_2 at 10 Torr and setting the lock-in integration time at 100 ms.

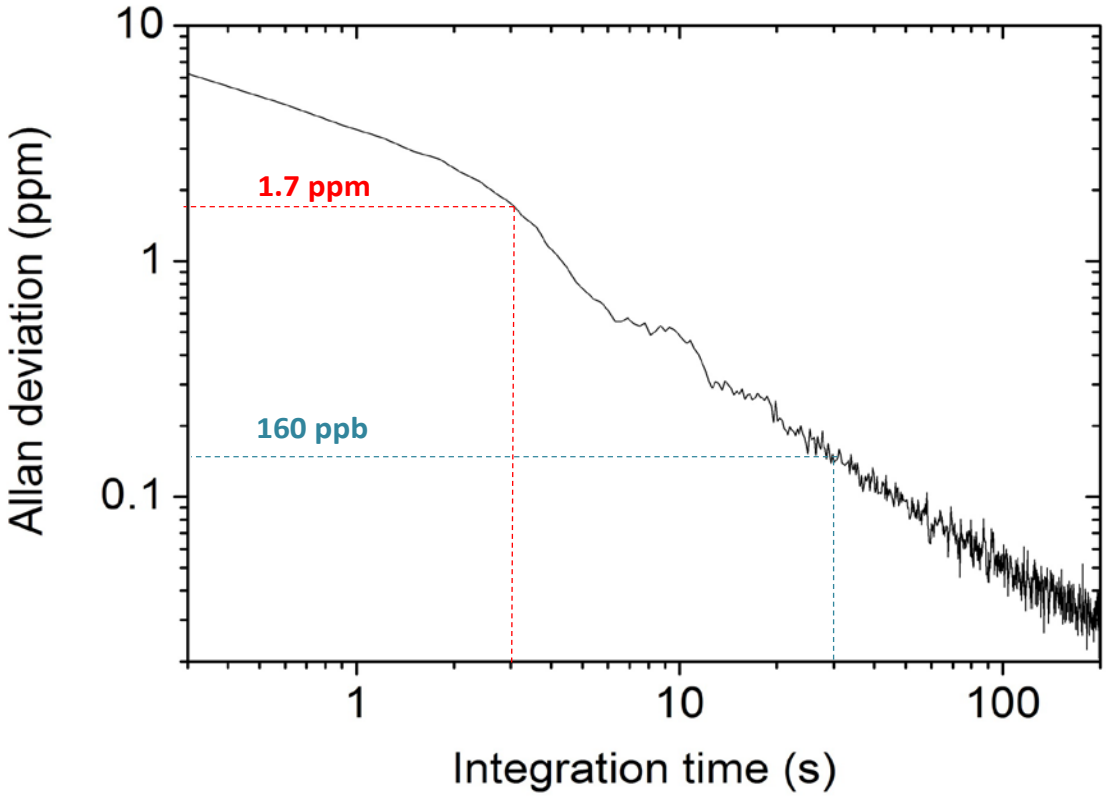

Comparison between fundamental and first overtone QTF flexural modes for QTF#5 – *QEPAS Characterization*

- **2f detection of a fixed H_2O concentration**

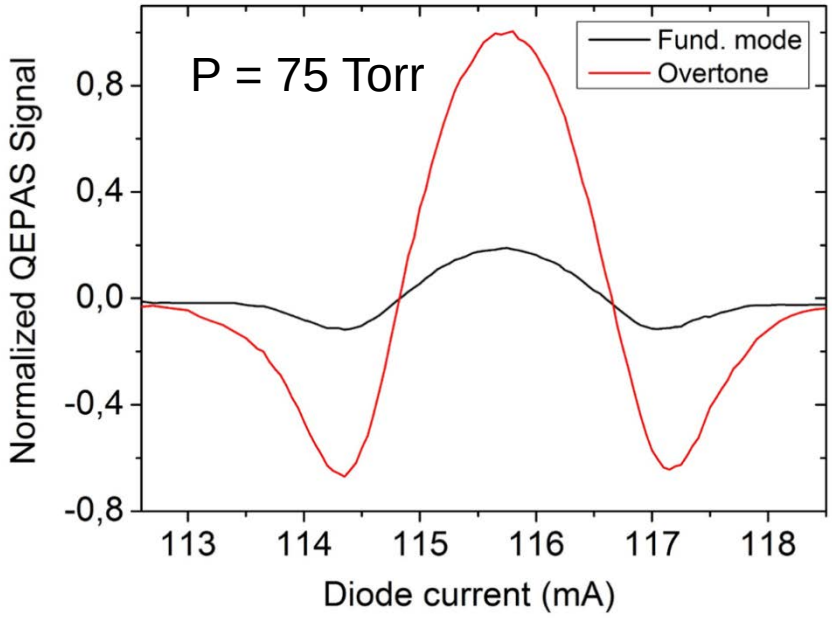

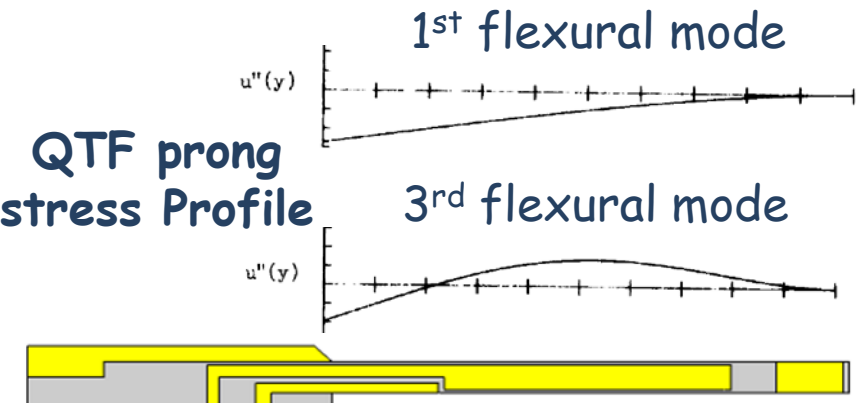

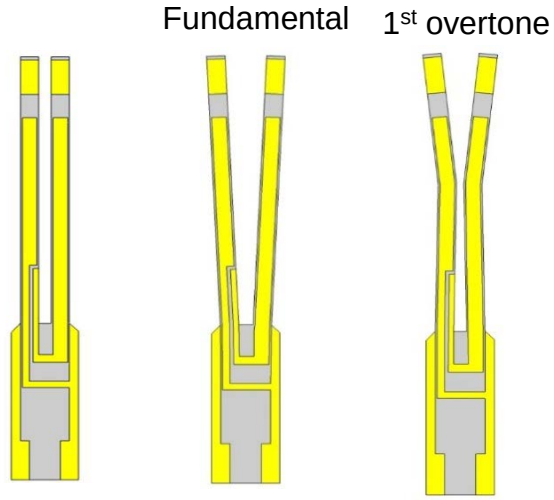

← Comparison between the 1st overtone (18KHz) and fundamental (3KHz) flexural modes of the B-C QTF @ P=75 torr.

The signal for the 3rd flexural mode is ~ 5 times higher.

The two vibrational modes differ in the stress profile. A larger charge is generated for the high order modes

Summary, Conclusions and Future Work

- Development of robust, compact, sensitive, selective mid-IR trace gas sensor technology based on RT, CW high performance DFB ICLs & QCLs for environmental monitoring and medical diagnostics.
- ICLs and QCLs were used in TDLAS and PAS/QEPAS based sensor platforms
- Performance evaluation of seven target trace gas species were reported. The minimum detection limit (MDL) with a 1 sec sampling time were :
  - C_2H_6: MDL of .24 ppbv at ~3.36 µm; CH_4: MDL of 13 ppbv at ~7.28 µm; N_2O: MDL of 6 ppbv at ~7.28 µm.
- I-QEPAS demonstration resulted in a factor of 240 increase in detection sensitivity
  - CO_2 MDL of 300 pptv at 50mbar was achieved for a 20 sec integration time.
- THz-QEPAS H_2S sensing demonstration using a custom QTF resulted in a NNEA of 10^{-10} $cm^{-1}W(Hz)^{-1/2}$. The MDL was 13 ppmv for a 30 sec integration time.
- Novel implementation of QTF 1st overtone flexural l mode for QEPAS sensing
- Development of "active" I-QEPAS system for CO and NO detection in the ppt range
- Future development of trace gas sensors for monitoring of broadband absorbers: acetone(C_3H_6O), propane (C_3H_8), benzene (C_6H_6)
- Future development of mid-IR electrically pumped interband cascade optical frequency combs (OFCs) jointly with JPL, Pasadena, CA , NRL, Washington, DC and Bari (Italy)

Acknowledgements

- DoE ARPA-E MONITOR Program: Aeries Technologies & Maxion Technologies;
- National Science Foundation (NSF) ERC MIRTHE award
- NSF-ANR (France) award for international collaboration in chemistry
- Robert Welch Foundation grant C-0586